Figure 43. Adsorption of formic acid on 90/5/5 Zn/Cu/Cr oxide at 200°C

a) reduced surface

b) exposure for 5 minutes

c) 1 hour after exposure

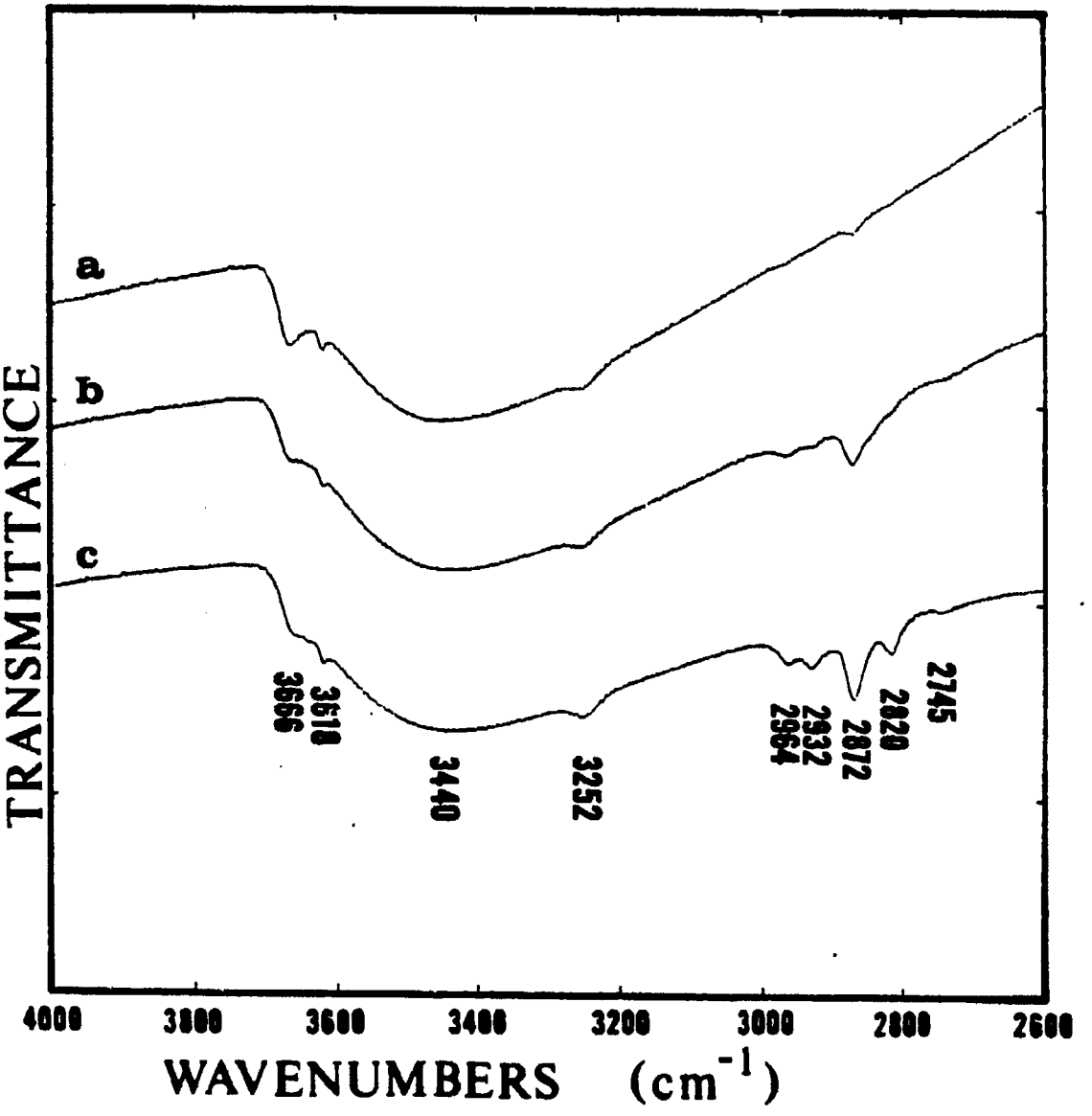
a
b
c
TRANSMITTANCE
3696
3618
3440
3252
2964
2932
2872
2820
2745
4000
3800
3600
3400
3200
3000
2800
2600
WAVENUMBERS (cm-1)

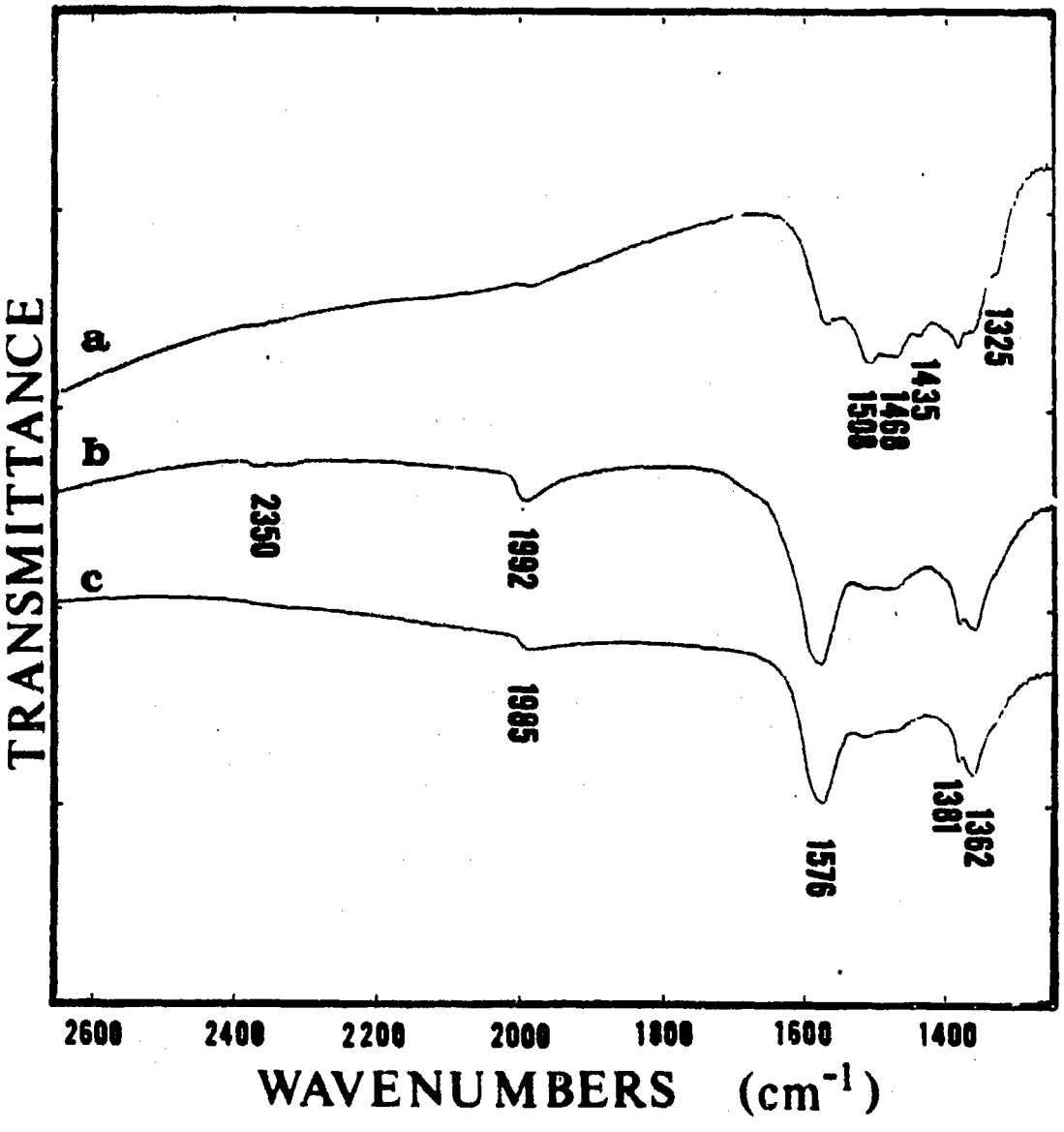

Figure 43. Continued

Figure 44. Adsorption of formic acid on 80/10/10 Zn/Cu/Cr oxide at 200°C

a) reduced surface

b) exposure for 5 minutes

c) exposure for 1 hour

d) 1 hour after exposure

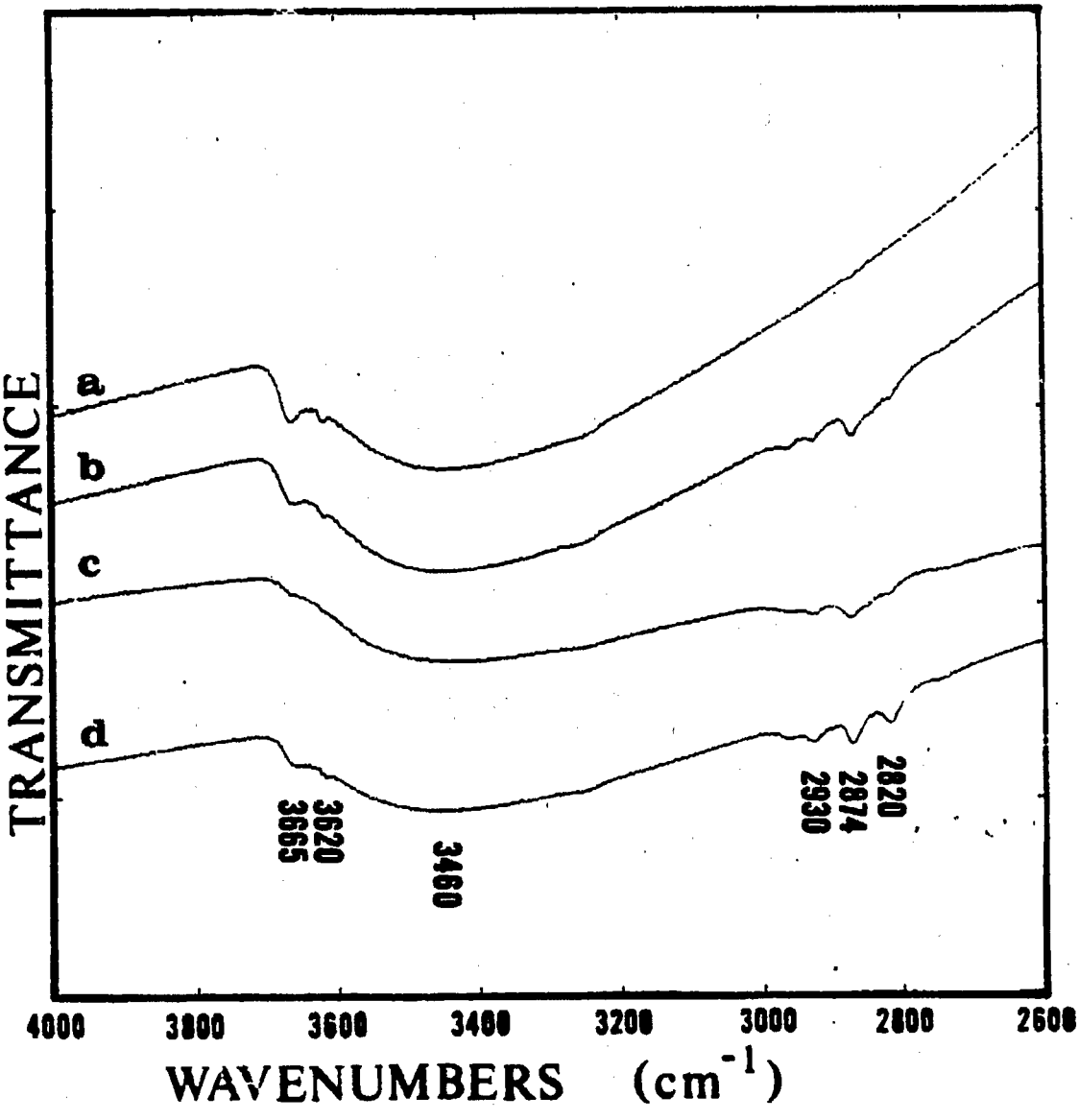
TRANSMITTANCE
a
b
c
d
3620
3695
3460
2820
2874
2930
4000
3800
3600
3400
3200
3000
2800
2600
WAVENUMBERS (cm-1)

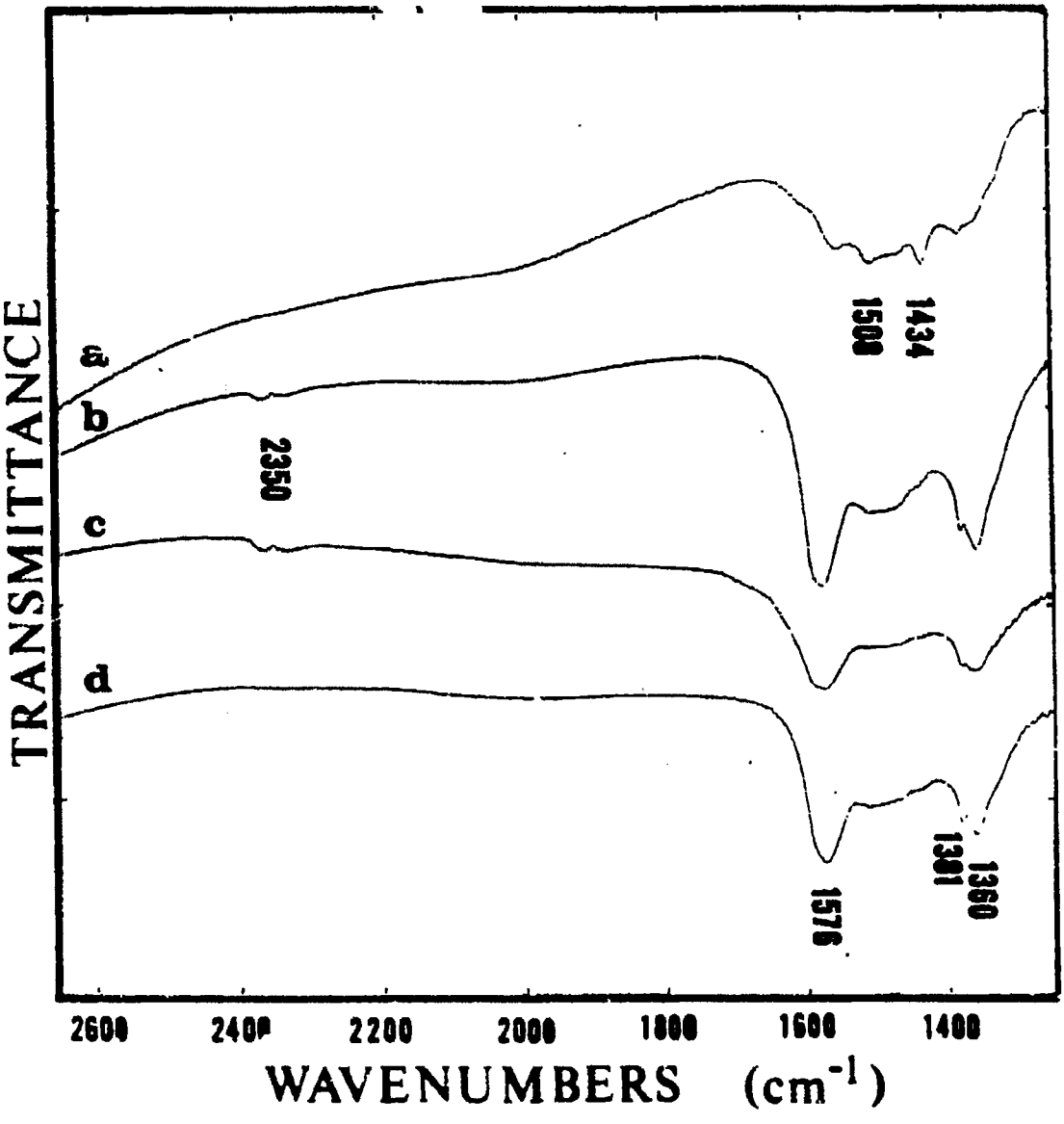

Figure 44. Continued

war assigned to an adsorbed formic acid molecule. There was negligible methoxy development until after the formic acid was flushed from the gas phase, possibly because the gas phase also contained some water (the formic acid solution has water) which inhibited methoxy formation.

A brief exposure (5 minutes) of formaldehyde to 90/5/5 and 80/10/10 Zn/Cu/Cr catalysts at 200°C and 1 atmosphere is shown in Figures 45 and 46, respectively. The formation of methoxy groups (bands at 2930 and 2822 cm^{-1}) and formate groups (bands at 2872, 1576, 1381, and 1360 cm^{-1}) occurred initially, followed by decomposition of the methoxy groups. Both catalysts had a weak band at 2087 cm^{-1} suggesting that carbon monoxide was a decomposition product during formaldehyde adsorption at 200°C. The rate of methoxy formation was more rapid on the 90/5/5 Zn/Cu/Cr catalyst than the 80/10/10 Zn/Cu/Cr catalyst. The weak band at 1670 cm^{-1} can be assigned to adsorbed water, probably another decomposition product during formaldehyde adsorption.

The adsorption of formaldehyde on 90/5/5 and 80/10/10 Zn/Cu/Cr catalysts at 100°C and 1 atmosphere is shown in Figures 47 and 48, respectively. Initially, the exposure to formaldehyde produced an adsorbed formaldehyde species (bands at 2935, 2850, and 2737 cm^{-1}), formate (bands at 2966, 2876, 1580, 1381, and 1365 cm^{-1}), and some methoxy groups (bands at 2932 and 2820 cm^{-1}). As the amount of adsorbed formaldehyde increased on the surface, the isolated hydroxyl groups (bands at 3666 and 3618 cm^{-1}) and the methoxy groups were displaced. The adsorbed formaldehyde gradually decomposed to formate species.

The adsorption and decomposition of methanol (CH_3OH) on 90/5/5 and

Figure 45. Adsorption of formaldehyde on 90/5/5 Zn/Cu/Cr oxide at 200°C

a) reduced surface

b) 10 minutes after exposure

c) 30 minutes after exposure

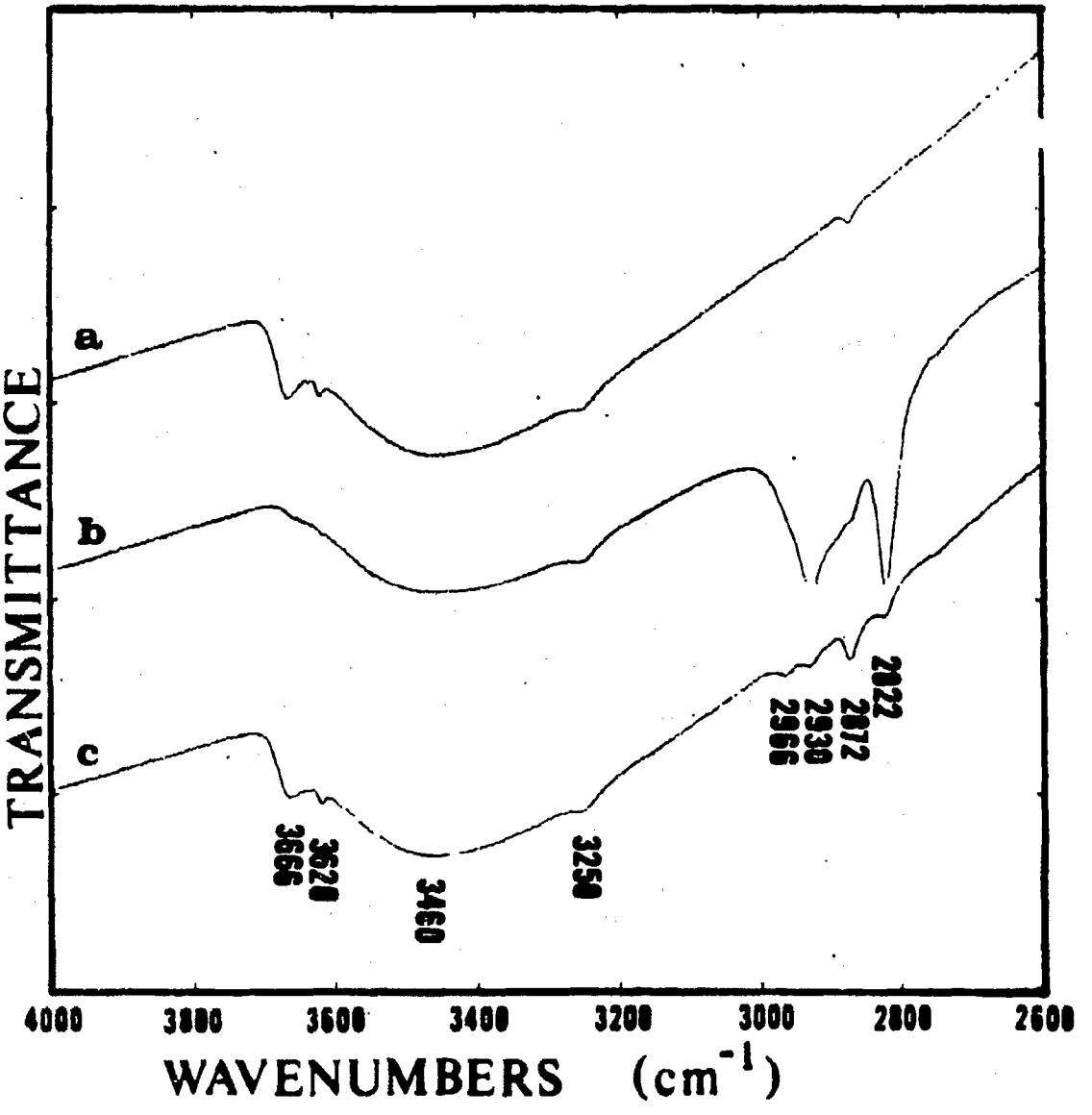
a
b
c
TRANSMITTANCE
3666
3620
3490
3250
2969
2930
2872
2822
4000
3800
3600
3400
3200
3000
2800
2600
WAVENUMBERS (cm-1)

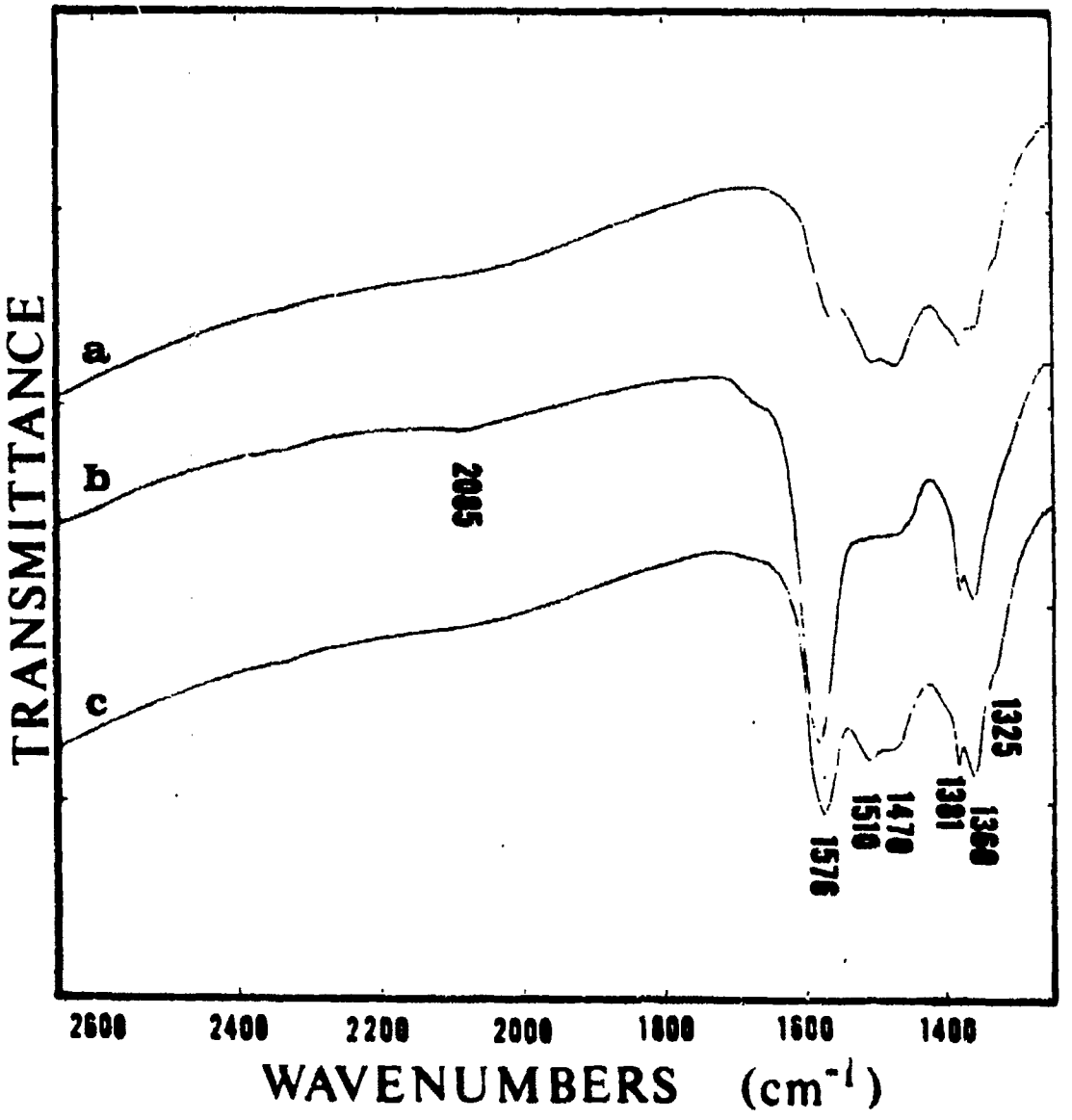

Figure 45. Continued

Figure 46. Adsorption of formaldehyde on 80/10/10 Zn/Cu/Cr oxide at 200°C

a) reduced surface

b) 10 minutes after exposure

c) 30 minutes after exposure

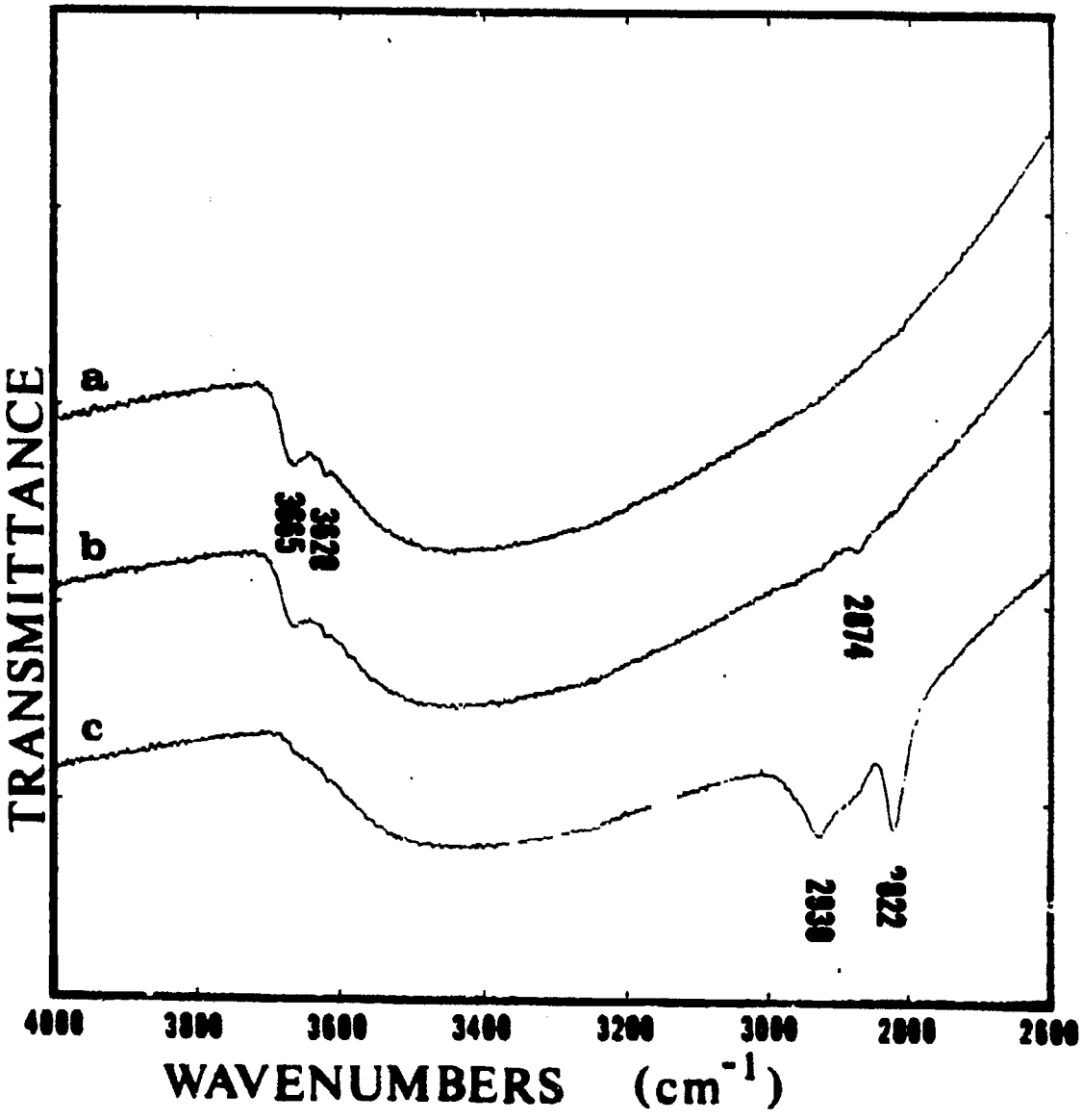
TRANSMITTANCE
a
b
c
3365
3520
2874
2930
2722
4000
3800
3600
3400
3200
3000
2800
2600
WAVENUMBERS (cm-1)

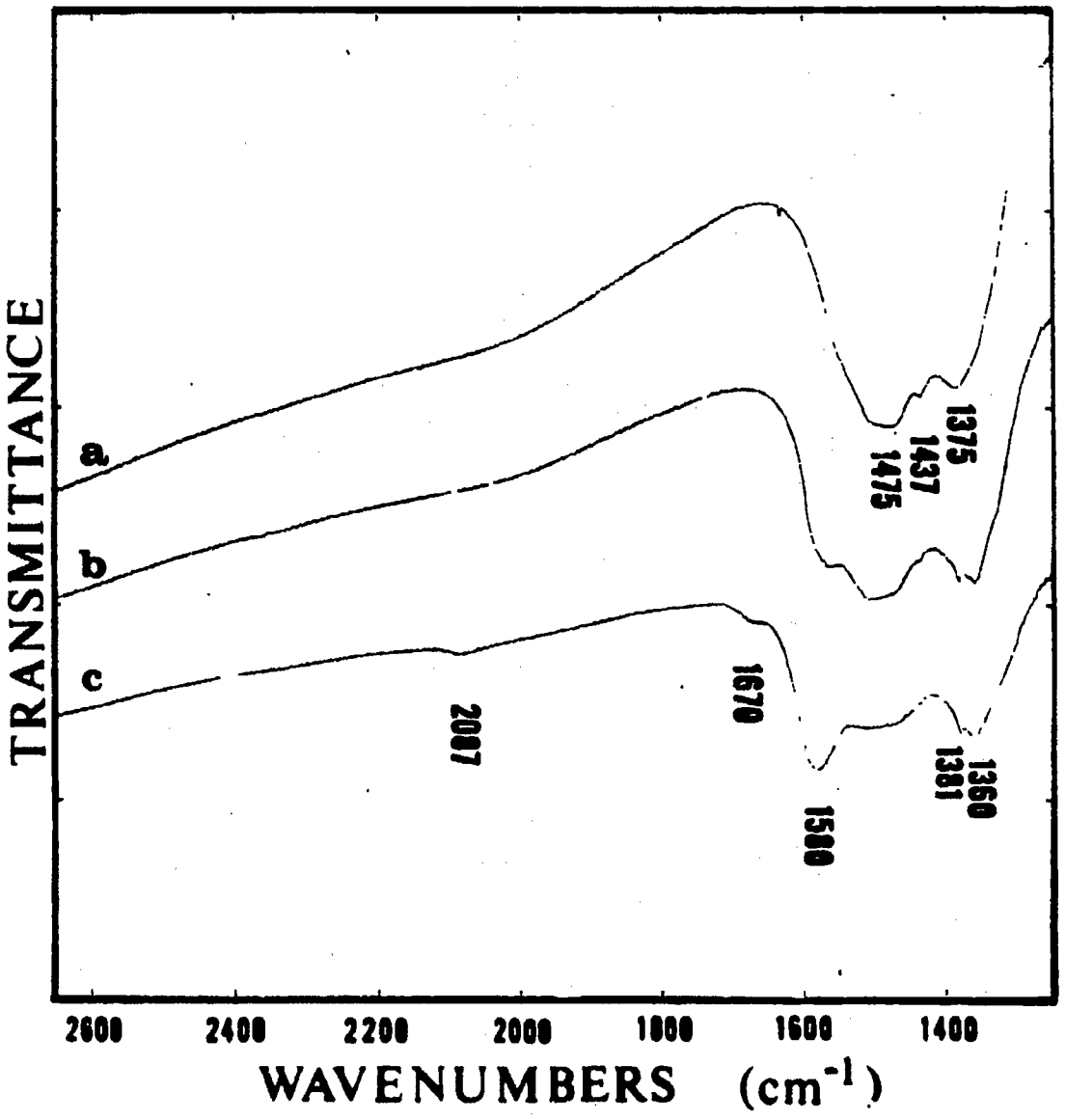

Figure 46. Continued

Figure 47. Adsorption of formaldehyde on 90/5/5 Zn/Cu/Cr oxide at 100°C

a) during exposure

b) 10 minutes after exposure

c) 30 minutes after exposure

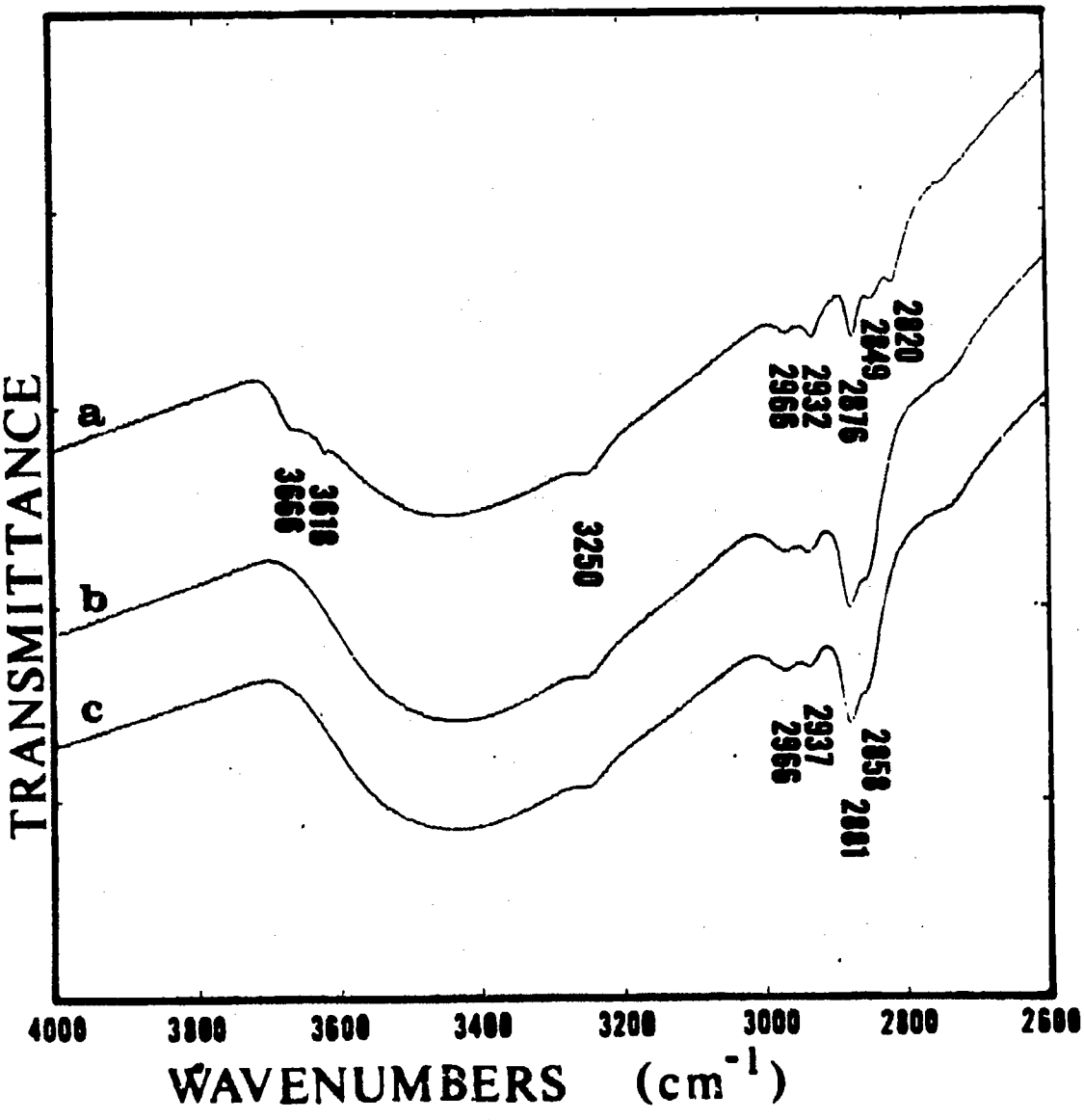
TRANSMITTANCE
a
b
c
3660
3610
3250
2966
2932
2876
2849
2820
2966
2937
2881
2858
4000
3800
3600
3400
3200
3000
2800
2600
WAVENUMBERS (cm-1)

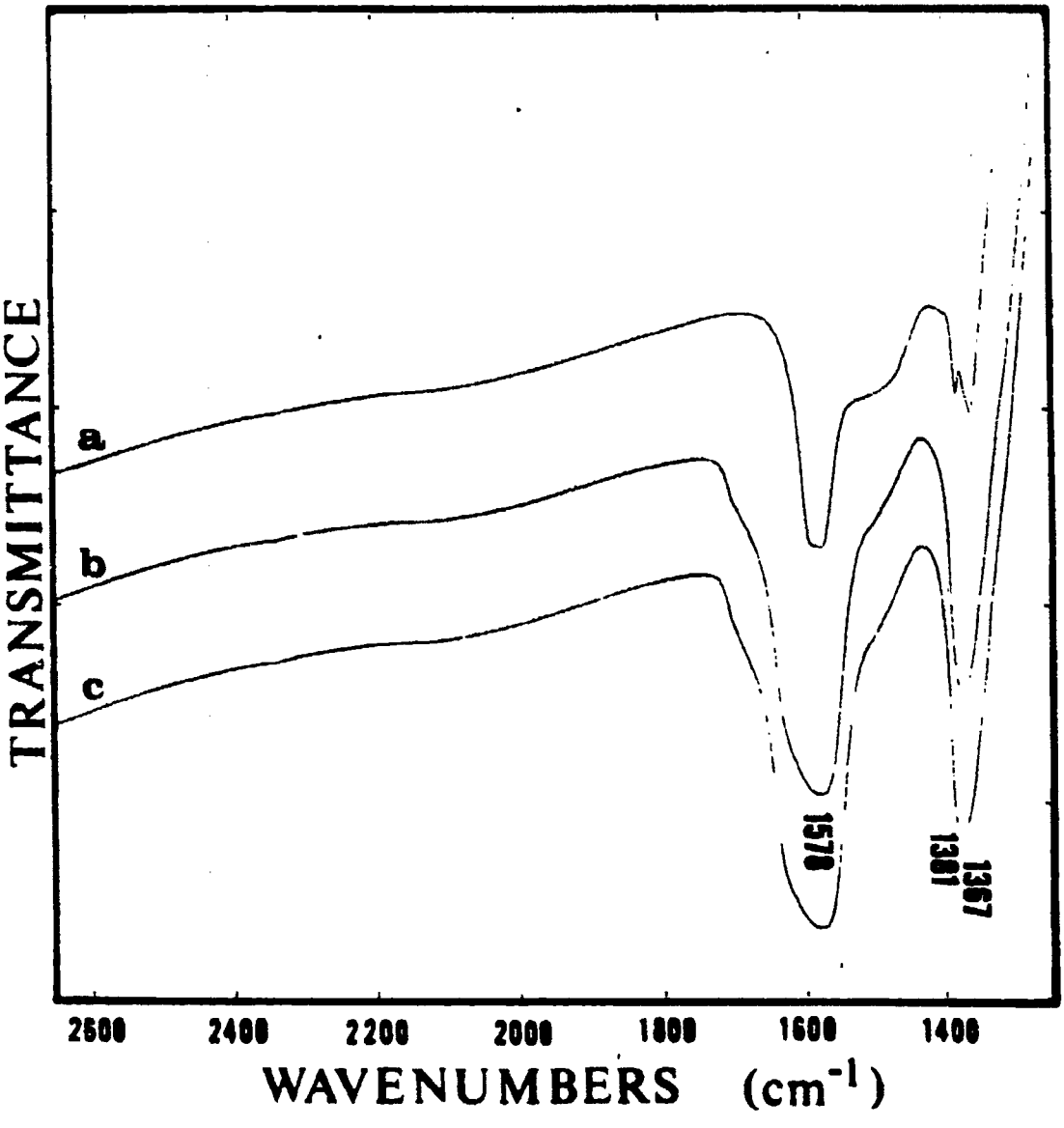

Figure 47. Continued

Figure 48. Adsorption of formaldehyde on 80/10/10 Zn/Cu/Cr oxide at 100°C

a) reduced surface

b) 10 minutes after exposure

c) 30 minutes after exposure

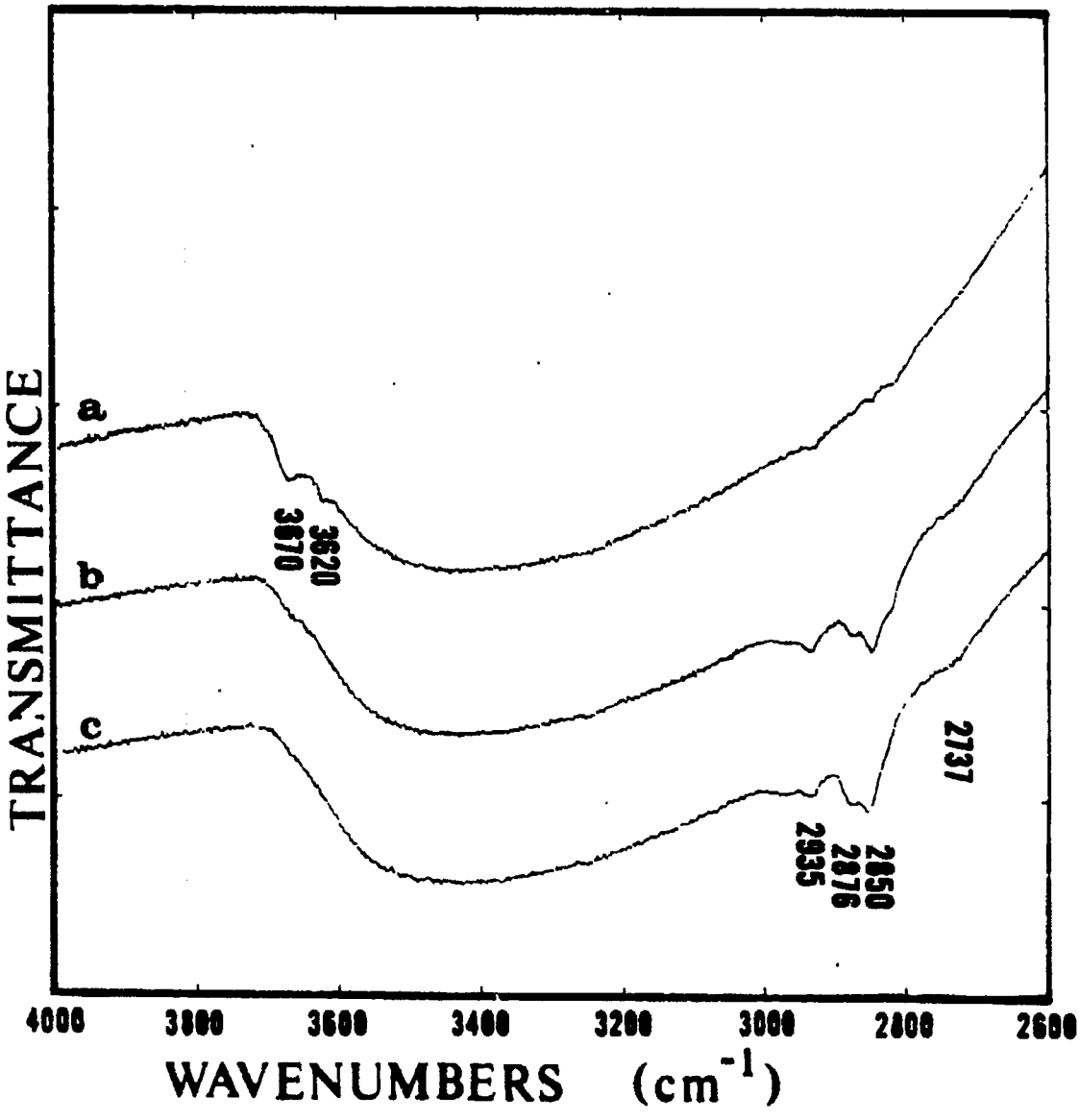
TRANSMITTANCE
a
b
c
3670
3620
2737
2935
2876
2850
4000
3800
3600
3400
3200
3000
2800
2600
WAVENUMBERS (cm-1)

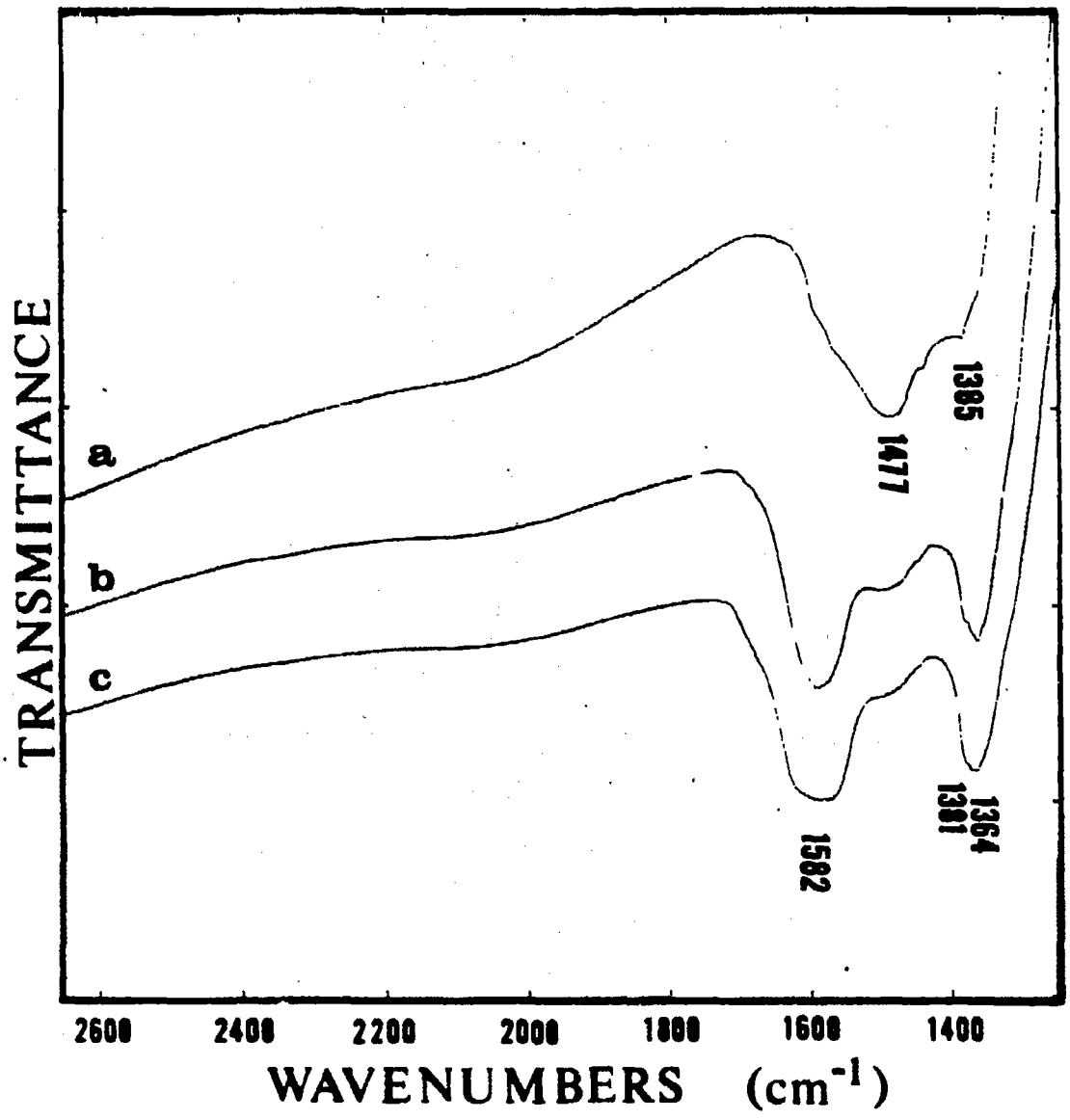

Figure 48. Continued

80/10/10 Zn/Cu/Cr catalysts were very similar at 200°C and 1 atmosphere (Figures 49 and 50). Exposure to methanol formed methoxy groups (bands at 2930 and 2820 cm^{-1}) and formate groups (bands at 2872, 1576, 1381, and 1360 cm^{-1}) with the concurrent disappearance of isolated hydroxyl groups (bands at 3666 and 3620 cm^{-1}). Some carbon dioxide was observed in the gas phase from methoxy decomposition. Removal of methanol from the gas phase caused rapid decomposition of the methoxy groups, leading to the development of formate and bidentate carbonate (bands at 1510 and 1327 cm^{-1}) groups. Methoxy groups did not decompose as readily after a second exposure to methanol.

Photoacoustic Spectra

Both oxidized and reduced methanol catalysts with Zn/Cu ratios below 85/15 were unsuitable for <u>in situ</u> infrared studies because they exhibited poor transmittance over the entire mid-infrared spectrum. Since the most active catalysts have Zn/Cu ratios near 67/33, it was desirable to compare spectra of catalysts with higher copper content to those catalysts employed in transmission infrared studies in order to determine if similar surface species exist on these various compositions. The technique of photoacoustic spectroscopy (PAS) was used to characterize several binary oxides subjected to different treatments. All spectra were taken at ambient conditions.

The spectra of several oxides that were not subjected to any pretreatment are shown in Figure 51. Each spectrum was taken with 256 scans at 8 cm^{-1} resolution. Surface carbonate bands can be seen in

Figure 49. Adsorption of methanol on 90/5/5 Zn/Cu/Cr oxide at 200°C

a) reduced surface

b) exposure for 1 hour

c) 1 hour after exposure

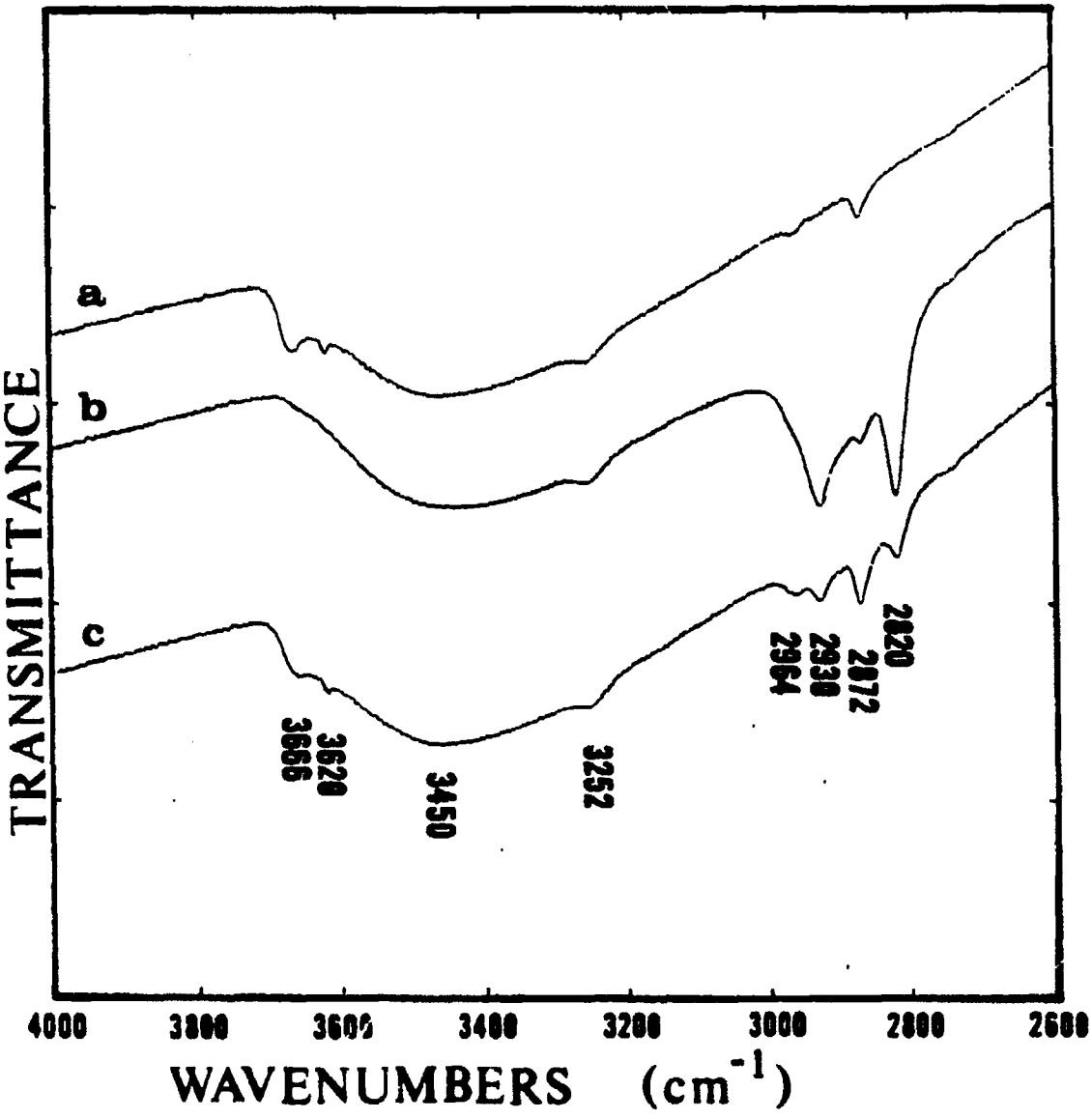
a
b
c
TRANSMITTANCE
3666
3620
3450
3252
2964
2930
2872
2820
4000
3800
3600
3400
3200
3000
2800
2600
WAVENUMBERS (cm-1)

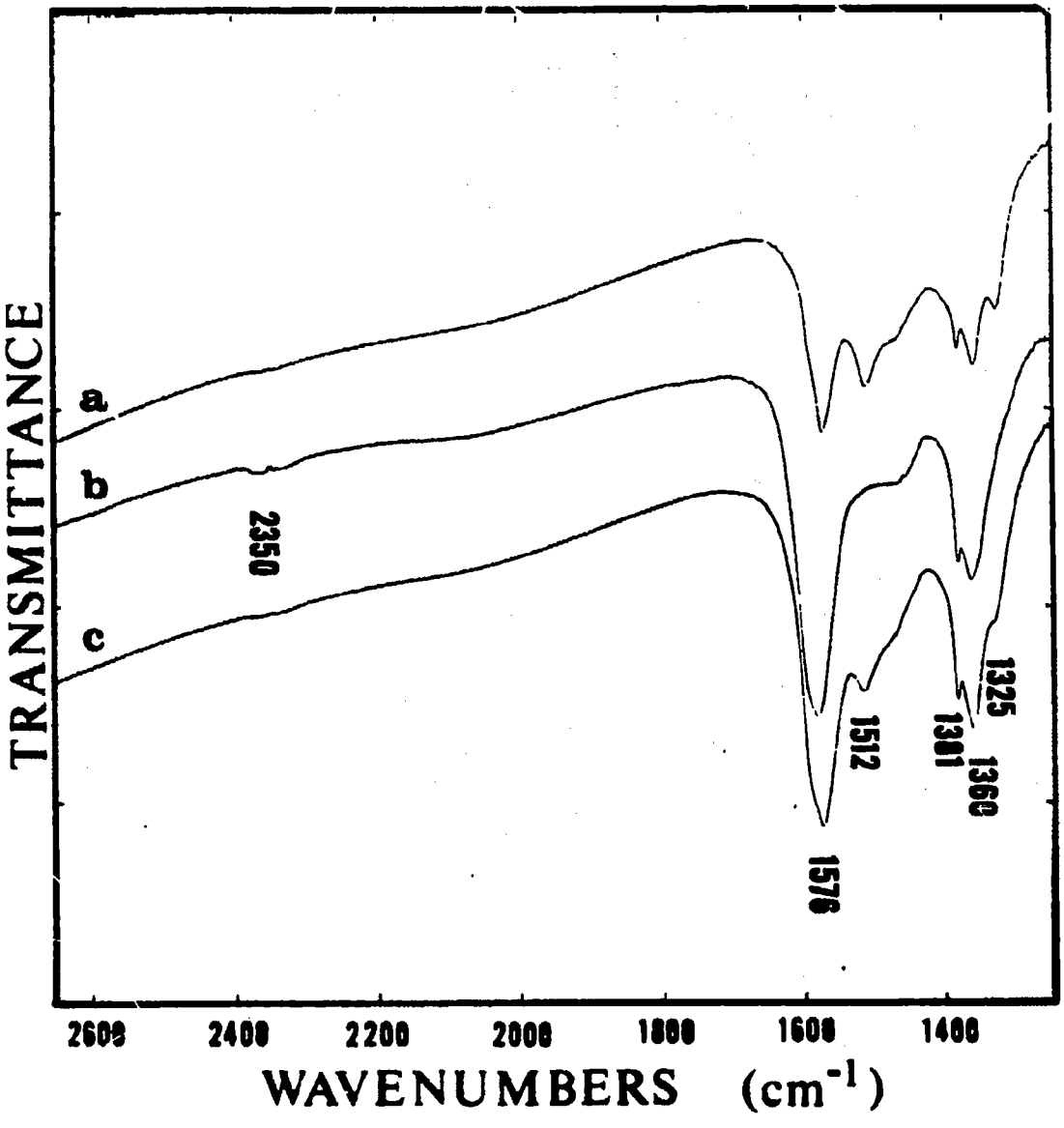

Figure 49. Continued

Figure 50. Adsorption of methanol on 80/10/10 Zn/Cu/Cr oxide at 200°C

a) reduced surface

b) exposure for 1 hour

c) 1 hour after exposure

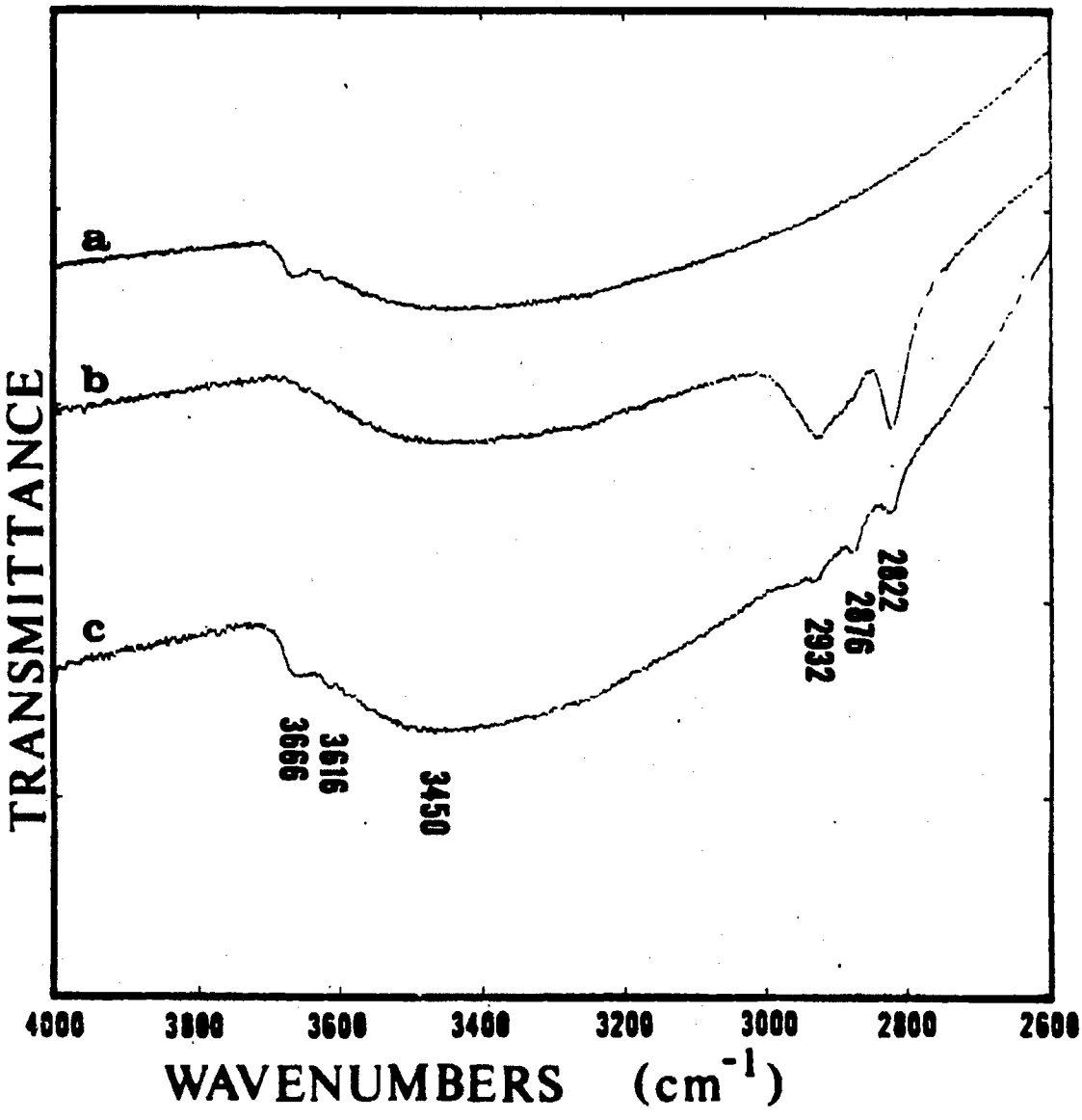
a
b
c
TRANSMITTANCE
3666
3616
3450
2932
2876
2822
4000
3800
3600
3400
3200
3000
2800
2600
WAVENUMBERS (cm-1)

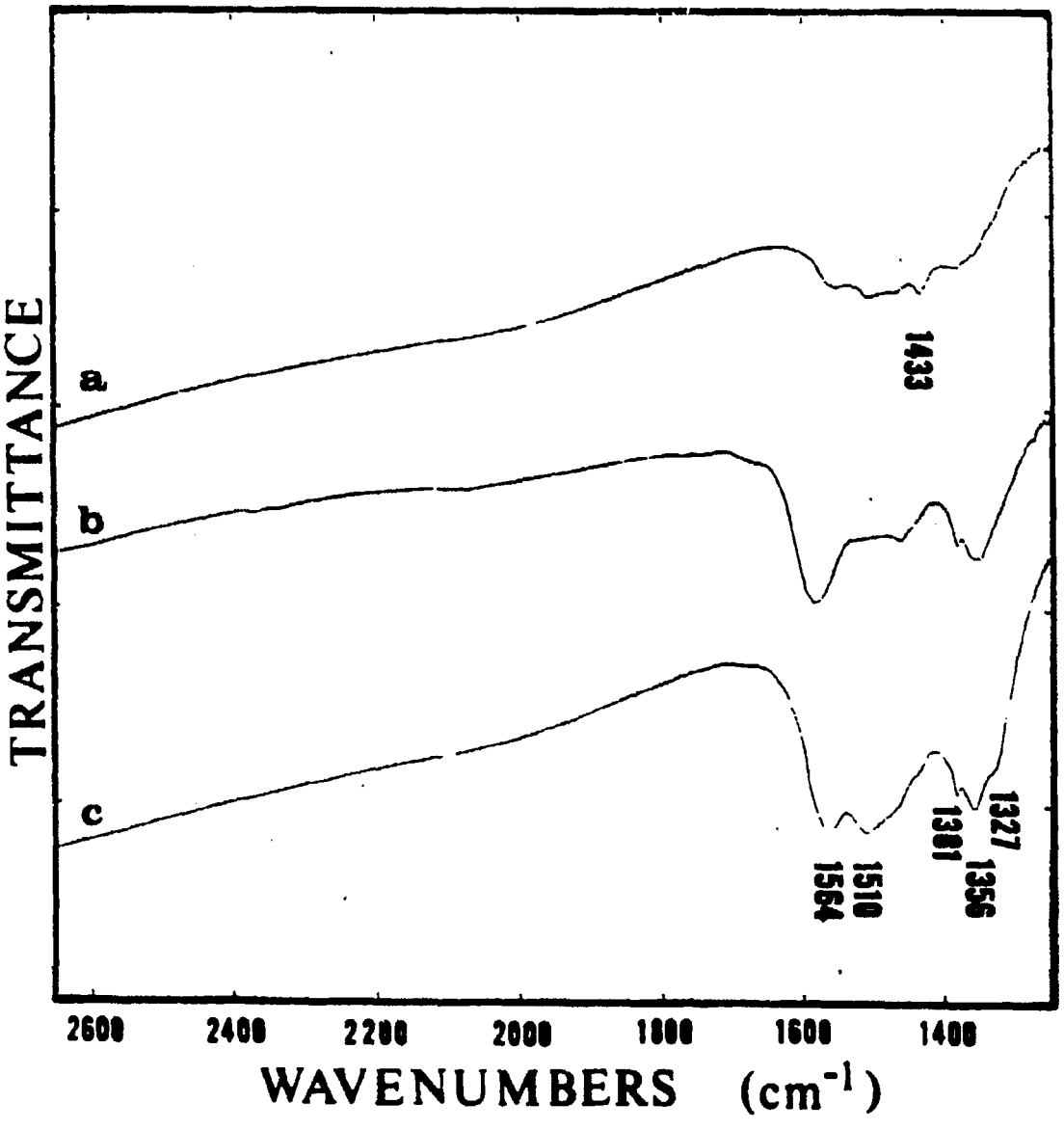

Figure 50. Continued

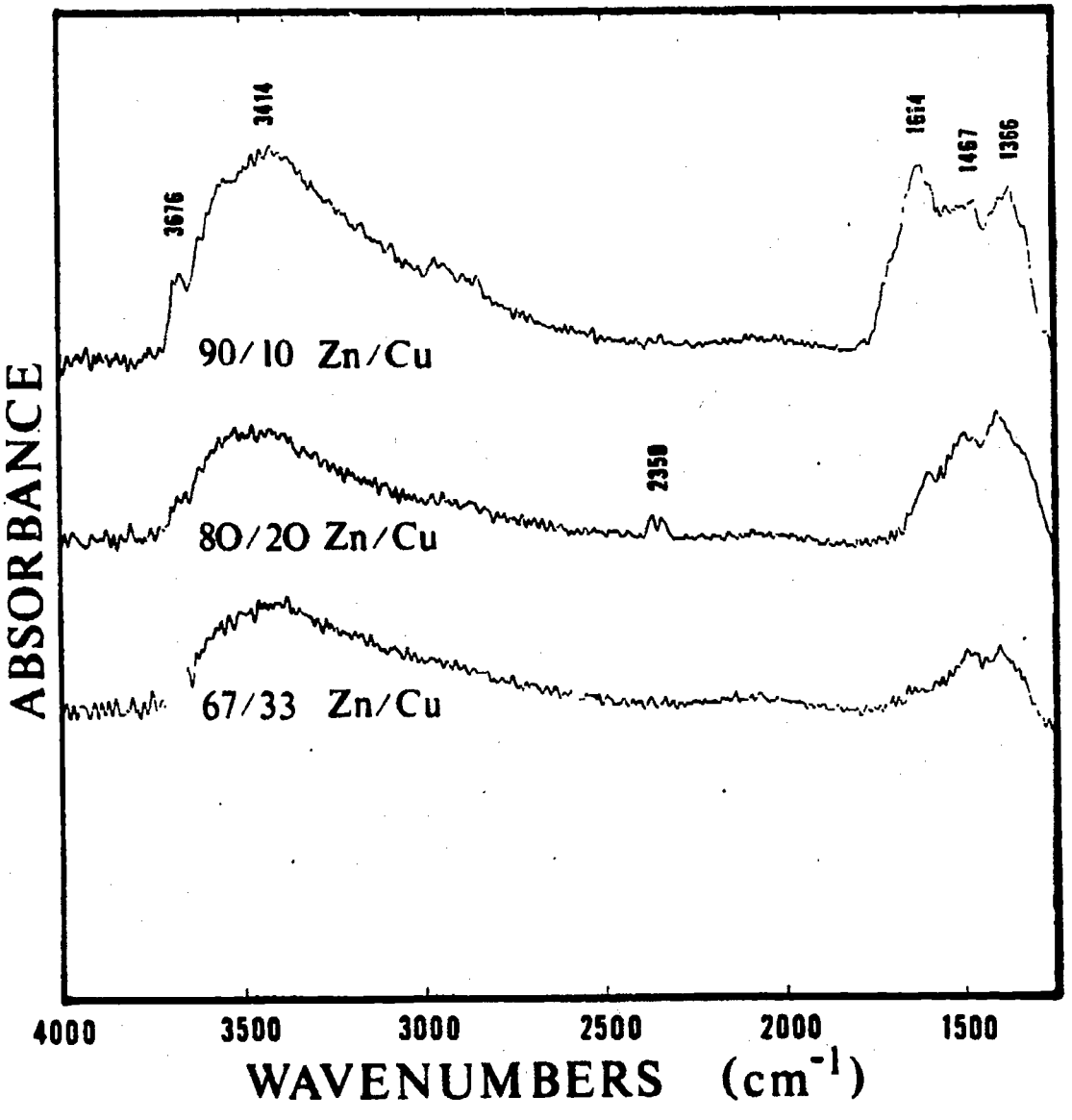

Figure 51. Binary oxides without any pretreatment

the 1700-1300 cm^{-1} region and adsorbed water near 3400 cm^{-1}. A gaseous impurity, carbon dioxide, was present in the spectrum of 80/20 Zn/Cu oxide. These oxides were pretreated at 350°C under vacuum for approximately 12 hours to remove some of the surface contaminants (adsorbed water and residual carbonates). Pretreated samples were transferred into the photoacoustic cell via a dry box to avoid contamination by atmospheric water vapor and carbon dioxide. The spectra of these oxides, shown in Figure 52, were taken with 128 scans at 8 cm^{-1} resolution. The reduction of adsorbed water revealed the isolated hydroxyl groups (bands at 3672 and 3622 cm^{-1}). The amount of residual carbonates (bands at 1535 and 1380 cm^{-1}) decreased as the zinc content of the binary oxide decreased.

The principal objective of this study was to determine if the adsorbed species formed on these binary oxides during exposure to a mixture of carbon monoxide and hydrogen (CO/H_2 = 1/2) were similar. Several binary oxides were heated at 350°C under vacuum for about 12 hours, cooled to 200°C, and exposed to the gas mixture for 4 hours. After cooling to room temperature, the samples were transferred via a dry box into the photoacoustic cell. These samples could not be subjected to a vacuum without decomposition of methoxy, formate, and carbonyl groups occurring. The spectra shown in Figure 53 were taken with 400 scans at 2 cm^{-1} resolution. The 95/5 Zn/Cu oxide had some adsorbed water (band at 3450 cm^{-1}), the hydroxyl band associated with reduced copper (band at 3230 cm^{-1}), methoxy groups (bands at 2935 and 2820 cm^{-1}), formate groups (bands at 2854, 1580, and 1370 cm^{-1}), and a carbonyl species (band at 2102 cm^{-1}). As the copper content of the

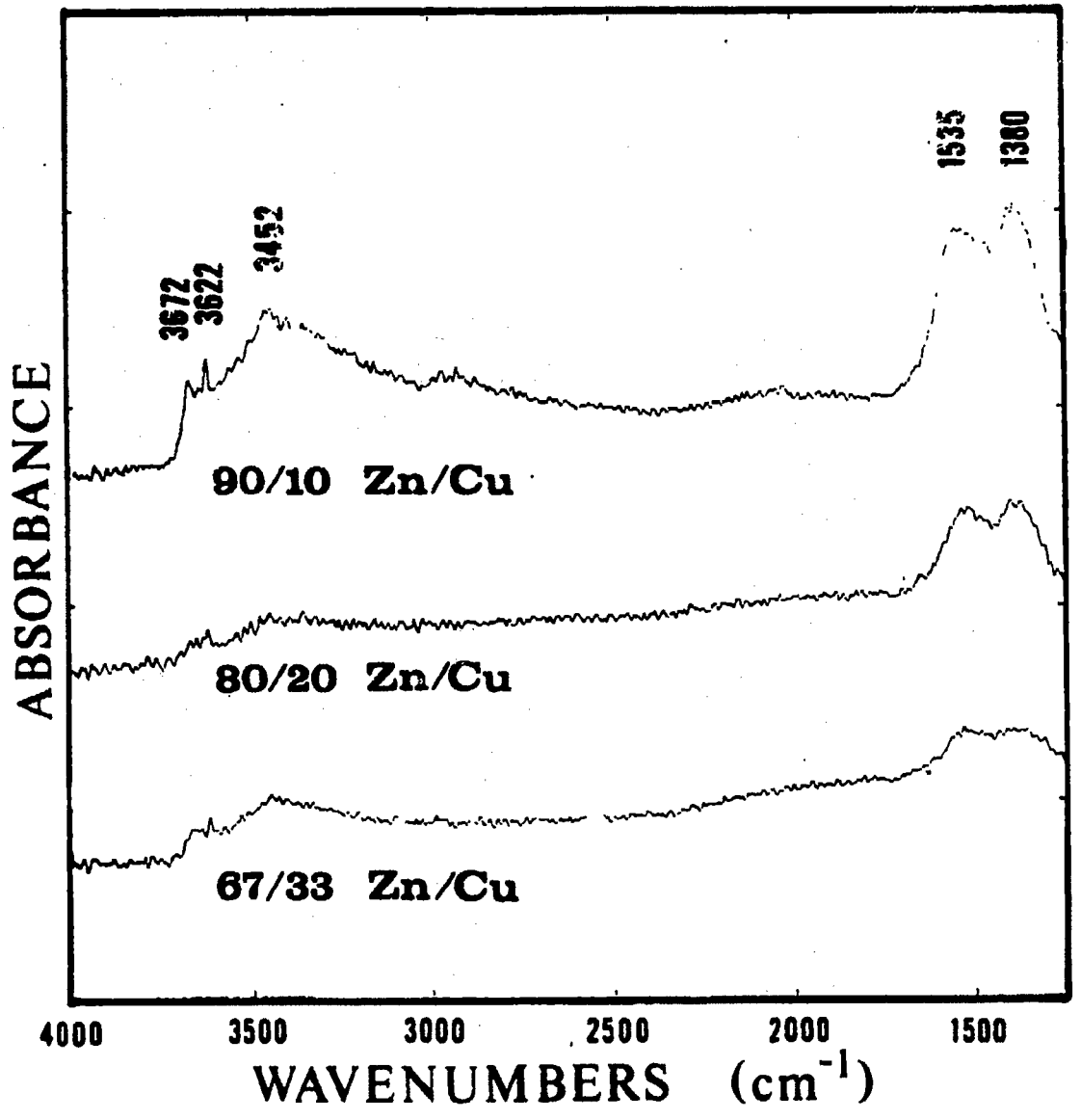

Figure 52. Binary oxides after thermal pretreatment

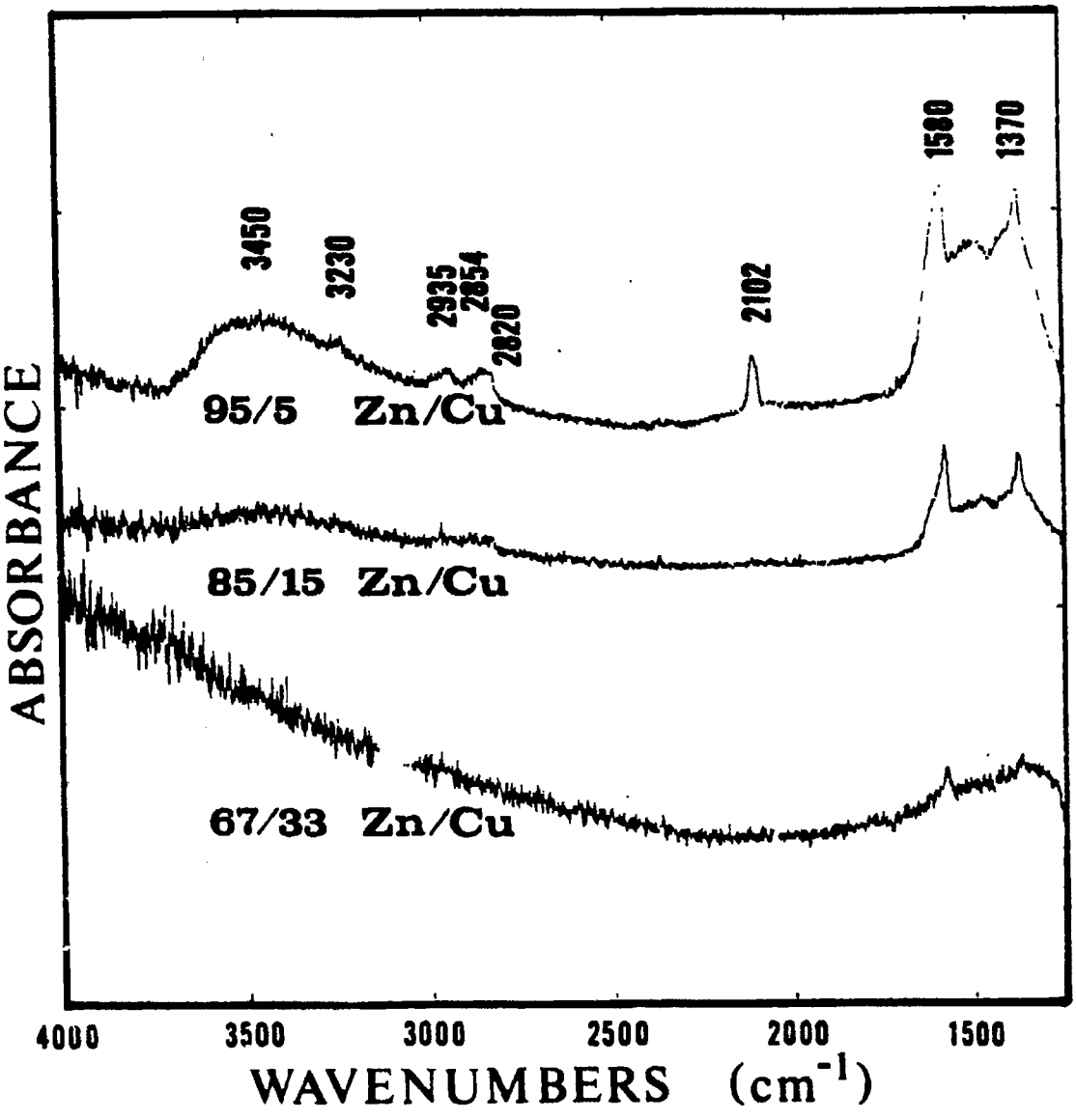

Figure 53. Adsorption of CO-H_2 mixture on binary oxides

oxide increased, the clarity of the photoacoustic spectra decreased to the extent that little information could be obtained from the spectrum of the 67/33 Zn/Cu oxide regarding surface species. The spectrum of the 85/15 Zn/Cu oxide showed a small amount of methoxy groups (bands at 2970 and 2825 cm^{-1}) and formate groups (bands at 1572 and 1370 cm^{-1}). The poor signal-to-noise ratio of these spectra and lack of detail at higher wavenumbers made the assignment of band locations quite difficult.

DISCUSSION OF RESULTS

The infrared spectra of adsorbed species on zinc oxide, binary Zn/Cu oxides, and ternary Zn/Cu/Cr oxides were sufficiently similar that infrared band assignments were applicable to all these oxides. Band positions assigned to various surface species in this discussion should be regarded as approximate because band positions can be affected by the extent of oxide reduction, temperature, surface concentration, and the presence of other species. Most results were obtained at 1 atmosphere and 200°C during flow conditions.

The infrared bands above 3000 cm^{-1} on all of these catalysts have been assigned to hydroxyl groups. Residual hydroxyl groups with bands at 3665, 3620, 3550, and 3450 cm^{-1} existed on both oxidized and reduced catalysts. A small band at 3640 cm^{-1} was also observed on some catalysts that had good transmittance. The sharp, narrow shape of the bands at 3665, 3640, and 3620 cm^{-1} were indicative of isolated hydroxyls, while the broad features of the bands at 3550 and 3450 cm^{-1} suggested that hydrogen bonding occurred among these hydroxyls. All the major hydroxyls readily exchanged with deuterium or deuterium oxide to produce OD bands at 2706, 2667, 2630, and 2560 cm^{-1}, establishing that these hydroxyls were surface species. The differences in the band positions of these hydroxyls have been attributed to the different crystal planes of zinc oxide on which these hydroxyls are located (Atherton et al., 1971).

A hydroxyl species indicated by a band at 3525 cm^{-1} developed when methanol or formic acid was adsorbed on the catalyst surface. An

exchange with deuterated compounds was not possible because this hydroxyl species was unstable at 200°C, but adsorption of deuterated methanol produced an analogous OD band at 2608 cm^{-1}. The dissociation of the hydroxyl hydrogen from the organic molecule during adsorption provided a large amount of atomic hydrogen (possibly as protons) on the surface which temporarily produced this hydroxyl species. At room temperature, this hydroxyl has been observed as a stable species on zinc oxide during hydrogen adsorption and labeled a Type I hydroxyl species (Dent and Kokes, 1969a). This hydroxyl was not formed by hydrogen adsorption at 200°C.

Binary and ternary oxides formed a hydroxyl band at 3250 cm^{-1} during reduction with hydrogen and a band at 2421 cm^{-1} during reduction with deuterium. Isotopic exchange of a hydrogen-reduced surface with deuterium shifted this hydroxyl species extremely slowly, indicating that this hydroxyl was not a surface species. During adsorption experiments, the intensity of this hydroxyl band was totally unaffected by adsorbed species as long as the catalyst remained in a reduced state. Catalyst oxidation with carbon dioxide or water caused this hydroxyl to disappear. These observations suggest that the hydroxyl at 3250 cm^{-1} is a bulk species associated with a reduced form of copper (oxidation state +1 or 0).

Fully oxidized catalysts had some residual carbonate groups on the surface which appeared as infrared bands at 1512, 1470, 1435, 1380, and 1325 cm^{-1}. The changes in band intensities during various surface conditions have indicated that the bands at 1512 and 1325 cm^{-1} belong to the same species, the bands at 1470 and 1380 cm^{-1} belong to another

species, and the band at 1435 cm^{-1} could be assigned to a third carbonate species. Infrared band assignments to specific carbonate and carboxylate complexes on surfaces reported in the literature have been dubious and sometimes contradictory because of the difficulties in making assignments based on comparisons with pure inorganic carbonates. Band frequencies can be affected by surface pretreatments and the temperature of adsorption. A choice must then be made among many different types of complexes that could be formed, e.g., bicarbonate, uncoordinated carbonate ion, unidentate carbonate, bidentate carbonate, and bridging carbonate species. The same carbonate species on zinc oxide with bands at 1530 and 1325 cm^{-1} has been assigned to a unidentate carbonate (Herd et al., 1974), bands at 1540 and 1330 cm^{-1} assigned to a carboxylate species (Bozon-Verduraz, 1970), and bands at 1560-1530 and 1342-1330 cm^{-1} assigned to a bidentate species (Hair, 1967). The single band at 1435 cm^{-1}, which was observed on ternary catalysts, was assigned to an uncoordinated carbonate ion. A carbonate ion on zinc oxide has been previously reported at 1430 cm^{-1} (Matsushita and Nakata, 1962). Based on the general assignments for unidentate and bidentate carbonate complexes given by Nakamoto (1978), the bands at 1470 and 1380 cm^{-1} were assigned to the asymmetric and symmetric O-C-O stretching frequencies of a unidentate carbonate species, while the bands at 1512 and 1325 cm^{-1} were assigned to the asymmetric and symmetric O-C-O stretching frequencies of a bidentate carbonate species, respectively.

The adsorption of carbon monoxide on zinc oxide was the same as previously reported by Taylor and Amberg (1961). A very weak band was observed at 2200 cm^{-1} after a brief flush with N_2 to remove the masking

by gaseous carbon monoxide. This band was assigned to a σ-bonded carbonyl species. A more intense band was observed near 2090 cm^{-1} on the binary and ternary oxides. This stretching frequency was in the 2080-2110 cm^{-1} region for π-bonded carbonyls on metallic copper (Pritchard and Sims, 1970; Pritchard et al., 1975; Horn and Pritchard, 1976). Although no infrared studies have been reported for carbon monoxide adsorption on cuprous oxide, carbonyl frequencies on copper(I) organometallic complexes have been characterized recently. The carbonyl frequencies, given in Table 13, fall into the 2050-2117 cm^{-1} region. Thus, the band near 2090 cm^{-1} on binary and ternary oxides was assigned to the stretching frequency of a carbonyl species adsorbed on a reduced copper site. The oxidation state of the reduced site could be either Cu(I) or copper metal.

Formate groups were formed by the hydrogenation of carbon monoxide and dioxide, the adsorption of formic acid, and the decomposition of methanol. Infrared bands at 2875, 1380, 1575, and 1365 cm^{-1} were assigned to the fundamental C-H stretching, C-H bending, asymmetric O-C-O stretching, and symmetric O-C-O stretching frequencies, respectively. Two additional bands at 2966 and 2740 cm^{-1} were assigned to combinations of fundamental frequencies; the former band was a combination of the C-H bending and asymmetric O-C-O stretching frequencies, while the latter band was a combination of the C-H bending and symmetric O-C-O stretching frequencies. These combined frequencies have been observed in the infrared spectra of inorganic formates. The infrared bands of some inorganic formates are given in Table 14. Infrared bands of a deuterated formate at 2166, 1575, and 1335 cm^{-1} were assigned to the

Table 13. Organometallic copper(I) complexes

Copper(I) complex	ν_{CO}, cm^{-1}	Reference
$[HB(C_3N_2H_3)_3]Cu(CO)$	2083	Churchill et al., 1975
$Cu(LBF_2)(CO)$	2068	Gagné et al., 1977
$[Cu(en)CO](BPh_4)$	2117	Pasquali et al., 1978
$[Cu(dien)CO](BPh_4)$	2080	Pasquali et al., 1978
$[Cu_2(tmen)_2(CO)_2Cl](BPh_4)$	2065	Pasquali et al., 1979
$[Cu_2(hm)_3(CO)_2](BPh_4)_2$	2055, 2066	Pasquali et al., 1980b
$[Cu(hm)CO](BPh_4)$	2091	Pasquali et al., 1980b
$[Cu(en)_2CO]I$	2060	Pasquali et al., 1980a
$[Cu_2(en)_3(CO)_2]I_2$	2062	Pasquali et al., 1980a
$[Cu_2(en)_3(CO)_2](BPh_4)_2$	2078	Pasquali et al., 1980a
CuCO(O-t-Bu)	2063	Geerts et al., 1983
$Cu(acac)(CO)_2$	2100	Chow and Buono-Core, 1983
$[Cu(q)CO]_4$	2050	Pasquali et al., 1983

fundamental C-D stretching, asymmetric O-C-O stretching, and symmetric O-C-O stretching frequencies, respectively.

Methoxy groups were also formed by the hydrogenation of carbon monoxide, the adsorption of formic acid, and the adsorption of methanol. Infrared bands at 2935 and 2820 cm^{-1} were assigned to the fundamental asymmetric and symmetric CH_3 stretching frequencies, respectively. Deuterated methoxy groups had infrared bands at 2220 and 2056 cm^{-1} which were assigned to asymmetric and symmetric CD_3 stretching frequencies, respectively. Infrared frequencies of methoxy groups were

Table 14. Infrared band assignments for inorganic formates

Fundamental frequencies, cm^{-1}	$NaHCO_2$ [a]	$NaHCO_2$ [b]	$NaHCO_2$ [c]	$NaHCO_2$ [d]	$Ca(HCO_2)_2$ [c]	$NaDCO_2$ [c]
$\nu_1(A_1)$ C-H stretching	2870	2841	2828	2828	2868	2130
$\nu_2(A_1)$ symmetric C-O stretching	1377	1366	1355	1364	1359	1327
$\nu_3(A_1)$ symmetric C-O bending	784	772	769	773	778	762
$\nu_4(B_1)$ asymmetric C-O stretching	1620	1567	1590	1600	1618	1580
$\nu_5(B_1)$ in-plane C-H bending	1365	1377	1385	1364	1386	1010
$\nu_6(B_2)$ out-of-plane C-H bending	1070	1073	1062	1070	1072	912
Binary frequencies, cm^{-1}						
ν_2 and ν_5	2750	2720	2715	2716	2694	–
ν_4 and ν_5	2990	2953	2950	2952	2942	–

[a] Newman, 1952.

[b] Ito and Bernstein, 1956.

[c] Harvey et al., 1963.

[d] Hammaker and Walters, 1964.

very similar to the infrared frequencies of liquid methanol. Liquid CH_3OH has asymmetric and symmetric CH_3 stretching frequencies at 2934 and 2822 cm^{-1}, respectively; liquid CD_3OD has asymmetric and symmetric CD_3 stretching frequencies at 2225 and 2082 cm^{-1}, respectively (Pinchas and Laulicht, 1971).

Infrared bands were formed at 2935, 2850, 2740, and 1600 cm^{-1} during the hydrogenation of carbon dioxide and the adsorption of formaldehyde. The assignment of these bands to a weakly adsorbed formaldehyde species was made since the CH_2 scissoring overtone, the out-of-phase CH_2 stretching, the in-phase CH_2 stretching, and the C=O stretching frequencies of gaseous formaldehyde occur at 2973, 2874, 2780, and 1745 cm^{-1}, respectively (Pinchas and Laulicht, 1971). The large shift in the C=O stretching frequency indicated that the formaldehyde species was adsorbed on the surface through the oxygen end of the molecule. The adsorption of a formaldehyde molecule on hematite (α-Fe_2O_3) produced infrared bands at 2920, 2870, 2770, and 1620 cm^{-1} (Busca and Lorenzelli, 1980). The possibility that this surface species might be a formyl group seems less likely. Infrared bands at 2770 and 2661 cm^{-1}, formed during CO hydrogenation on zinc were assigned to a formyl species (Saussey et al., 1982). The C-H and C=O stretching frequencies for various organometallic complexes containing a formyl ligand, reported in Table 15, have C-H stretching frequencies lower than those observed in this study.

Formate groups were formed during carbon monoxide adsorption on zinc oxide, binary oxides, and ternary oxides, demonstrating that surface hydrogen mobility at 200°C was increased by oxide reduction since

Table 15. Organometallic formyl complexes

Metallo-formyl complex	ν_{CO}, cm^{-1}	ν_{CH}, cm^{-1}	Reference
$(CO)_4Fe(CHO)^-N(PPh_3)_2^+$	1607	2690 2540	Collman and Winter, 1973
$Os(CHO)H(CO)_2(PPh_3)_2$	1601	2760 2680 2540	Brown et al., 1979
$[IrH(CHO)(P(CH_3)_3)_4]PF_6$	1600	2622	Thorn, 1980
RhOEP(CHO)	1700	–	Wayland and Woods, 1981
$[Ru(CHO)CO(Ph_2PCH_2PPh_2)]_2$	1600	2585	Smith and Cole-Hamilton, 1982
$[Ru(CHO)CO(Ph_2PCH_2)_2]_2$	1596	2550	Smith and Cole-Hamilton, 1982

no hydrogen was available from the gas phase. Formate formation was enhanced by the presence of gaseous hydrogen, presumably by increasing the amount of adsorbed hydrogen although no new hydroxyl or hydride species were observed. Carbon monoxide hydrogenation developed methoxy groups on binary and ternary oxides but not on zinc oxide at 200°C. Carbon dioxide hydrogenation on binary oxides at 200°C formed formate and some adsorbed formaldehyde groups but few methoxy groups, even when the gas phase was completely replaced with hydrogen. These results showed that the adsorbed carbonyl species on a reduced copper site was necessary for the formation of a methoxy group from a formate group at 200°C. Carbon monoxide hydrogenation at 100°C easily developed the copper carbonyl species but hydrogenation to formate species was very slow and no methoxy groups were formed. Thus, at 200°C, the primary function of copper in methanol synthesis catalysts was to activate carbon monoxide by forming an adsorbed carbonyl species. This carbonyl species enhanced the hydrogenation of formate groups to methoxy groups.

Formate acid decomposition on zinc oxide simply formed formate groups that decomposed to CO_2 (any H_2 formed could not be observed). Formic acid decomposition on binary and ternary oxides produced formate, methoxy, and a new hydroxyl species. Since there was no carbonyl species on these reduced surfaces, the hydrogenation of formate to methoxy groups arose from the unstable hydrogen added to the surface by the dissociative adsorption of formic acid (Type I hydrogen). At 200°C, the zinc hydride species was too unstable to be observed in the infrared spectra. The amount of gaseous hydrogen present during formic acid decomposition had no effect on the rate of methoxy formation, indicating

that an Eley-Rideal mechanism for formate hydrogenation to methoxy species was unlikely.

Methanol adsorption occurred by dissociative chemisorption to produce a methoxy and hydroxyl species and by the reaction of methanol with a surface hydroxyl to produce a methoxy species and water. The disappearance of isolated hydroxyl groups (bands at 3665 and 3620 cm^{-1}) during methanol adsorption was evidence of the reaction of methanol with surface hydroxyls. The development of the hydroxyl species at 3525 cm^{-1} (Type I hydrogen) was evidence of the dissociative chemisorption. The adsorption of isotopic methanol clearly showed that the hydrogen in the new hydroxyl species came from the hydroxyl hydrogen in the methanol molecule. Methoxy groups decomposed to formate groups, accompanied by the gradual appearance of the isolated hydroxyls.

Formaldehyde adsorption at 100°C produced an adsorbed formaldehyde species that caused the disappearance of isolated hydroxyl groups. Decomposition of adsorbed formaldehyde produced formate groups. Formaldehyde adsorption at 200°C formed methoxy and formate species. At this higher temperature, adsorbed formaldehyde was not stable under reducing conditions but the hydrogen from the decomposition of formaldehyde was readily utilized to form methoxy groups. No hydroxyl band was observed at 3525 cm^{-1}, indicating that formaldehyde adsorption was not dissociative and that hydrogenation of this unstable formaldehyde species was more favorable than the formation of a Type I hydroxyl group during decomposition.

A few concluding remarks have been addressed to the nature of surface sites for adsorbed species. The only species believed to be

adsorbed on copper sites was the carbonyl near 2090 cm^{-1}. All other species were adsorbed on zinc oxide. Isolated hydroxyl groups have been associated with polar ZnO surfaces and hydrogen-bonded hydroxyl groups associated with nonpolar ZnO surfaces using geometric arguments (Atherton et al., 1971). The band intensities of the bidentate carbonate species varied inversely with those of the formate species, suggesting that the same surface site was involved. Carbonate formation on zinc oxide has been found to occur on dehydroxylated sites (Morimoto and Morishige, 1975); these dehydroxylated sites have been associated with the sites of hydrogen-bonded hydroxyls (Atherton et al., 1971). The formation of carbonate and formate groups did not affect the isolated hydroxyls, but the formation of adsorbed formaldehyde and methoxy groups caused these isolated hydroxyls to disappear. Thus, it appears that adsorbed formaldehyde, methoxy, and isolated hydroxyls are all adsorbed on the same sites, which are zinc atoms on the polar ZnO surfaces. Formaldehyde was produced during the decomposition of methanol on a polar ZnO surface but not on any other type of surface (Cheng and Kung, 1982). The remaining species, the Type I hydroxyl at 3525 cm^{-1}, apparently adsorbs on an energetic surface or defect site. Because both formic acid and methanol adsorption produced this hydroxyl species, it will be proposed that stepped surfaces between polar and nonpolar planes are the sites for this hydroxyl group.

PART III.

IN SITU CHARACTERIZATION OF METHANOL SYNTHESIS CATALYSTS

LITERATURE REVIEW

Thermodynamics

Carbon monoxide and hydrogen can react to form a great variety of products. Some of the possible reactions are:

$$CO + H_2 = HCHO \quad (1)$$

$$CO + 2H_2 = CH_3OH \quad (2)$$

$$CO + 3H_2 + CH_4 + H_2O \quad (3)$$

$$2CO + 2H_2 = CH_4 + CO_2 \quad (4)$$

$$2CO = CO_2 + C \quad (5)$$

$$2CO + 4H_2 = (CH_3)_2O + H_2O \quad (6)$$

$$nCO + 2nH_2 = C_nH_{2n} + nH_2O \quad (7)$$

$$nCO + (2n+1)H_2 = C_nH_{(2n+2)} + nH_2O \quad (8)$$

$$nCO + 2nH_2 = C_nH_{(2n+1)}OH + (n-1)H_2O \quad (9)$$

$$(n+1)CO + 2nH_2 = C_nH_{(2n+1)}COOH + (n-1)H_2O \quad (10)$$

An important reaction involving products from previous reactions is:

$$CO_2 + 3H_2 = CH_3OH + H_2O \quad (11)$$

Because the desired product is methanol, the reaction conditions should be chosen to favor reaction 2 while minimizing the others. Free energies of reaction for several of these reactions are given in Table 16; over the range of practical temperatures, the formation of methanol from carbon monoxide and hydrogen is least favorable. Methanol synthesis can be enhanced by using high pressures since the molar reduction for reaction 2 is greater than the others with the exceptions of dimethyl

Table 16. Free energy of reaction[a]

T, °K	ΔG° (kcal/mol)				
	300°	400°	500°	600°	700°
Reaction (2)	- 6.3	- 0.8	5.0	10.8	16.7
Reaction (3)	-33.9	-28.6	-23.0	-17.3	-11.4
Reaction (4)	-40.7	-34.4	-27.9	-21.2	-14.5
Reaction (5)	-28.6	-24.3	-20.0	-15.7	-11.4
Reaction (7)	-27.2	-19.3	-11.1	- 2.7	5.9
Reaction (8)	-51.3	-40.5	-29.2	-17.6	- 5.9

[a]Natta, 1955.

ether (reaction 6) and ethanol (n = 2 in reaction 9) formation. A catalyst is required to selectively form methanol.

The methanol content at equilibrium is determined from the equilibrium constant:

$$K = f_{CH_3OH}/(f_{CO})(f_{H_2})^2 \tag{12}$$

Using the subscripts CH_3OH = 1, CO = 2, and H_2 = 3, then

$$K = p_1\gamma_1/(p_2\gamma_2)(p_3\gamma_3)^2 \tag{13}$$

$$= K_y K_\gamma \tag{14}$$

where K_y is the equilibrium constant at low pressures and K_γ is the fugacity coefficient ratio. Numerical equations for K have been developed by Cherednichenko (Strelzoff, 1970):

$$\log K = 3971T^{-1} - 7.492 \log T + 0.00177T - 3.11 \times 10^{-8}T^2 + 9.218 \quad (15)$$

and by Thomas and Portalski (1958):

$$\log K = 3921T^{-1} - 7.971 \log T + 0.00250T - 2.95 + 10^{-7}T^2 + 10.20 \quad (16)$$

Values for K_γ are shown in Figure 54, as calculated and plotted by Ewell (1940). Rearranging Equation 13 and using mole fractions, the methanol mole fraction is:

$$y_1 = Ky_2y_3^2P^2/K_\gamma \quad (17)$$

Since K decreases with increasing temperature and K_γ increases with increasing temperature, the temperature for methanol synthesis should be as low as practicable to maximize conversion.

The reaction is strongly exothermic ($\Delta H^o_{298^oK}$ = -21.7 kcal/mol). A numerical expression for the heat of reaction is (Thomas and Portalski, 1958):

$$\Delta H^o_T = -17,920 - 15.84T + 0.01142T^2 = 2.699 \times 10^{-6}T^3 \quad (18)$$

and at elevated pressures:

$$\Delta H_{T,P} = \Delta H^o_T - 0.5411P - 3.255 \times 10^6 P/T^2 \quad (19)$$

Because the heat of reaction increases with increased pressure, methanol reactors must be designed for large amounts of heat removal to maintain adequate conversion and to protect the catalyst from deactivation.

A more fundamental approach for determining equilibrium concentra-

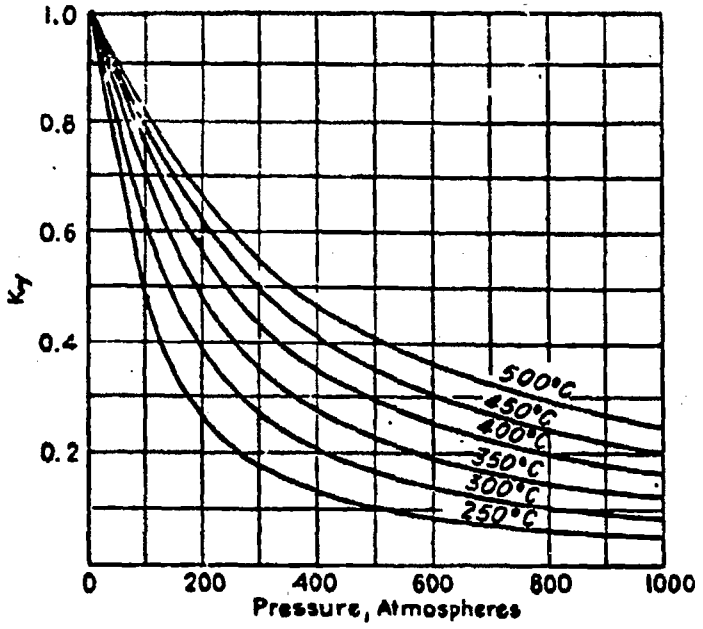

Figure 54. Values of K_γ (Ewell, 1940)

tions requires information about the free energy of formation, heat of formation, heat capacity, and fugacity coefficient of each component in the reaction. The equilibrium constant can also be expressed as:

$$K = \exp[-\Delta G/RT] = \exp[-\Sigma \nu_i \Delta G_i/RT] \tag{20}$$

For the methanol synthesis reaction at 298°K and 1 atm:

$$\Delta G^o = \Delta G^o_{CH_3OH} - \Delta G^o_{CO} - 2\Delta G^o_{H_2}$$

Values for ΔG^o_i can be obtained from Table 17, giving a value:

$$\Delta G^o = -38.6 + 32.8 = -5.8 \text{ kcal/gmol}$$

The standard-state equilibrium constant becomes:

$$K^o = \exp[5800/(1.99)(298)] = 1.8 \times 10^4$$

The effect of temperature on the equilibrium constant can be determined using the van't Hoff equation:

$$\left(\frac{\partial \ln K}{\partial T}\right)_P = \frac{\Delta H^o_T}{RT^2} \tag{21}$$

The heat of formation is calculated from the expression:

$$\Delta H^o_T = \Delta H^o + \int_{T_o}^{T} \Delta C^o_p dT \tag{22}$$

where the standard-state heat of formation, ΔH^o, can be expressed as:

$$\Delta H^o = \Sigma \nu_i \Delta H_i \tag{23}$$

and the heat capacity of the reaction mixture is:

$$\Delta C^o_p = \Sigma \nu_i C^o_{P_i} \tag{24}$$

Table 17. Heat and free energy of formation[a]

Compound	ΔH^o_{298}, kcal/mol	ΔG^o_{298}, kcal/mol
CH_3OH	-48.08	-38.62
H_2	0.0	0.0
CO	-26.416	-32.808
CO_2	-94.052	-94.260
H_2O	-57.798	-54.635
HCOOH	-86.67	-80.24
HCHO	-28.29	-26.88

[a]Chemical Engineers' Handbook, 1973.

Values for ΔH^o_i are given in Table 17. The heat capacity is temperature dependent, and may be expressed as:

$$C^o_{pi} = a + bT + cT^2 + dT^3 \tag{25}$$

where values for the constants are given in Table 18. Substituting Equations 25 and 22 into Equation 21, and integrating yields the expression:

$$\ln K = \ln K^o + (\Delta a/R)\ln(T/T_o) + (\Delta b/2R)(T - T_o) + (\Delta c/6R)(T^2 - T_o^2) + (\Delta d/12R)(T^3 - T_o^3) + \frac{1}{R}\left[-\Delta H^o + \Delta a T_o + \frac{\Delta b}{2} T_o^2 + \frac{\Delta c}{3} T_o^3 + \frac{\Delta d}{4} T_o^4\right]\left[\frac{1}{T} - \frac{1}{T_o}\right] \tag{26}$$

The temperature of the reaction is T and the standard-state temperature, T_o, is 298°K. The effect of pressure on the equilibrium concentrations

Table 18. Heat capacity[a]

Compound	$c_p^o = a + bT + cT^2 + dT^3$, cal/mol-°K			
	a	b x 10^2	c x 10^5	d x 10^9
CH_3OH	5.052	1.694	0.6179	-6.811
H_2	6.483	0.2215	-0.3298	1.826
CO	7.373	-0.307	0.6662	-3.037
CO_2	4.728	1.754	-1.338	4.097
H_2O	7.701	0.04595	0.2521	-0.859
HCOOH	2.798	3.243	-2.009	4.187
HCHO	5.607	0.7540	0.7130	-5.494

[a]Reid et al., 1977.

can be determined by calculating the value of the fugacity coefficient ratio:

$$K = K_y K_\gamma = [\prod_i (y_i^{\nu_i})][\prod_i (f/p)_i^{\nu_i}](\frac{P}{1\ atm})^{\Sigma\nu_i} \qquad (27)$$

Using the critical properties given in Table 19, reduced pressures and temperatures are calculated and used with Figure 55 to estimate fugacity coefficients. The mole fraction of methanol can then be expressed as:

$$y_1 = K y_2 y_3^2 P^2 (f/P)_2 (f/P)_3^2 / (f/P)_1 \qquad (28)$$

The detailed numerical results for several reactions are given in Appendix C, using a stoichiometric mixture of reactants at 200°C and 50 atmospheres. Table 20 gives reduced pressures, reduced temperatures, and fugacity coefficients at these conditions. Methanol formation is

Table 19. Critical properties[a]

Compound	T_c, °K	P_c, atm
CH_3OH	512.6	79.9
H_2	33.2	12.8
CO	132.9	34.5
CO_2	304.2	72.8
H_2O	647.3	217.6
HCOOH	580.	(70.)[b]
HCHO	408.	65.

[a]Reid et al., 1977.

[b]Estimate, acetic acid plus 10 atm.

Table 20. Fugacity coefficients at 200°C and 50 atmospheres

Compound	T_R	P_R	f/P
CH_3OH	0.92	0.63	0.70
CO	3.56	1.45	0.98
H_2	14.2	3.91	1.03
H_2O	0.73	0.23	0.38
CO_2	1.56	0.69	0.96
HCOOH	0.82	0.70	0.30
HCHO	1.16	0.77	0.85

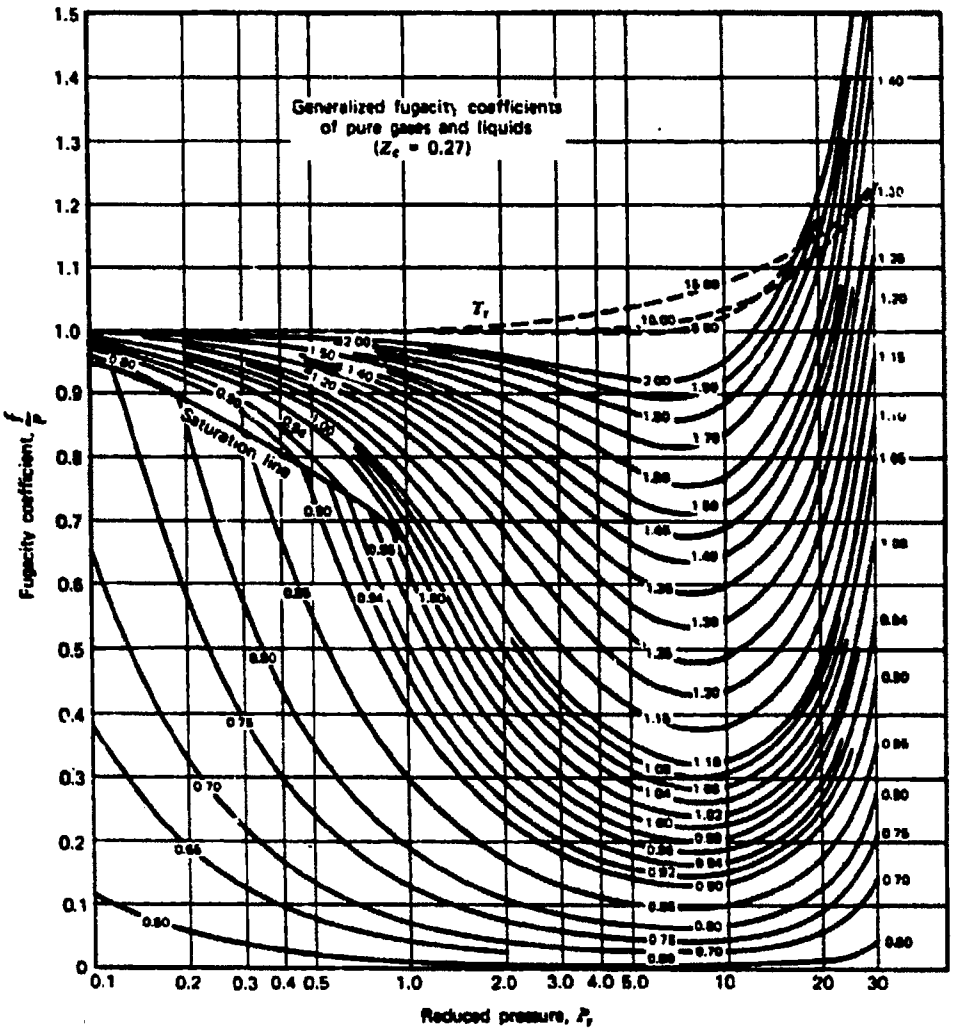

Figure 55. Generalized fugacity chart (Hougen et al., 1960)

favorable in carbon monoxide hydrogenation, carbon dioxide hydrogenation, formic acid hydrogenation, and formaldehyde hydrogenation.

Mixed metal oxides having compositions very similar to those used for methanol synthesis catalyze the water-gas shift reaction (Newsome, 1980). The methanol synthesis and water-gas shift reactions could occur at the same time on the catalyst and might involve a common intermediate. A surface formate has been determined to be an intermediate species on ZnO (Ueno et al., 1970) and on Cu/ZnO catalysts (van Herwijnen and de Jong, 1980; van Herwijnen et al., 1980) during studies of the water-gas shift reaction. The thermodynamics of the water-gas shift reaction, using a stoichiometric mixture of reactants at 200°C and 50 atmospheres, are given in Appendix D. The products were strongly favored under these conditions.

Kinetics

Although thermodynamics establishes the maximum possible conversion of carbon monoxide and hydrogen to methanol, the actual methanol yield also depends on the rate of reaction. Because the reaction is heterogeneous, the overall rate of reaction may depend on rates of adsorption of the reactants, surface reaction rates, and the rate of product desorption. Rate expressions are derived from reaction schemes involving a sequence of elementary steps with various assumptions concerning the assignment of the rate determining step. Kinetic data are applied to the rate expressions to determine rate constants for those models compatible with the data and to discard those models in which the data

will not fit.

Using the method of Hougen and Watson (1943), Natta developed an expression for the rate of methanol synthesis on a zinc oxide-chromia catalyst and a ternary $ZnO\text{-}CuO\text{-}Cr_2O_3$ catalyst assuming that a trimolecular surface reaction was rate determining (Natta, 1955):

$$r = \frac{f_{CO}f_{H_2}^2 - f_{CH_3OH}/K}{(A + Bf_{CO} + Cf_{H_2} + Df_{CH_3OH})^3} \qquad (29)$$

The values of the empirical rate constants A, B, C, and D were dependent on the catalyst and experimental conditions. During the two decades since Natta's work, experimental data have been successfully applied to other kinetic models with significantly different assumptions concerning the rate determining step. Various models have assumed that the adsorption of hydrogen, a bimolecular surface reaction, the reaction of adsorbed hydrogen with a methoxy species, a Rideal-type reaction between gaseous hydrogen and a surface formaldehyde species, or the desorption of methanol was the rate determining step (Denny and Whan, 1978). In most expressions, the rate of reaction was found to be proportional to $(P_{CO}P_{H_2}^2)^n$, where n had values between 0.5 and 1.

The industrial reaction mixture normally contains some carbon dioxide in the feed to improve the activity for methanol synthesis. The role of carbon dioxide has been described both as a primary reactant and as an oxidant to maintain the catalyst in an active state. At first glance, the extent of CO_2 hydrogenation to methanol appears to be easily determined by simply measuring the amount of water formed. However, as a result of the water-gas shift reaction, the amount of water in the gas phase would be quite small at equilibrium conditions. If the reaction

rate for the water-gas shift occurs more rapidly than methanol synthesis from carbon dioxide, it would be possible for the carbon dioxide concentration to remain constant and the water concentration to be very low even during CO_2 hydrogenation to methanol.

Experimental studies of methanol synthesis by Rozovskii and coworkers during the past decade have shown that carbon dioxide was hydrogenated to methanol under reaction conditions. Methanol was formed from a feed containing CO, CO_2, and H_2 but synthesis activity ceased when CO_2 was removed from the gas phase (Rozovskii et al., 1975). Studies of methanol synthesis from CO_2 and H_2, taking into account the CO formed by the water-gas shift reaction, showed no correlation between methanol yield and CO concentrations for various contact times; in some cases, the methanol yield exceeded the equilibrium amount for CO hydrogenation (Kagan et al., 1976; Kuznetsov et al., 1983). Using feed mixtures containing either isotopic CO or CO_2, radioactivity measurements of the reaction products established that methanol was formed by direct hydrogenation of carbon dioxide and provided estimates of reaction rates for individual steps, i.e., water-gas shift and methanol synthesis (Rozovskii et al., 1977; Rozovskii, 1980). High concentrations of CO_2 decreased the product yield by oxidative dehydrogenation of methanol (Rozovskii et al., 1976a):

$$CH_3OH + CO_2 = 2CO + H_2 + H_2O \qquad (30)$$

Klier and coworkers have also investigated the effect of carbon dioxide on methanol synthesis (Klier et al., 1982). Carbon dioxide was hydrogenated to methanol but at a lower rate than carbon monoxide hydro-

genation. The loss of methanol synthesis activity when using a feed of only CO and H_2 was attributed to deactivation of active surface sites due to strong reduction of the catalyst rather than the reactivity of feed itself. This conclusion was based on an increase in the rate of methanol synthesis by small additions of water or oxygen as well as carbon dioxide. The decrease in the rate of methanol synthesis at higher CO_2 concentrations was attributed to strong CO_2 adsorption on the same sites involved in the adsorption of carbon monoxide and hydrogen. A kinetic rate expression incorporating both the promoting and inhibiting effects of carbon dioxide had the general form

$$r = C_o L^m \frac{P_{CO}P_{H_2}^2 - P_{CH_3OH}/K}{(A + BP_{H_2} + CP_{CO} + DP_{CH_3OH} + EP_{H_2O} + FP_{CO_2})^n} + k[P_{CO_2} - K_o^{-1}(P_{CH_3OH}P_{H_2O}/P_{H_2}^3)] \quad (31)$$

where C_o and k were constants, L was the concentration of active sites, and K and K_o were equilibrium constants for methanol synthesis from CO and CO_2, respectively.

Several investigators have compared the rates of methanol synthesis by CO hydrogenation and CO_2 hydrogenation (Bardet et al., 1981; Kieffer et al., 1981; Denise et al., 1982). It was determined that carbon dioxide was hydrogenated directly to methanol at lower temperatures than CO hydrogenation. A chemical trapping technique was used to identify a stable formate species on the catalyst surface after these reactions.

Reaction Mechanisms

An understanding of how catalysts function to selectively form the desired product is an important factor in the development of improved catalysts. This requires a detailed understanding of the reaction mechanism. A methanol catalyst serves as a classic example of how a selective catalyst can be utilized to produce a product that is thermodynamically disfavored.

An indirect method for mechanistic studies involves the proposal of a mechanism from which a rate expression can be derived, then making a comparison between the proposed rate and experimental data. Invalid mechanisms may be discounted by this method, but agreement between a rate expression and experimental data does not constitute proof that the mechanism is correct. Natta used this approach to propose a mechanism for methanol synthesis (Natta, 1955). Using Hougen and Watson models and kinetic data with the assumption that a trimolecular surface reaction occurred, the following steps were proposed:

$$CO + * = CO*$$

$$H_2 + * = H_2*$$

$$CO* + 2H_2* = CH_3OH* + 2*$$

$$CH_3OH* = CH_3OH + *$$

where * was an active site on the catalyst surface. A rate expression based on the assumption that the surface reaction was controlling (Equation 29) agreed very well with experimental data. However, many other kinetic models have been found to satisfy the data, making any

conclusions concerning the reaction mechanism ambiguous (Denny and Whan, 1978).

Additional indirect mechanistic information was obtained from adsorption experiments. Measurements of the simultaneous adsorption of carbon monoxide and hydrogen at low pressures on a methanol catalyst suggested that an intermediate surface species having the formula $-OCH_3$ existed on active sites (Tsuchiya and Shiba, 1965). A critical assumption in this approach was that the $-OCH_3$ species dominated the surface, since the total amount of carbon monoxide and hydrogen adsorbed was used to predict the surface species. These investigators concluded that the rate determining step for methanol synthesis was the reaction of hydrogen with the surface species $-OCH_3$. This conclusion was supported by a high pressure study using a methanol catalyst and labeled hydrogen (Borowitz, 1969). After exposing the catalyst to a $CO-H_2$ mixture, the reactor was evacuated and a $CO-D_2$ mixture admitted. Analysis of the product methanol by nmr spectroscopy showed a predominance of deuterium in the hydroxyl groups. This finding indicated that a surface methoxy species was a stable intermediate and that the source of the hydrogen in the hydroxyl group of methanol was gaseous hydrogen. However, it was not clear whether gaseous hydrogen reacted directly with methoxy groups or if an adsorbed form of hydrogen was involved because the exchange rates of deuterium with adsorbed hydrogen (hydroxyl or hydride species) were not determined.

Several mechanisms for methanol synthesis have been proposed in recent years. The scheme in Figure 56 was suggested by Deluzarche, Kieffer, and Muth (1977) for methanol synthesis on an industrial ZnO-

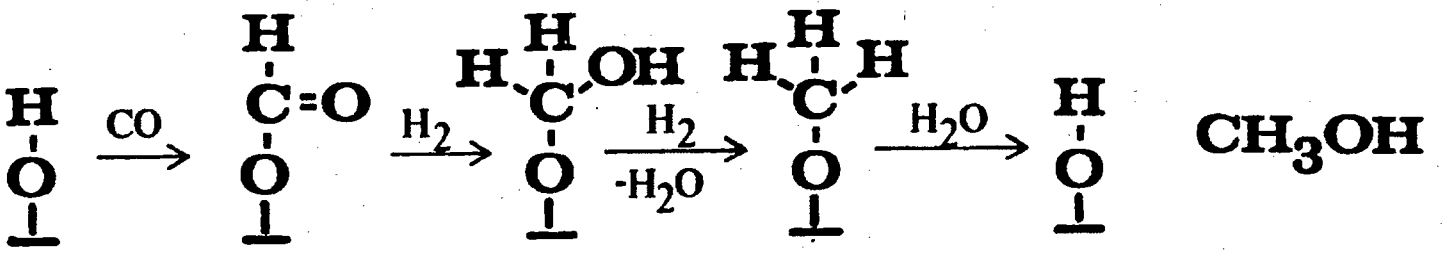

Figure 56. Methanol synthesis mechanism #1 (Deluzarche et al., 1977)

Cr_2O_3 catalyst. Carbon monoxide insertion into a surface hydroxyl group formed a formate (formyloxy) species which was hydrogenated to produce a methyloxy species. Dehydration and hydrogenation of the methyloxy species formed a methoxy group which was hydrated to produce methanol and a surface hydroxyl group. This mechanism did not involve carbon monoxide adsorption on metal ions. The proposed mechanism was based on the results of a chemical trapping technique which identified the stable intermediates on used catalysts. Only the formate and methoxy groups were detected by this method. The conclusion that the methoxy species was hydrated rather than hydrogenated to methanol was based on the observation that methanol synthesis required some CO_2 or H_2O in the $CO-H_2$ feed mixture (the presence of CO_2 ensures some H_2O formation via the water-gas shift reaction).

The mechanism shown in Figure 57 proposed that carbon monoxide was adsorbed on a metal ion followed by successive hydrogenation to formyl, hydroxycarbene, and hydroxymethyl species until further hydrogenation produced methanol (Herman et al., 1979). The active site for CO adsorption was proposed to be Cu(I) ions while adjacent zinc ions were the centers for hydrogen adsorption. None of these intermediate species were proven to exist on an active methanol catalyst. The presence of carbon dioxide provided an alternate pathway to methanol and methane formation via formate and methoxy intermediates (Klier et al., 1982). This concept of different routes to methanol synthesis for CO and CO_2 hydrogenation involving carbon-bonded and oxygen-bonded intermediates, respectively, was reached independently in kinetic studies (Denise et al., 1982). It was proposed that an adsorbed formate species was

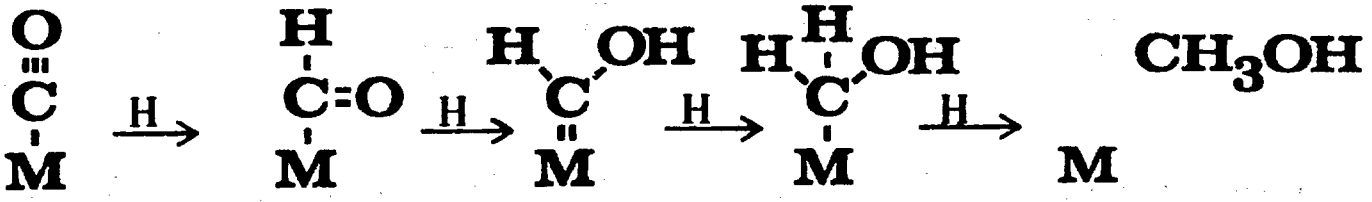

Figure 57. Methanol synthesis mechanism #2 (Herman et al., 1979)

formed both b. CO insertion into an adsorbed hydroxyl group and by CO_2 insertion into a surface hydride species. The mechanism for CO_2 hydrogenation suggested by these investigators is presented in Figure 58.

The studies of Rozovskii and coworkers concluded that methanol was formed by direct hydrogenation of carbon dioxide; carbon monoxide was hydrogenated indirectly via the water-gas shift reaction. The general form of the mechanism for methanol synthesis was proposed to be

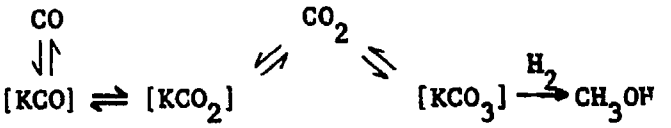

where [KCO], [KCO_2], and [KCO_3] were intermediate surface complexes (Rozovskii et al., 1976b). The intermediates in the water-gas shift reaction were believed to be different from the intermediates in methanol synthesis.

A methanol synthesis mechanism incorporating both carbon-bonded and oxygen-bonded intermediates was recently proposed by reviewing the literature up to 1981 (Henrici-Olivé and Olivé, 1982). This reaction scheme, shown in Figure 59, proposed that carbon monoxide was adsorbed on Cu(I) active sites within the zinc oxide lattice. Hydrogen was dissociatively adsorbed to form Cu(I) hydride and zinc hydroxide. Carbonyl insertion into the Cu-H bond produced a formyl species which was hydrogenated to form a side-bonded formaldehyde species. Further hydrogenation yielded a methoxy species and ultimately methanol. This type of mechanism has also been suggested for methanol synthesis by CO hydrogenation in homogeneous catalysis using ruthenium complexes (Dombek, 1980) and cobalt or rhodium complexes (Fahey, 1981).

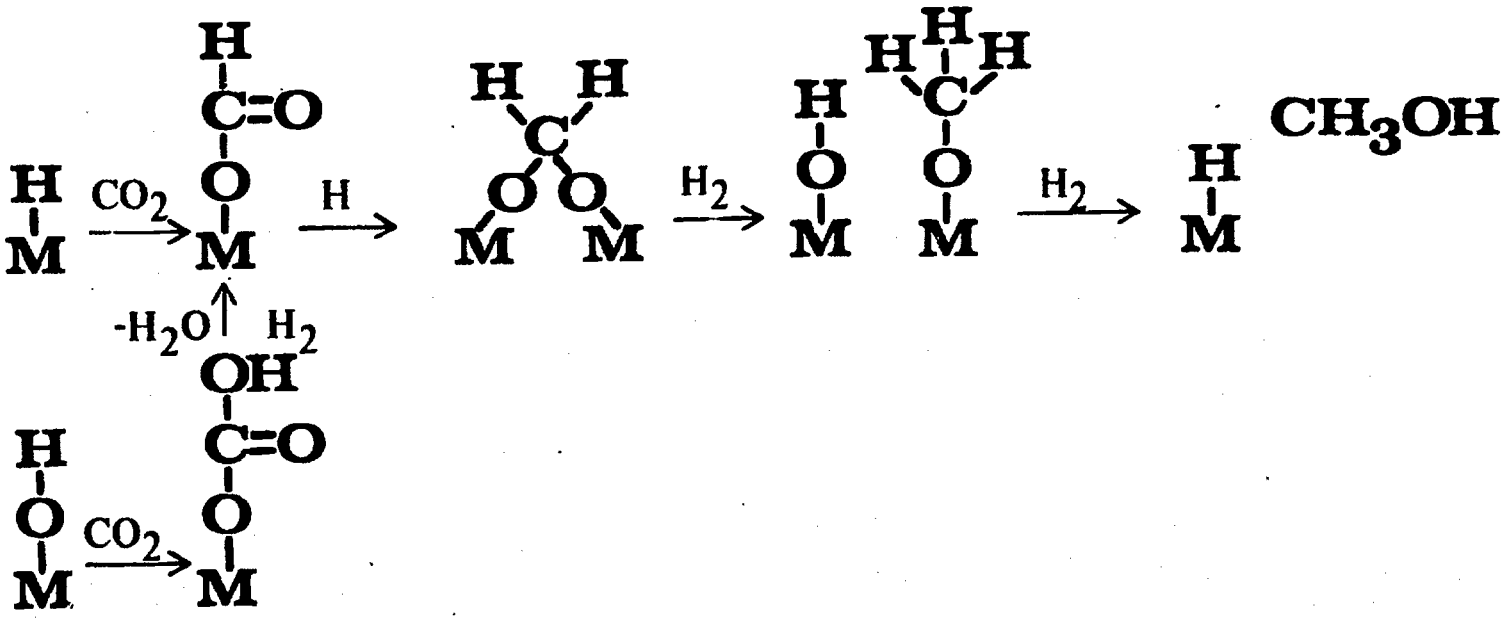

Figure 58. Methanol synthesis mechanism #3 (Denise et al., 1982)

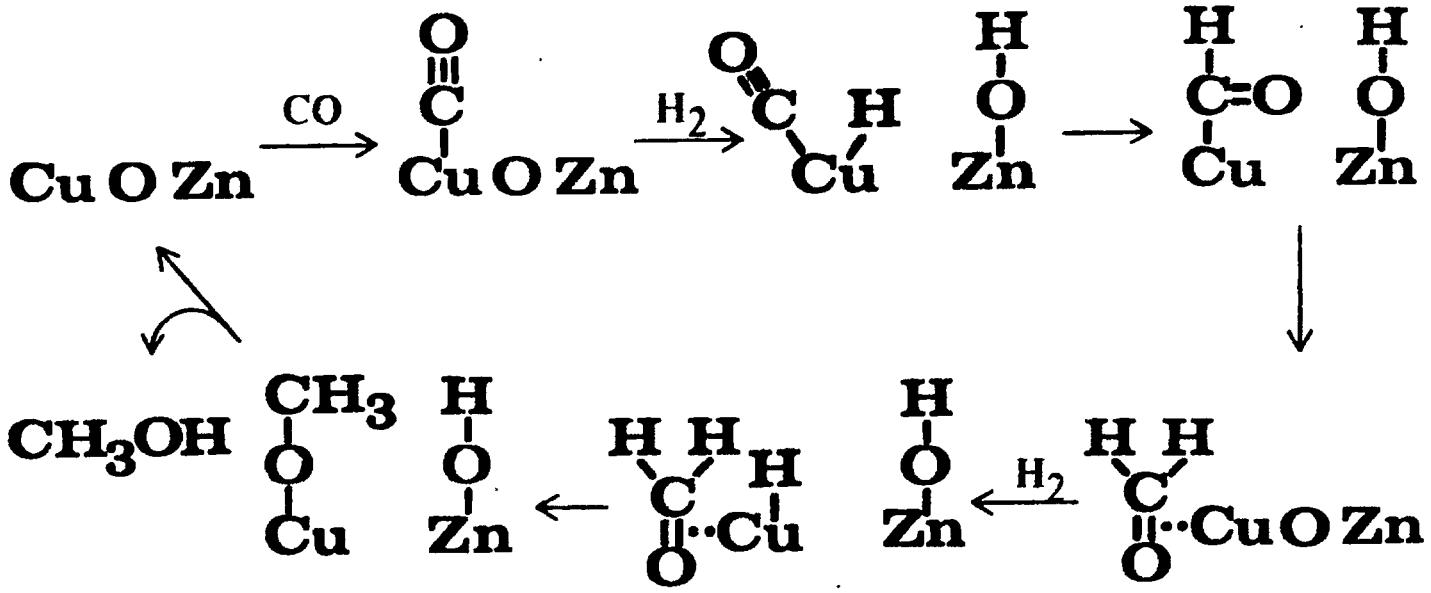

Figure 59. Methanol synthesis mechanism #4 (Henrici-Olivé and Olivé, 1982)

Some studies have investigated the adsorption of various organic molecules, their decomposition, and desorption from the surface of zinc oxide to obtain an insight on methanol synthesis. The temperature programmed desorption of adsorbed species on zinc oxide powder using the adsorbates H_2, CO, CO_2, HCHO, CH_3OH, CO + H_2, and CO_2 + H_2 indicated that an adsorbed formate intermediate was involved in the decomposition of methanol and formaldehyde as well as the hydrogenation of carbon dioxide (Bowker et al., 1981). The decomposition of methanol and formaldehyde also produced a surface methoxy species. The mixture of hydrogen and carbon monoxide did not yield an adsorbed formate species. This same technique has been applied to specific crystal faces of zinc oxide (Cheng and Kung, 1982; Cheng et al., 1983). It was established that the type of crystal face and the presence of defects affected the nature of adsorbed species. In particular, the decomposition of deuterated methanol yielded DCDO, D_2O, CO, CO_2, and D_2 on the polar (0001) surface whereas CD_4, CO, CO_2, and D_2 were the products from the stepped and nonpolar surfaces. Nonpolar surfaces with steps or anion vacancies, as well as polar surfaces, were believed to be active for methanol synthesis. The reaction mechanism depicted in Figure 60 demonstrates the role of an anion vacancy in CO hydrogenation to methanol (Kung, 1980). The active site was proposed to be an oxygen vacancy surrounded by metal ions. Carbon monoxide adsorbed on a metal ion, carbon end down, and was hydrogenated by a neighboring adsorbed hydrogen atom to form a formyl species. The oxygen on the formyl species then interacted with the electron-deficient vacancy as further hydrogenation occurred, eventually forming a methoxy species as the bonding between the oxygen

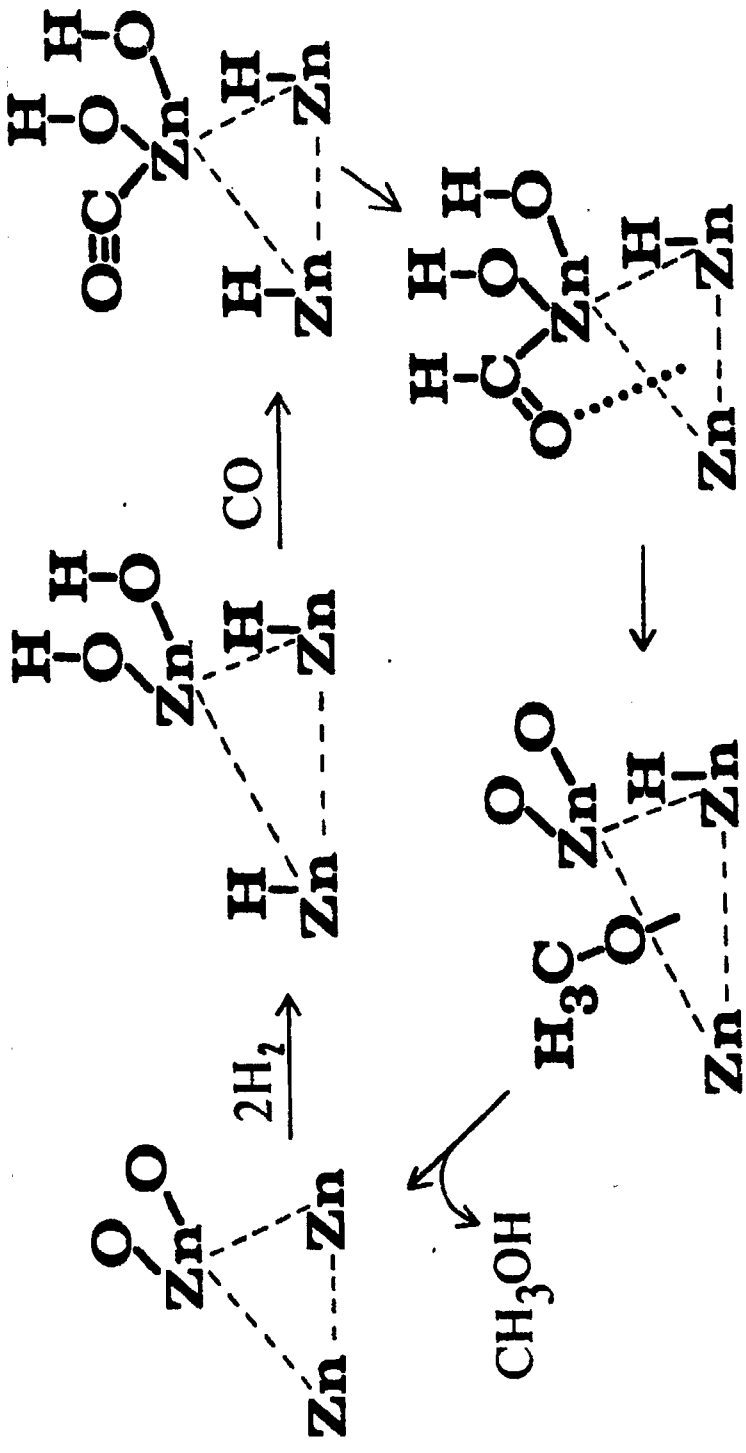

Figure 60. Methanol synthesis mechanism #5 (Kung, 1980)

and the vacancy strengthened while the bonding between the carbon and the metal ion weakened. Additional hydrogenation produced methanol.

High Pressure Spectroscopic Cells

Several infrared cells have been made for studying catalytic reactions at elevated pressures and temperatures, primarily for gas-liquid systems (Tinker and Morris, 1972; Gallei and Schadow, 1974; King et al., 1978; Ballintine and Schmulbach, 1979; Penninger, 1979). A common feature of these cells has been the use of thick calcium fluoride, magnesium fluoride, or quartz windows which have relatively large optical diameters. Short, variable path length designs have been used. High pressure studies of gas-solid systems involving gases which strongly absorb infrared radiation, such as CO, require a cell with a short path length. These cells generally have been designed for a maximum pressure of several hundred atmospheres, limited by the strength of the windows. The maximum temperature of the cell is limited by the seal material employed. Temperatures up to 600°C could be achieved with the cell of Gallei and Schadow because the windows were water-cooled; this cell also had high vacuum capability.

A high pressure cell has been developed for studying gas-solid reactions on a catalyst wafer (Hicks et al., 1981). Temperatures up to 317°C and pressures up to 70 atmospheres can be achieved with this cell. The design allows infrared windows and catalyst wafers to be removed and replaced easily.

EXPERIMENTAL APPARATUS AND METHODS

Reactor System

The flow system shown in Figure 61 was designed for catalytic studies at pressures in the range from 10^{-4} torr to 100 atm. There are three major sections in this system: 1) a high pressure section constructed with stainless steel components for optimum safety, 2) an atmospheric section to handle the effluent from the system for venting or sampling, and 3) a vacuum section composed of glass and stainless steel to desorb impurities in the system or on catalyst surfaces. The entire system was built on a mobile frame permitting the system to be connected with various other analytical instruments (i.e., gas chromatograph or infrared spectrometer) at different locations.

High pressure section

Gas streams for nitrogen, carbon monoxide, hydrogen, and oxygen were included in the system. The oxygen line provided additional flexibility which was not utilized in the studies of methanol catalysts. Gas cylinders were used as the pressure source for the system. A full cylinder of carbon monoxide (99.5% min. purity) provided 1650 psig (113 atm), a full cylinder of nitrogen (99.9% min. purity) provided 2490 psig (170 atm), and a full cylinder of hydrogen (99.9% min. purity) provided 2200 psig (150 atm). Cylinders were replaced when the tank's pressure dropped to 50 atm since most experiments were conducted at this pressure. The size of the CO cylinder (#2, 1.87 m^3) was smaller than the others because of the toxicity of the gas (to minimize the amount of gas lost in the case of an accidental release). Because these

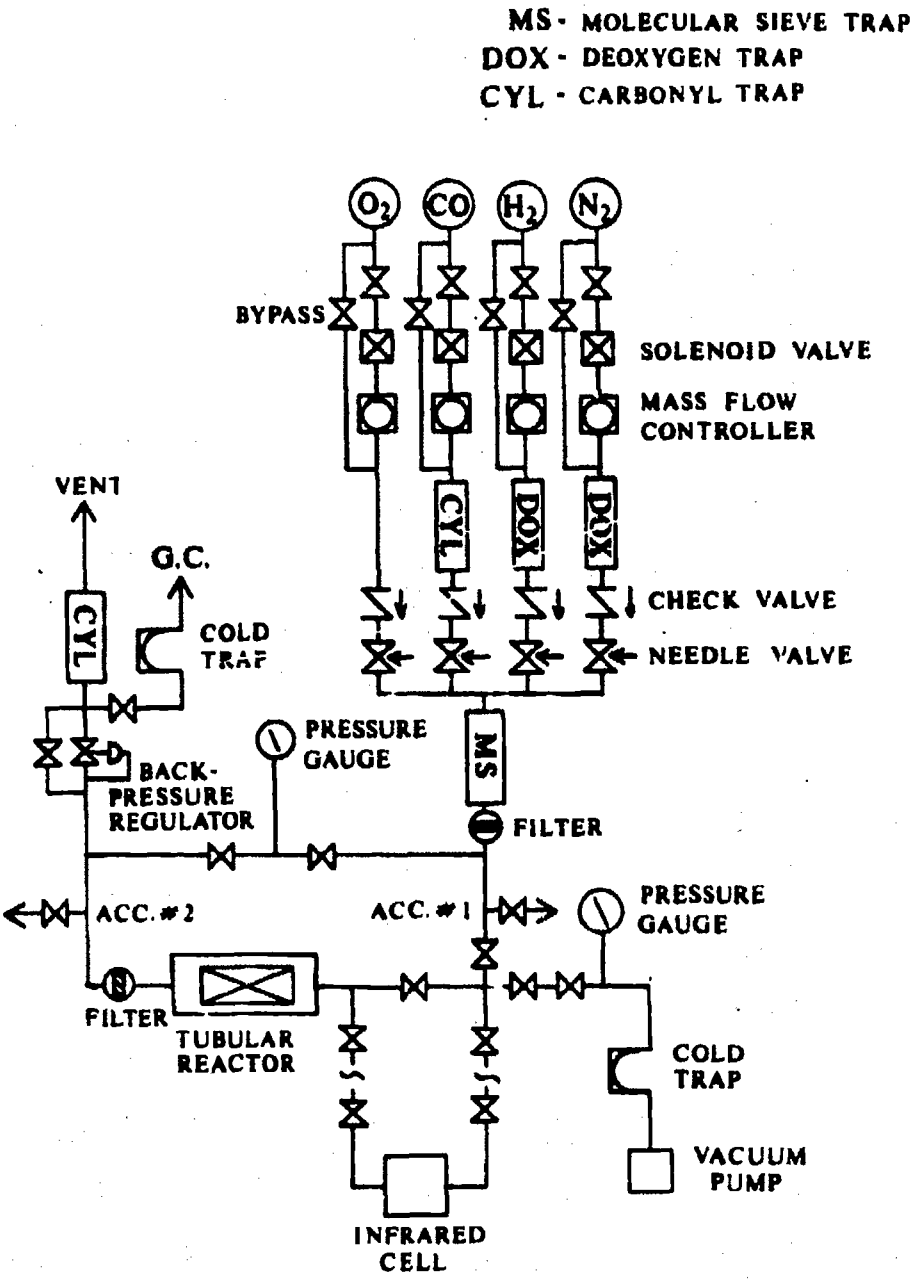

Figure 61. High pressure system

cylinder pressures were above the safe operating pressure of some components in the system (1500 psig), each cylinder had a high pressure regulator (Matheson, Model 3064) capable of delivering any pressure in the safe operating range (0-100 atm).

The gas lines were 1/8" 316SS tubing (0.062" ID) connected to various fittings (Autoclave Engineers, Speedbite) specifically made for high pressures. Three types of hand-operated valves were used: 1) a vee stem for on-off use having a metal-to-metal seal, 2) a soft-seating stem for bubble-tight on-off use, and 3) a regulating stem for control as well as shut-off use. Figure 61 indicates where each type of valve has been used in the system. Each gas has a flow line with a solenoid valve (Atkomatic, Type SBTD) and a thermal mass flow controller (Brooks, Model 5810/5835A). All the solenoid valves have been wired via the alarm relay of a CO detector system (Mine Safety Appliances, Model 571) to provide an automatic shut-down feature if a major gas leak (CO or H_2) develops downstream. The solenoid valves close when the CO level exceeds 200 ppm (or about 2000 ppm H_2) as measured by the electrochemical sensor. The mass flow controllers measure and regulate the flow over a range of 0-500 sccm with an accuracy of 1% full scale. These controllers are rated for 1500 psig maximum operating pressure. The flow sensors are attached to the secondary electronics and digital indicators (Brooks, Models 5871/5872) where the flowrates are set. Calibration curves for flowrate vs. digital indicator reading over a range of pressures for each of the gases are given in Appendix E. A bypass line in each gas stream allows quick gas bleedoff from the cylinders and, if necessary, can be used with the regulating valve downstream to set flowrates (e.g.,

if a flowrate greater than 500 sccm were desired).

Each gas passed through a trap to remove impurities. All high pressure traps were comprised of a 12" length of tubing (9/16" OD x 0.312" ID) wrapped with heating tape and insulation. The trap in the nitrogen line contained a copper-supported catalyst (BASF, R3-11) which removed trace amounts of oxygen at room temperature by the oxidation of copper to copper oxide. The trap in the hydrogen line also contained the same copper-supported catalyst which removed trace amounts of oxygen at 70°C by reacting hydrogen with oxygen to form water. Both traps were activated by reducing the 10-20 mesh particles in hydrogen at 180°C. The trap in the carbon monoxide line contained activated alumina (Alcoa, F-1) as 28-48 mesh particles. During operation of the CO flow line, this trap was heated at about 300°C to decompose any metal carbonyls that might be present in the feed. All gases passed through a trap containing a molecular sieve (Linde, 13X) to remove any water in the feed stream. This final trap in the feed system was followed by a dual-disc filter to remove particles larger than 35 μm. Each gas line had a check valve to prevent backflow and a regulating valve.

Pressures from atmospheric to 2000 psig can be measured with the pressure gauge (Heise, Model CMM) to an accuracy of ± 2 psi. This tubing configuration permitted both the upstream (pre-reactor) and downstream (post-reactor) pressures to be recorded, from which the pressure drop through the reactor could be determined. Several ports were installed in the high pressure section which could be connected to external equipment. The ports labeled IR #1 and IR #2 were normally utilized as inlet and outlet connections to a high pressure infrared cell. This

design made it possible to conduct simultaneously infrared and catalyst activity studies. The ports labeled Accessory #1 and Accessory #2, which provided additional flexibility to the system, were used in infrared studies involving a saturator. In these studies, the reactor was removed and the connections plugged, the Accessory #1 and IR #2 ports connected to the saturator, and the IR #1 and Accessory #2 ports connected to the infrared cell.

The reactor, shown in Figure 62, was a 12-inch length of 316SS tubing (9/16 inch OD by 0.312 inch ID) fitted with a 316SS sheathed thermocouple (Omega, Sub-Miniature) that passed axially through the reactor inlet to the catalyst bed. An 8-inch section of the outer reactor wall was wrapped with 12 feet of alumel wire (Leeds & Northrup, 22 gauge) insulated electrically by fish-spine porcelain beads (Leeds & Northrup, #034365) for the purpose of heating the reactor; the total resistance of the wire was 4 Ω. The beads were held in place with electric resistor cement (Sauereisen, #78) having good thermal conductivity. The entire heating section was wrapped with refractory fiber insulation (Manville, Cerafelt) and aluminum foil. The reactor preheater was packed with silicon carbide particles (Norton, 10 grit); the catalyst bed followed and then additional silicon carbide particles were used to fill the remaining volume in the reactor. The contents were kept in place with 316SS screens (~ 100 mesh) at each end of the reactor. The reactor was followed by a dual-disc filter to remove particles larger than 35 μm from the flow stream.

The reactor thermocouple was used to operate a proportional controller (Omega, Model 49) and a high limit controller (Omega, Model

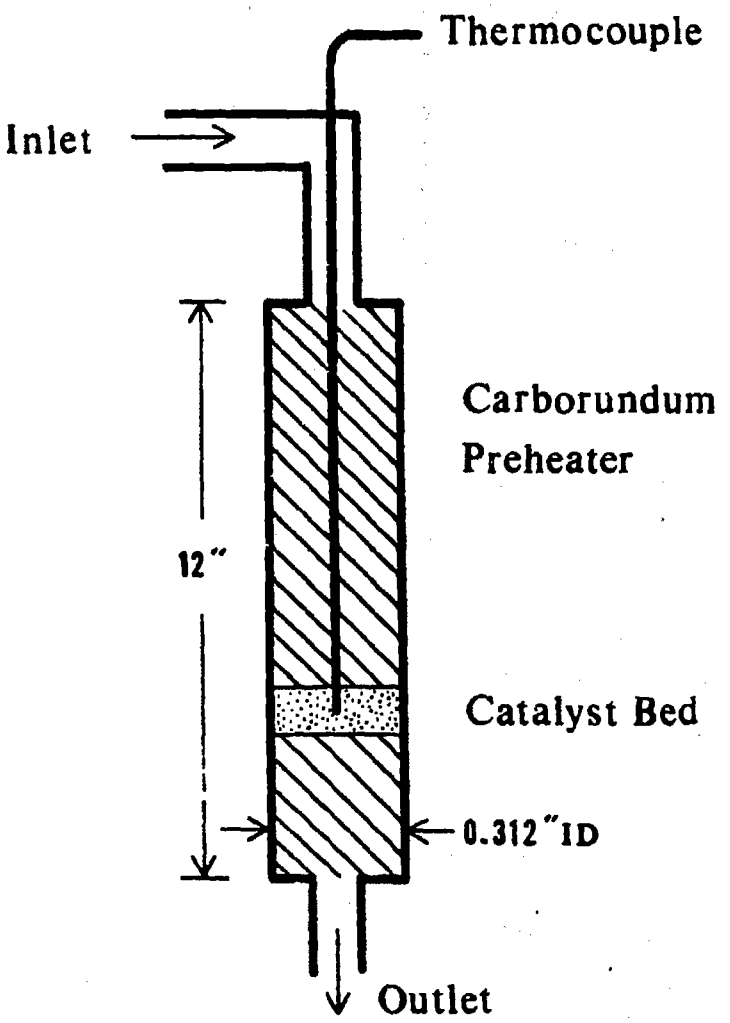

Figure 62. Methanol synthesis reactor

50) which supplied power to the reactor heating jacket. The electrical circuit, depicted in Figure 63, is composed of the limit controller and proportional controller in series with a Variac transformer. The high limit controller was set 50°C above the reactor operating temperature to protect the catalyst from an abnormal temperature increase that could arise if the catalyst reduction takes place too rapidly or an electrical malfunction occurs. The proportional controller was very responsive to the thermocouple measurement, providing temperature control better than ± 1°C (the temperature indicator, Omega Model 199, was only accurate to ± 1°C). Power from the proportional controller was passed through a transformer set at 15% of full voltage, limiting the rate of the reactor temperature rise and providing additional protection against a temperature overshoot.

At the downstream end of the high pressure section was a back pressure regulator (Tescom, #26-1724) providing pressure relief over the range 15-2500 psig with an accuracy of ± 25 psi. Generally, the back pressure regulator was kept at a setting corresponding to 50 atm (720 psig) because of the difficulty in reproducing the same pressure (setting the back pressure is a trial-and-error procedure and the accuracy is poor); both pressure increases and decreases were made by closing and opening, respectively, the valve in the bypass line. The bypass line was also used for studies at atmospheric pressure.

Atmospheric section

The gas lines downstream from the back pressure regulator were 304SS tubing (1/4 inch OD by 0.18 inch ID) connected with Swagelok

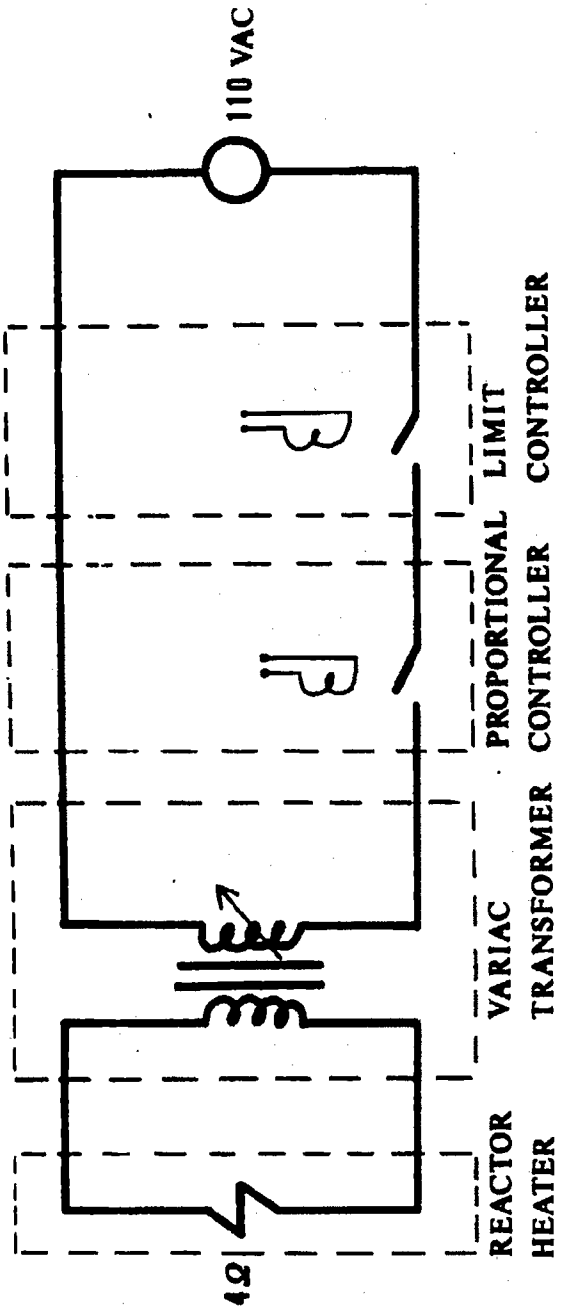

Figure 63. Reactor electrical circuit

fittings. The vent line contained a 12-inch section filled with activated alumina (Alcoa, F-1) heated at approximately 300°C to decompose any carbonyls formed in the reactor system. The gas-sampling line could be attached to a gas chromatograph for analysis of the reactor effluent. This line contained a cold trap which could be used to condense the heavier components in the effluent stream for subsequent gas chromatographic analysis to detect trace products. The regulating valve (Whitey, SS-1RS4) allowed a part of the flow to pass through the sampling line and the remaining flow to pass through the vent line. In practice, no carbonyl formation was detected, so for convenience, the sampling line was also used for venting.

Vacuum section

A vacuum section was incorporated into the design primarily to provide pretreatment of infrared samples for removing surface contaminants prior to analysis. The line from the high pressure section led to a vacuum valve (Veeco, 1/2 inch brass) which would allow the vacuum section to operate isolated from the rest of the system. This valve was connected to a flexible piece of 321SS tubing with a metal-to-glass seal for making the transition to the Pyrex components; the flexible tubing compensated for vibration and stresses to protect the glassware. The pressure was measured with an ionization gauge controller, using a Pirani gauge over the 1000 to 10^{-3} torr range. Both gauges were attached to the vacuum line near a liquid nitrogen trap. The pumping system consisted of a two-stage vacuum pump (Welch, Model 1402) and an air-cooled diffusion pump (Edwards, Model E02) producing an ultimate

vacuum of 10^{-6} torr with silicon oil (Dow Corning, Silicon 704). Most of the glass portion of the system could be easily detached when the vacuum system was not in use, making it easier to clean the glassware and avoiding damage when transferring the system to a new location.

High Pressure Infrared Cell

The infrared cell used in these studies was a modification of the design by Tinker and Morris (1972). The cell was constructed to examine catalysts at pressures ranging from 10^{-6} torr to 240 atmospheres and temperatures from ambient to 300°C. The cross section of a partially disassembled cell is shown in Figure 64. The cell body (A) was constructed of 304 stainless steel. The inner surface of the cell body was copper plated and copper tubing was inserted into the inlet and outlet ports to prevent metal carbonyl formation at elevated CO pressures. Four equally spaced holes were drilled around one end of the body for the insertion of 150 watt heating cartridges. The outer circumference of the cell body was insulated, and a thermocouple well was positioned directly between the inlet ports.

A copper-plated 304 stainless steel spacer (C) held the windows in place and distributed the gas around the sample wafer (G). Gases entering from the inlet ports (H) contacted the sample and exited through eight 1.6 mm holes drilled around the circumference of the spacer. A pair of grooves around the outer circumference was used to channel the exiting gases to the outlet port (I). This type of configuration, which admitted gases to both sides of the sample, decreased the chance for

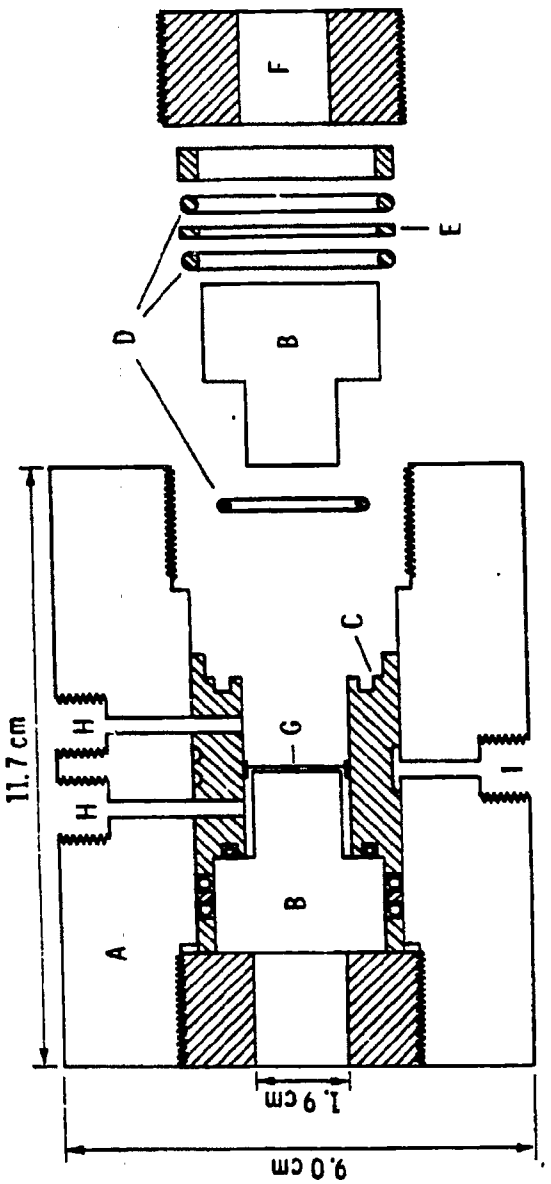

Figure 64. High pressure infrared cell

sample breakage due to pressure differences. Samples were pressed into the form of a wafer, generally between 0.05 and 0.20 mm thick. A thin aluminum ring could be used to hold the wafer in the center of the spacer.

Calcium fluoride step windows (B), manufactured by Harshaw Chemical Co., were used which have an outer diameter of 3.34 cm, an inner diameter of 1.80 cm, and an overall length of 3.66 cm. The small-diameter end of the window displaced most of the gaseous volume in the spacer. The maximum operating pressure for these windows, using a safety factor of 4, was calculated from the formula (Eastman Kodak Company, 1971):

$$P = M(t/2.1\ r)^2$$

where M is the modulus of rupture, t is the window thickness, and r is the radius of the unsupported window area. For these windows at room temperature, M = 5300 psi, t = 1.9 cm, and r = 1.1 cm; the maximum pressure was calculated to be 3530 psi (240 atm). The cell had separate seals (D) for vacuum or elevated pressure conditions. The innermost o-ring provided the vacuum seal, and a pair of o-rings separated by a thin aluminum ring (E) encircling the larger diameter of the window provided the seal at high pressures. The use of two o-rings around each window at high pressures distributed the radial stress caused by compression better than a single o-ring, avoiding one cause of window failure. A single o-ring can be utilized successfully if the o-ring is not compressed too much. Screw plugs (F) at each end of the cell were used to compress the o-rings. Because the windows could be chipped or cracked fairly easily during compression, the polished ends

of the windows were protected from the plugs and spacer with thin-gaskets (1 mil) of Mylar film in applications at 200°C and less. Viton o-rings were used at temperatures below 230°C; Kalrez o-rings may be used at temperatures up to 300°C.

Gas Chromatography

A gas chromatograph (Antek, Model 310/40-ALP) with dual column thermal conductivity detectors coupled with a reporting integrator (Hewlett-Packard, Model 3390A) was used for the analysis of gaseous mixtures. Samples of the reactor effluent were taken with a 6-port sampling valve and analyzed with the column arrangement depicted in Figure 65. A Porapak N column (6 ft by 1/8 inch SS) in series with a Porapak T column (6 ft by 1/8 inch SS) separated all species normally found in the effluent; a typical chromatogram is shown in Figure 66. If nitrogen was added to the feed as an internal standard, a Carbosieve S column (6 ft by 1/8 inch SS) provided the separation of nitrogen and carbon monoxide. These two light gases eluted together from the Porapak columns and passed into the Carbosieve column. A stand-off 4-port switching valve allowed the heavier species to bypass the Carbosieve column while trapping the light gases. After all the heavier species had eluted, the switching valve was turned back to pass the carrier through the Carbosieve column and separate the N_2-CO mixture. The operating conditions for all analyses have been given in Table 21.

In order to measure quantitatively the amount of each component in the sample, it was necessary to determine the response factor of each

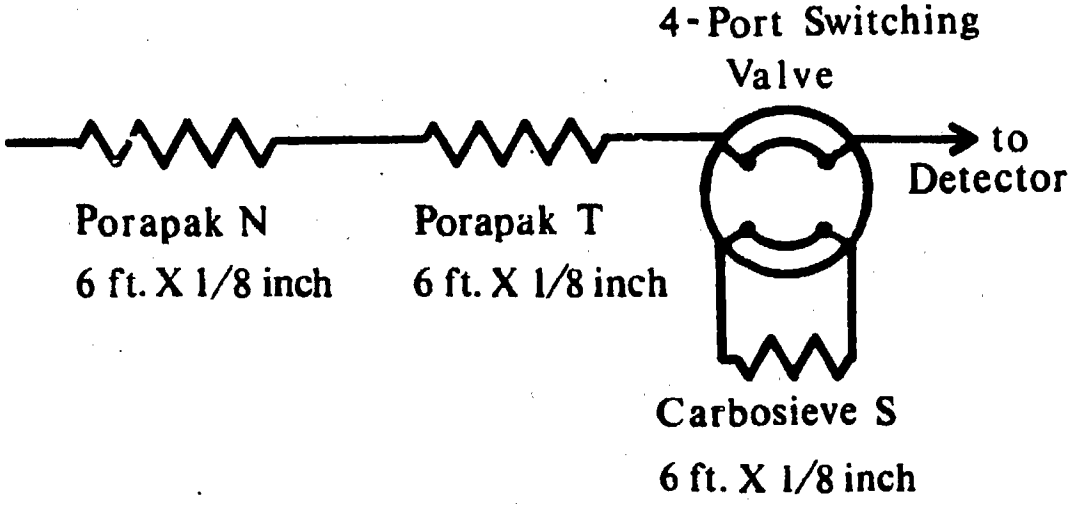

Figure 65. Gas chromatograph analysis system

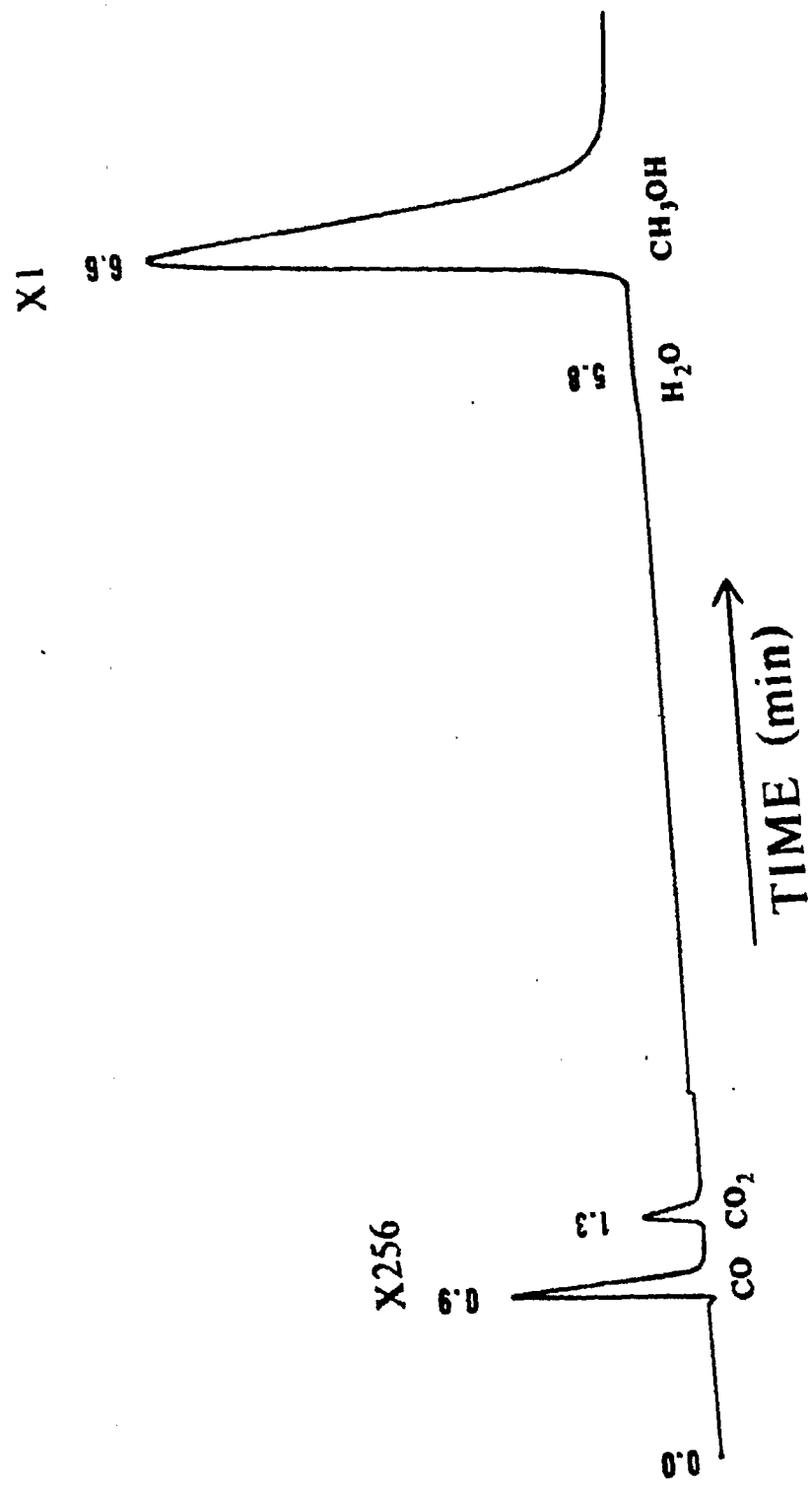

Figure 66. Chromatogram of methanol synthesis effluent

Table 21. Chromatographic operating conditions

Detector:	thermal conductivity
Filament current:	180 mA
Detector temperature:	250°C
Carrier gas:	helium
Carrier flowrate:	30 cc/min
Oven temperature:	150°C

species. Relative molar response factors were determined using prepared mixtures in a gas sampling bulb from which 0.5 cc samples were injected into the gas chromatograph. The response factor for CO was defined as having the value 1.00, and all other response factors were established relative to this value. A known mixture was injected into the gas chromatograph and peak areas measured, repeating the injections enough times to ensure the reproducibility and accuracy of the results. Because carbon monoxide was a component in each mixture, the relative molar response factor for any species could be determined using the relationship:

$$RF_i = (moles_i/moles_{CO})(area_{CO}/area_i)RF_{CO}$$

The exact amount injected did not need to be known since the relative area and relative composition would be independent of sample size. The use of relative response factors avoided problems that arise from variations in operating conditions over a period of time. The details for mixture preparations and chromatographic results have been given in

Appendix F. The relative molar response factors were determined to be 1.15 for CH_3OH, 0.91 for H_2O, 0.98 for CO_2, and 1.10 for N_2.

Safety Considerations

There were several major safety concerns in this study. Both hydrogen and carbon monoxide are hazardous gases; hydrogen is highly flammable and carbon monoxide is toxic and flammable. A continuous carbon monoxide detection system (MSA, Model 571) was incorporated into the high pressure system to close the solenoid valves in all flow lines if the concentration of carbon monoxide exceeded 200 ppm or the concentration of hydrogen exceeded 2000 ppm. The electrochemical sensor was placed at head level on the front side of the rack to provide maximum protection to the operator. In addition, a hand-held carbon monoxide indicator (MSA, MiniCO) provided the flexibility for spot checks and for locating gas leaks.

Carbon monoxide in contact with stainless steel at the pressures and temperatures used in this study can form metal carbonyls which are extremely toxic (Ludlum and Eischens, 1973; Brynestad, 1976). Carbonyl traps consisting of activated alumina at 300°C were placed in the CO feed line and in the exit line before venting to decompose any carbonyls present. The vented gases were sent to an exhaust hood.

The main concern to personnel when using high pressure gases is the danger of flying projectiles in the event of failure of some part of the system. The high pressure section of the system was enclosed on five sides by 1/8-inch thick steel sheet, leaving the top open for maintenance

(mostly to install and remove the reactor) and for gas expansion in the unlikely event of an explosion. The pressure gauge had a blowout back within this section and valves were mounted with only the stems protruding through the steel sheet. The valve stems were anchored to the steel sheet. The pressures in the system were obtained directly from the gas cylinders, requiring that all cylinder pressures had to be above 50 atmospheres. The weakest part of the system was the flow controllers whose maximum operating pressure was rated at 100 atmospheres. Because it was desirable to minimize the amount of CO in the cylinder owing to its toxicity to personnel in the event of a major leak yet also provide a sufficient amount for extended flow experiments at high pressure, a size #2 CO cylinder was chosen. Additional protection was provided to the system by using this cylinder size because the maximum cylinder pressure was 110 atmospheres; if the pressure regulator should fail, exposing the flow controller to the cylinder pressure, the system would still be safe (the 10% overpressure would not be dangerous). Failure of the CO pressure regulator should not be regarded as an unlikely event because it has occurred twice during a two-year period. Most components of the high pressure system have been rated for 200 atmospheres or better.

RESULTS OF IN SITU CHARACTERIZATION

Catalytic Reactivity

Because the catalysts developed for infrared studies had copper contents considerably lower than those in an industrial methanol synthesis catalyst, it was important to determine the activity and selectivity of these various catalysts to verify that they functioned as methanol synthesis catalysts. Activities and selectivities were measured under the same conditions as those used in the high-pressure infrared studies, i.e., a pressure of 50 atm and a temperature of 200°C. Additional studies were made at higher temperatures. Catalyst evaluations were conducted in a fixed-bed tubular reactor containing a bed of broken catalyst wafers surrounded by SiC particles. Silicon carbide was found to have no activity for CO hydrogenation at 50 atm of 2/1 H_2/CO up to a temperature of 250°C. The binary oxides were evaluated with a flow rate of 1800 GHSV and the ternary oxides evaluated with a flow rate of 3600 GHSV, to compensate for the difference in surface areas between the two types of oxides.

The standard procedure for catalyst testing involved heating the catalyst at 200°C overnight in 60 cc/min STP of N_2. The N_2 flow was replaced with a 5% H_2-in-N_2 flow for 1 hr to reduce the oxide. Then the reducing feed was replaced with the reaction feed mixture and the pressure gradually increased to 50 atm. Reaction runs were generally conducted over a period of 8 hrs, taking samples of the reactor effluent periodically to observe changes in activity and selectivity. The effluent was analyzed by gas chromatography using Porapak T and N columns in

series at 150°C and a thermal conductivity detector. The gc output was quantitatively analyzed by a HP 3390A reporting integrator.

Binary catalysts

The selectivity for CO hydrogenation to methanol was 100% for all binary catalysts under the experimental conditions used in these reactions. The effects of catalyst composition, reactor temperature, and feed composition on CO conversion were examined and the results are summarized in Table 22. Pure zinc oxide, either as a precipitated oxide (wet process) or Kadox 25 (dry process), has no measurable activity at 200°C but some activity at 250°C. The reactor system was carefully checked to verify that this low activity was due to the zinc oxide and did not arise from impurities or components of the reactor. The precipitated binary catalysts had comparable activities, which were an order of magnitude higher than pure zinc oxide at 250°C. The impregrated binary catalyst was prepared by adding a copper nitrate solution to Kadox 25, followed by drying and calcination. Unlike the precipitated oxide of some composition, the impregnated catalyst possessed no activity at 200°C. The addition of an oxidizing agent to the feed mixture produced little change in activities at 200°C but significantly improved conversions at 250°C for the precipitated binary catalysts. Carbon dioxide was added as a gas premixed with hydrogen (10% CO_2 in H_2), while water was added by bubbling the H_2/CO mixture through liquid water at high pressure. The reactor effluent from experiments using water in the feed had no water but some carbon dioxide,

Table 22. Reactivity of binary catalysts at 50 atmospheres

Composition ZnO/CuO[a]	CO conversion to CH_3OH (%) 200°C	250°C	Methanol yield (x 10^{-5} moles/m^2/hr) 200°C	250°C
With feed composition H_2/CO = 67/33 vol %				
Kadox 25	0.0	0.6	0.0	0.6
100/0	0.0	0.6	0.0	0.5
95/5	1.6	6.3	1.1	4.5
Imp. 95/5	0.0	–	0.0	–
90/10	1.3	5.2	0.9	3.7
With feed composition $H_2/CO/CO_2$ = 66/28/6.6 vol %				
95/5	0.7	11.4	0.5	8.2
90/10	1.1	15.6	0.8	11.2
With feed composition $H_2/CO/H_2O$ = 67/33/0.5 vol %				
95/5	1.9	8.8	1.4	6.3
90/10	1.1	12.6	0.8	9.0

[a]Mole percent.

indicating that the catalysts had good activity for the water-gas shift reaction:

$$CO + H_2O \rightleftharpoons CO_2 + H_2$$

Methanol yields have been based on BET surface areas; values of 9.1, 20, and 27 m^2/g were used for Kadox 25, precipitated ZnO, and the precipitated binary oxides, respectively.

The initial yield of methanol was generally higher than the steady-state yield (value after 8 hr), usually in the range of 20 to 50% higher. This loss of activity could arise from several causes, and has been examined by taking the transient behavior of 90/10 Zn/Cu

catalyst as an example. The concentrations of CO_2, CH_3OH, and H_2O were measured periodically during the first 8 hr of a reaction run for each of the feed mixtures utilized in these studies; these transients are shown in Figure 67. When a feed of H_2 and CO was used, the initial methanol yield was 50% higher than the steady-state yield. The activity of the catalyst gradually decreased during the transient. At the reaction temperature of 200°C, however, this deactivation is quite slow and thus the activity after 8 hr is relatively good. The small amount of CO_2 in the initial effluent sample most likely arose from the water-gas shift reaction berween CO and some residual water formed previously from the reduction of CuO by H_2. The transient behavior of the effluent components from a reaction run using a feed of CO, H_2, and CO_2 had some significant differences compared to the previous run using a feed of CO and H_2. The initial methanol yield was twice the amount obtained without any CO_2 present, while the amount of CO_2 was approximately one-tenth the feed concentration. The CO_2 concentration returned to the value in the feed and a steady-state methanol yield was established in under 4 hours at a level less than the steady-state value of the reaction with CO and H_2. Water was also a product in the effluent stream. The initial low level of CO_2 arose from absorption by the catalyst; relatively high CO_2 concentrations were found in the effluent from the reactor system following the pressure drop at the end of a reaction run. At steady state, the methanol yield could result from CO hydrogenation and CO_2 hydrogenation; the water could be formed by CO_2 hydrogenation or the water-gas shift reaction. Because the methanol yield was less with a feed containing CO_2 at 200°C, the diffusive

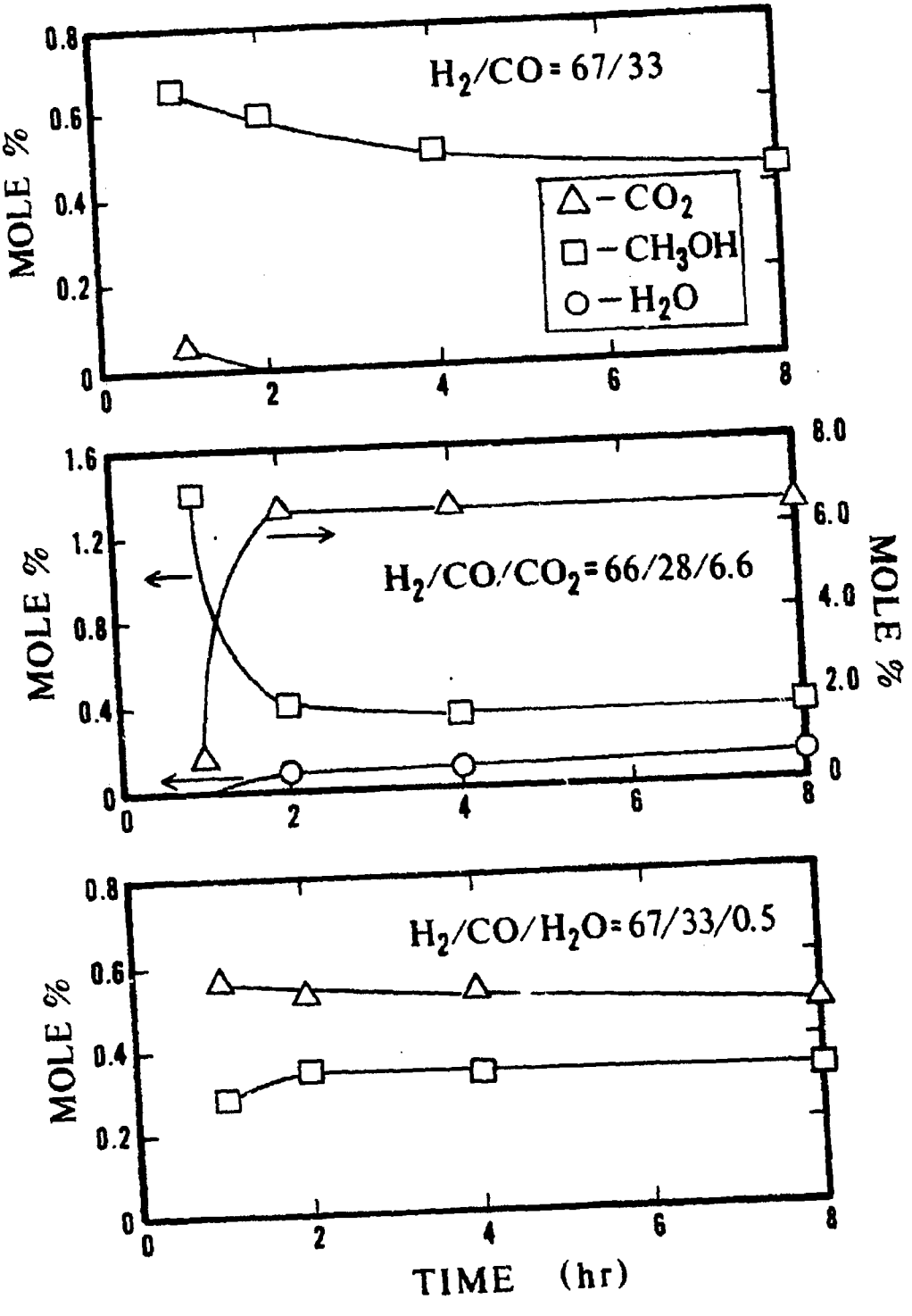

Figure 67. Transient behavior

restrictions caused by CO_2 in the catalyst pores overrode any advantage that CO_2 may provide as a reactant or in preventing deactivation (strong reduction) of active sites.

At 250°C, however, these conditions were reversed; CO_2 had a positive effect on the methanol yield. The feed mixture with water produced effluent concentrations essentially constant over the entire 8-hour period. The methanol yield was approximately the same as the yield obtained from the feed mixture containing CO_2, which is logical since the water in this feed mixture was converted to CO_2 by the water-gas shift reaction. A pressure drop at the end of the reaction run resulted in relatively high levels of CO_2 and H_2O in the effluent, indicating some absorption of these two species. These pressure drops were also used to detect for condensation of methanol, since a pressure decrease would increase the amount of CH_3OH in the gas phase if any condensation had occurred.

Because a formate intermediate has been proposed in methanol synthesis from H_2 and CO, a reaction run was conducted with some 95/5 ZnO/CuO catalyst using a gas feed of H_2/N_2 = 50/50 bubbling through a formic acid solution (73% HCOOH, 27% H_2O) at 50 atm. The reaction,

$$HCOOH + 2H_2 \rightarrow CH_3OH + H_2O$$

went to completion at 200°C. No other reaction products other than methanol were observed.

Ternary catalysts

The selectivity for CO hydrogenation to methanol was 100% for the ternary catalysts at 200°C and > 98% (dimethyl ether was the other product) at 250°C. Because the surface areas of ternary oxides were approximately double the values of binary oxides, the amount of ternary catalyst (by weight) used in reactor tests was half the amount of binary catalysts. The effects of catalyst composition, reaction temperature, and feed composition on conversion to methanol have been summarized in Table 23. In general, the methanol yield per unit surface area was comparable between binary and ternary catalysts. BET surface areas of 49, 58, and 65 m^2/g were used for 90/5/2.5 $ZnO/CuO/Cr_2O_3$, 80/10/5 $ZnO/CuO/Cr_2O_3$, and 80/10/5 $ZnO/CuO/Al_2O_3$, respectively. These results support the observation (Herman et al., 1979) that the primary effect of the addition of Cr_2O_3 or Al_2O_3 to the composition of a binary oxide was to increase activity by increasing the surface area. An exception was the 80/10/5 $ZnO/CuO/Cr_2O_3$ catalyst which exhibited high activity at 200°C (approximately an order of magnitude higher yield per unit surface area than the binary catalyst). Thus, the role of the promoters Cr_2O_3 and Al_2O_3 appears to be electronic as well as physical. The activities of ternary catalysts showed better stability (less deactivation occurred) than binary catalysts. The addition of an oxidizing agent (CO_2 or H_2O) to the H_2/CO feed mixture had little effect on yields at 200°C but increased yields significantly at 250°C, using the yields for 80/10/5 $ZnO/CuO/Al_2O_3$ as the benchmark. Carbon dioxide was also absorbed by the ternary catalysts, as indicated by initially low levels of CO_2 in the reactor effluent and high levels after the pressure drop. These catalysts

Table 23. Reactivity of ternary catalysts at 50 atmospheres

Catalyst composition (mol %) $ZnO/CuO/Cr_2O_3$	Feed composition (vol %) $H_2/CO/CO_2/H_2O$	CO conversion to CH_3OH (%) 200°C	250°C	Methanol yield[a] (x 10^{-5} mol/m^2/hr) 200°C	250°C
90/5/2.5	66/28/6.6/0	0.9	10.7	0.5	6.4
80/10/5	65/33/0/0	7.8	13.8	4.8	8.4
80/10/5	67/33/0/0.1	1.8	11.0	1.1	6.7
$ZnO/CuO/Al_2O_3$					
80/10/5	67/33/0/0	0.8	3.7	0.4	2.0

[a] $\text{Yield} = \dfrac{(\text{molar flowrate})(\text{fraction CO in feed})(\text{fraction CO to } CH_3OH)}{(\text{weight catalyst})(\text{surface area catalyst})}$

were also active for the water-gas shift reaction, converting small amounts of water to carbon dioxide (the conversion has been expressed in this manner because the amounts of water and carbon dioxide can be measured more accurately than hydrogen or carbon monoxide).

The activity of the 80/10/5 $ZnO/CuO/Cr_2O_3$ catalyst was evaluated for converting formic acid to methanol. At 200°C and 250°C, no activity for methanol synthesis was observed using a gaseous mixture of 50/50 H_2/N_2 bubbling through a solution of formic acid (73% HCOOH, 27% H_2O) at 50 atm.

Infrared Spectra at High Pressure

Gaseous carbon monoxide

The high pressure cell was used initially to determine the extent to which gaseous carbon monoxide adsorbed infrared radiation in the wavelength region near 2143 cm^{-1} and to determine the effect of pressure on the spectra. The contribution by gaseous carbon monoxide to the spectrum can be subtracted to reveal the presence of adsorbed carbon monoxide on a catalyst surface only if the transmittance is nonzero. The effect of increasing pressure on the spectrum of gaseous carbon monoxide is shown in Figure 68. Each spectrum was produced by taking 500 scans at 0.24 cm^{-1} resolution. The results demonstrated that a very short pathlength was required to avoid total absorption by gaseous carbon monoxide. The transmittance in the region of 2180 cm^{-1} at a pressure of 70 atm. was close to 10% for a pathlength of 0.4 mm. These spectra demonstrated the need for an accurate reference spectrum in order to correct for

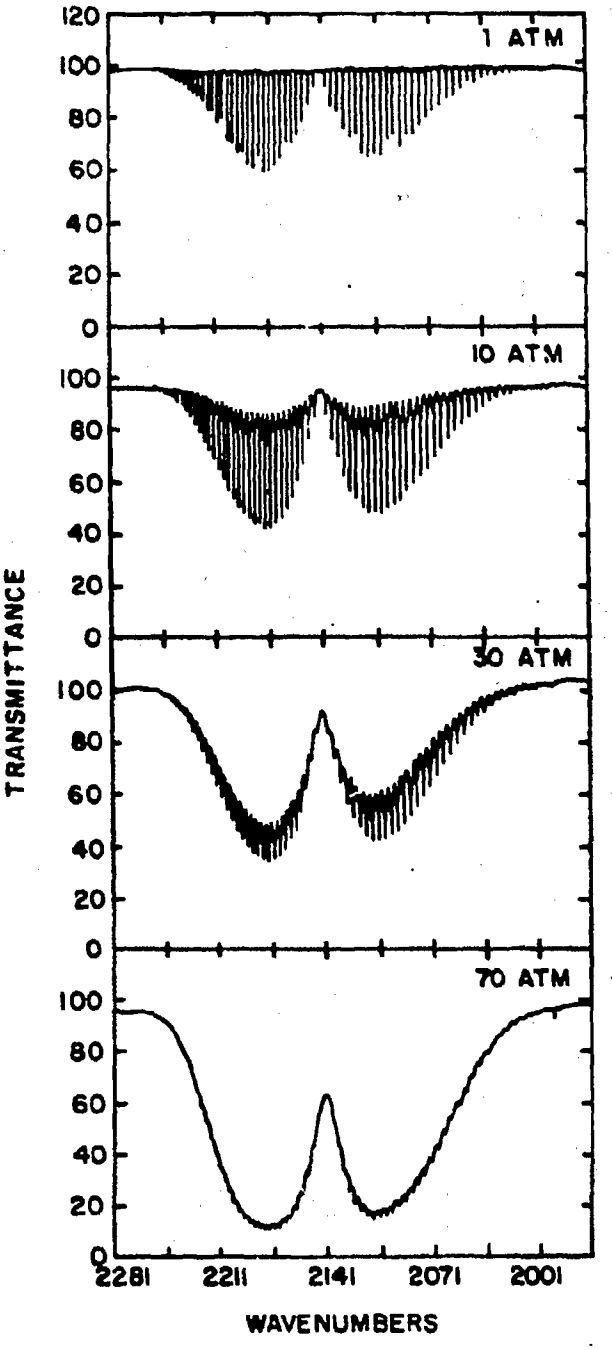

Figure 68. Infrared spectra of gaseous CO

absorption by gaseous carbon monoxide since the shape of the rotational-vibrational bands was a strong function of the pressure. The additional complications arising from the variability in sample background absorptions and the various wafer thicknesses made it impractical to subtract the effect of gaseous carbon monoxide from the spectra of metal oxides during in situ studies.

Species on zinc oxide

Although zinc oxide was inactive for methanol synthesis at 200°C, spectra of adsorbed species can be helpful for identifying which intermediates on mixed metal oxides would be adsorbed on zinc sites. The effect of pressure on the nature of surface species on zinc oxide (Kadox 25, New Jersey Zinc Company) at 200°C was established for pressures from 1 to 50 atmospheres of carbon monoxide. Each spectrum has had the background (zinc oxide) subtracted and was produced by taking 100 scans at 1.0 cm^{-1} resolution. The spectra of adsorbed species on zinc oxide are shown in Figure 69. Bands at 1580 and 1363 cm^{-1} (1 atm) were assigned to the asymmetric and symmetric C-O stretching bands, respectively, of a surface formate species. As the pressure was raised to 50 atmospheres, the asymmetric band shifted toward lower wavenumbers and the symmetric band shifted to 1366 cm^{-1}. The band at 1377 cm^{-1} has been assigned to the C-H bending frequency of a surface formate species. The band appearing at 1688 cm^{-1} and shifting to 1678 cm^{-1} at 50 atmospheres has been assigned to zinc hydride species which Boccuzzi (1978b) had designated as Band III; no additional bands were observed in this region of the spectra. A strong band at 2867 cm^{-1}, shifting to

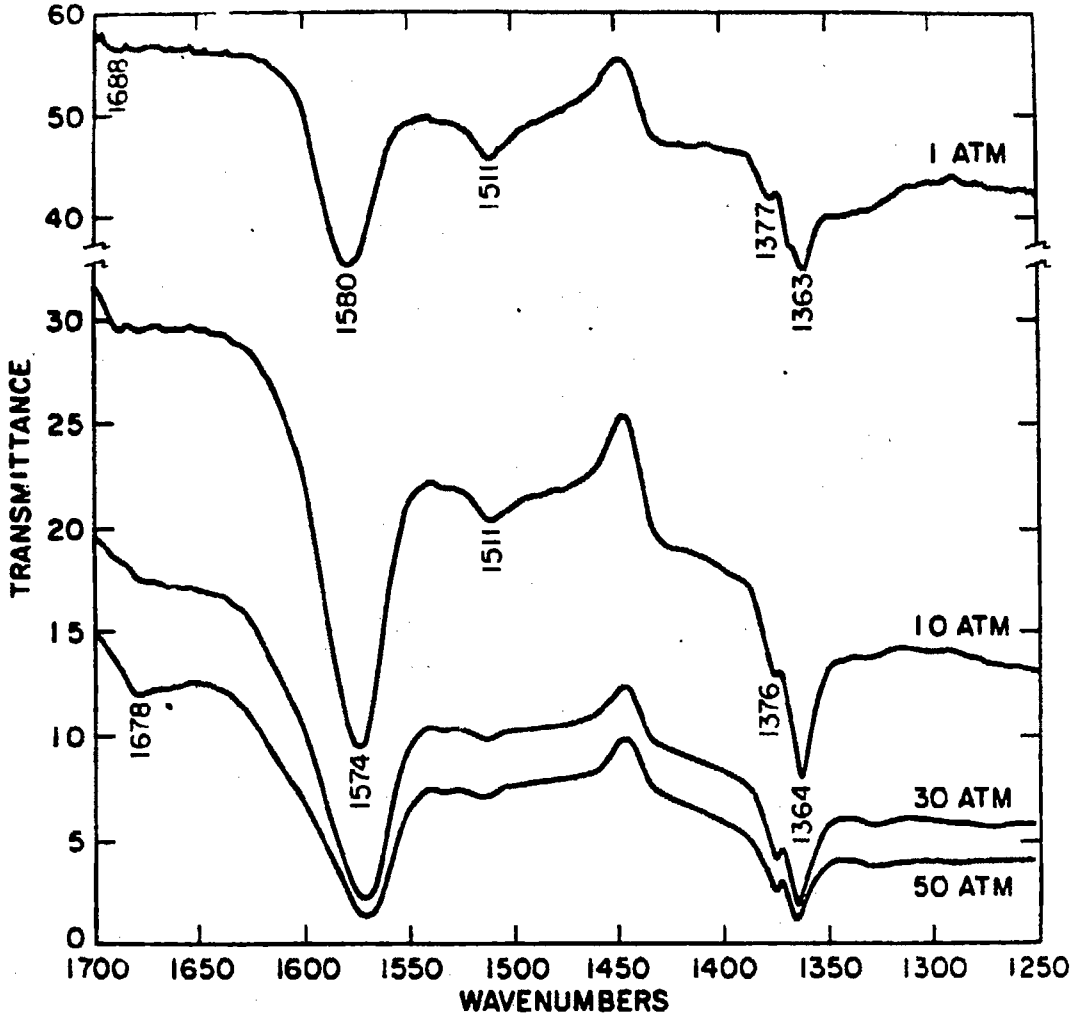

Figure 69. Infrared spectra of adsorbed CO on ZnO

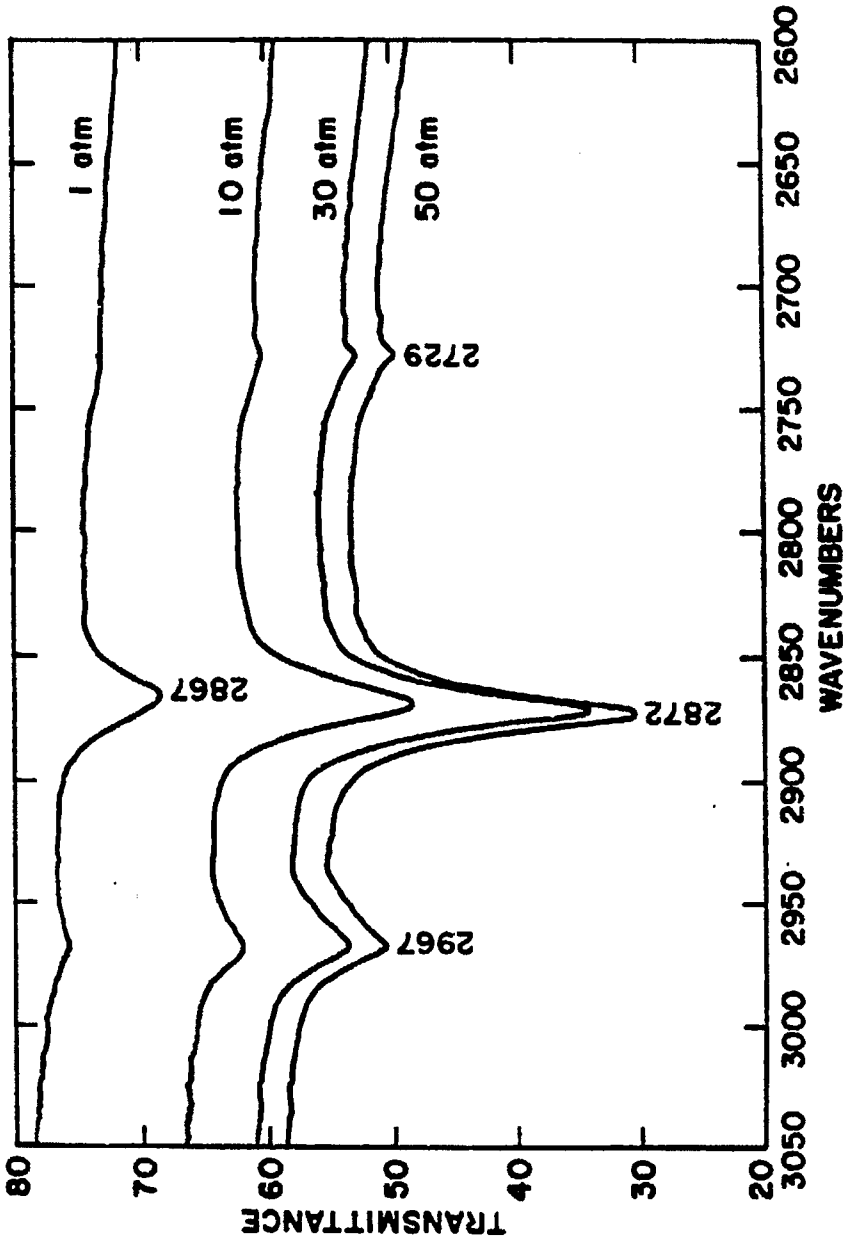

Figure 69. Continued

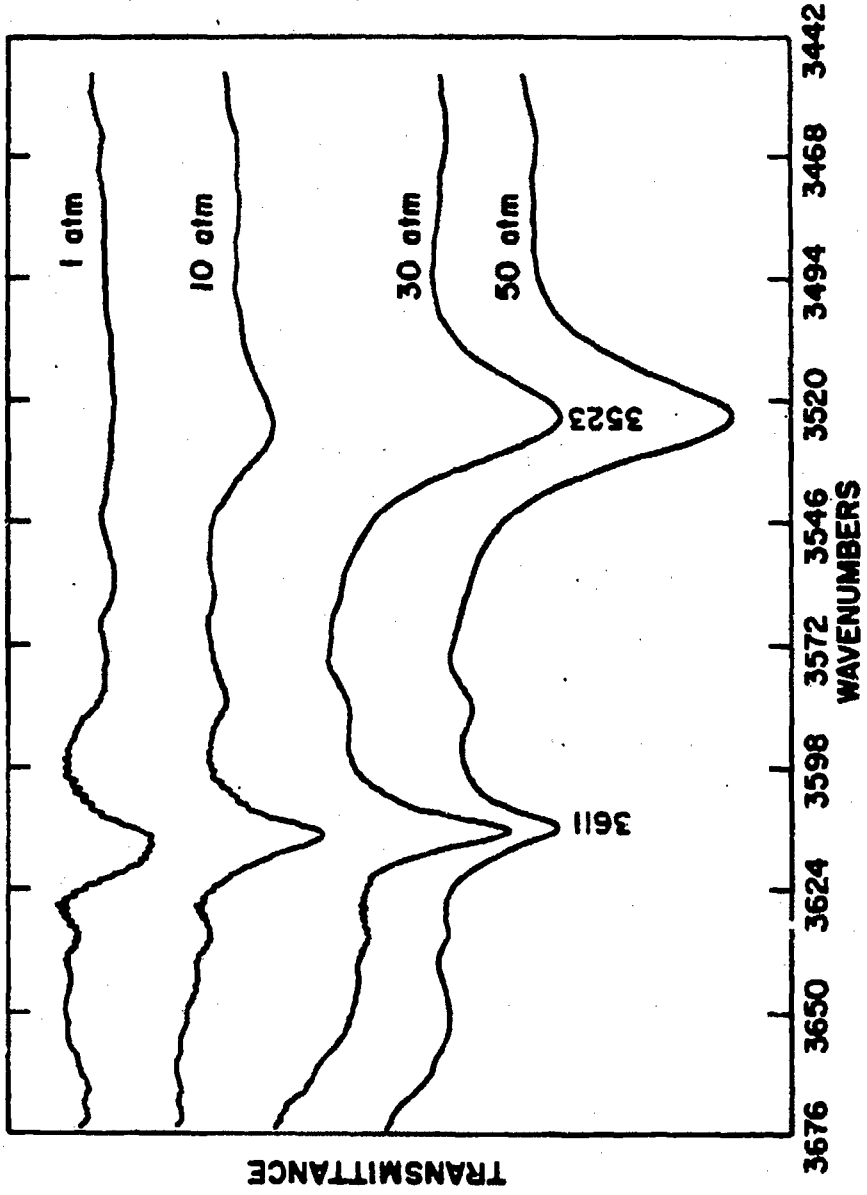

Figure 69. Continued

higher wavenumbers with increasing pressure, which was assigned to the C-H stretching frequency of the formate species. The bands appearing at 2967 and 2729 cm^{-1} have been assigned to combinations of fundamental frequencies; the 2967 cm^{-1} band is a combination of the 1570 and 1377 cm^{-1} bands of the formate species while the 2729 cm^{-1} band is a combination of the 1366 and 1377 cm^{-1} bands of the formate species. A strong band at 3523 cm^{-1} was attributed to a surface hydroxyl group having greater stability at higher pressures. Because the spectrum of zinc oxide was subtracted from each adsorption spectrum, the normal residual hydroxyl groups on zinc oxide have been removed. However, there was a shift in the residual hydroxyl species at 3620 cm^{-1} toward lower wavenumbers as the pressure increased, resulting in the appearance of the hydroxyl band seen at 3611 cm^{-1}.

Species on binary catalysts

The binary catalysts with Zn/Cu ratios of 95/5 and 90/10 were satisfactory for infrared investigations. Although the transmittance was very poor, some information was also obtained from a 85/15 Zn/Cu catalyst. Binary catalysts with copper contents above the 15/85 Cu/Zn ratio were unsatisfactory for transmission infrared studies in both oxidized and reduced states. All of these catalysts had a significant transmittance loss at lower wavenumbers during in situ studies. The experimental results for all binary compositions were not presented because the infrared spectra of adsorbed species on these catalysts were qualitatively quite similar under equal experimental conditions.

The adsorption of carbon monoxide on a 95/5 Zn/Cu catalyst (pre-

treatment #1) at 200°C and 50 atmospheres is shown in Figure 70. Prolonged exposure reduced the catalyst, indicated by the formation of the hydroxyl band at 3252 cm^{-1}. Formate groups (bands at 2969, 2878, 2731, and 1573 cm^{-1}) developed first, then an adsorbed formaldehyde species (bands at 2935, 2834, 2731, and 1660 cm^{-1}) was formed. At high pressure, the Type I hydroxyl species (band at 3520 cm^{-1}) gradually emerged as a stable surface species. The residual hydroxyl group originally at 3620 cm^{-1} shifted to 3611 cm^{-1} and the carbonyl band shifted to 1975 cm^{-1}.

The hydrogenation of surface species was accelerated by incorporating hydrogen with the carbon monoxide feed. Figure 71 shows the adsorption of a mixture of carbon monoxide and hydrogen (CO/H_2 = 9/1) on a 95/5 Zn/Cu catalyst (pretreatment #1) at 200°C and 50 atmospheres. Initially formate groups (band at 2879 cm^{-1}) and the hydroxyl of reduction (band at 3252 cm^{-1}) were formed. The development of methoxy groups (bands at 2934 and 2822 cm^{-1}) was accompanied by the disappearance of the isolated hydroxyl groups (bands at 3660 and 3612 cm^{-1}). The formate band shifted significantly from 2879 to 2868 cm^{-1}, owing to the presence of methoxy groups.

The adsorption of a 2/1 H_2/CO mixture on 95/5, 90/10, and 85/15 Zn/Cu catalysts at 200°C and 50 atmospheres after an hour of exposure is shown in Figure 72. At these conditions, very little detail could be observed at lower wavenumbers because of low transmittance. The surface condition was representative of the surface species during methanol synthesis. These spectra showed the hydroxyl of reduction (band at 3252 cm^{-1}), methoxy groups (bands at 2933 and 2822 cm^{-1}), and the formate species (bands at 2865 and 1575 cm^{-1}) in addition to

Figure 70. Carbon monoxide adsorption on 95/5 Zn/Cu oxide at 50 atm

a) oxidized surface

b) exposure for 8 hours

c) exposure for 24 hours

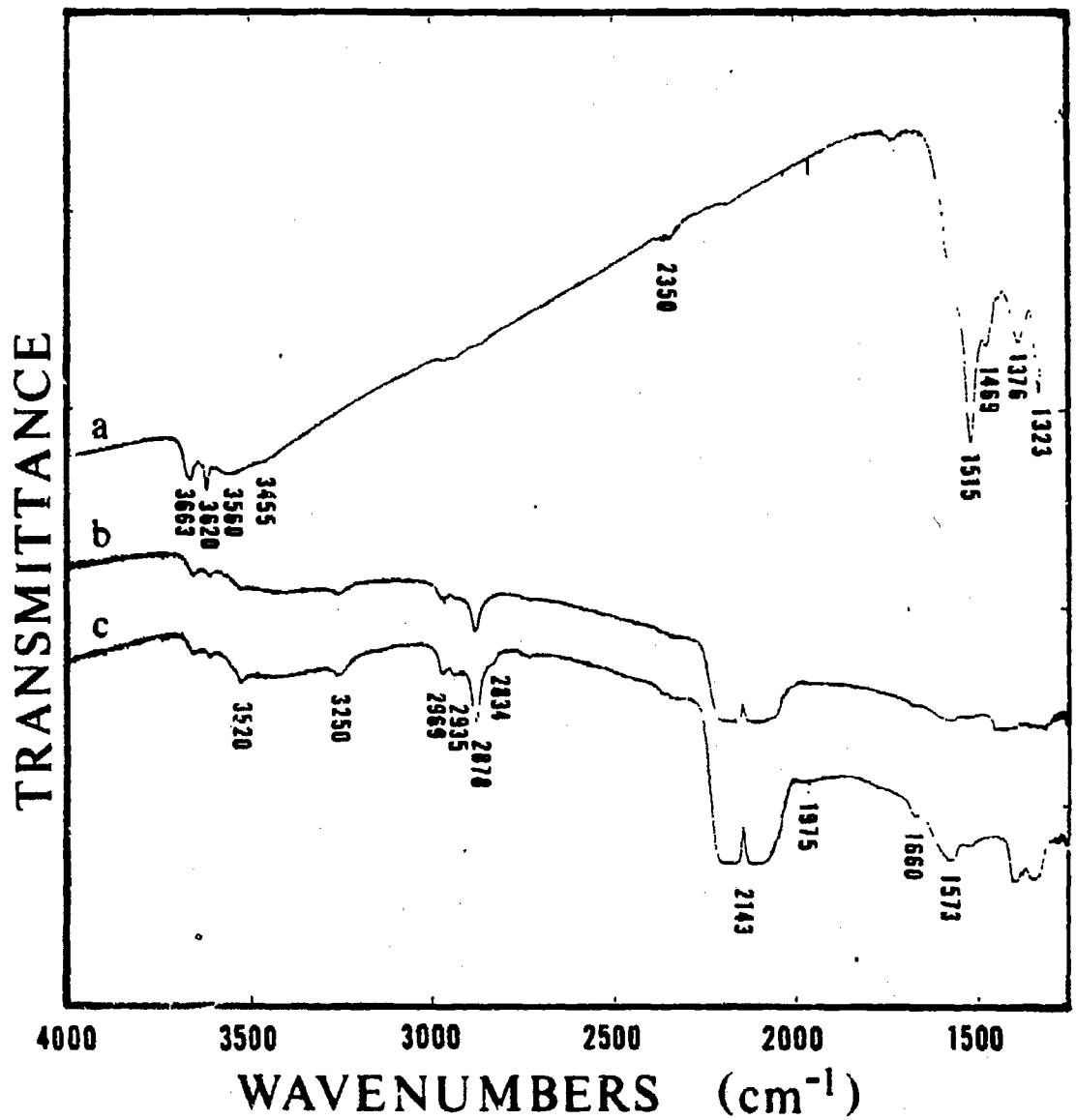
TRANSMITTANCE
a
b
c
3455
3550
3620
3693
2350
1515
1469
1376
1323
3520
3250
2959
2855
2814
2078
2143
1975
1660
1573
4000
3500
3000
2500
2000
1500
WAVENUMBERS (cm-1)

Figure 71. Adsorption of CO-H_2 mixture on 95/5 Zn/Cu oxide at 50 atm

a) oxidized surface

b) exposure for 15 minutes

c) exposure for 1 hour

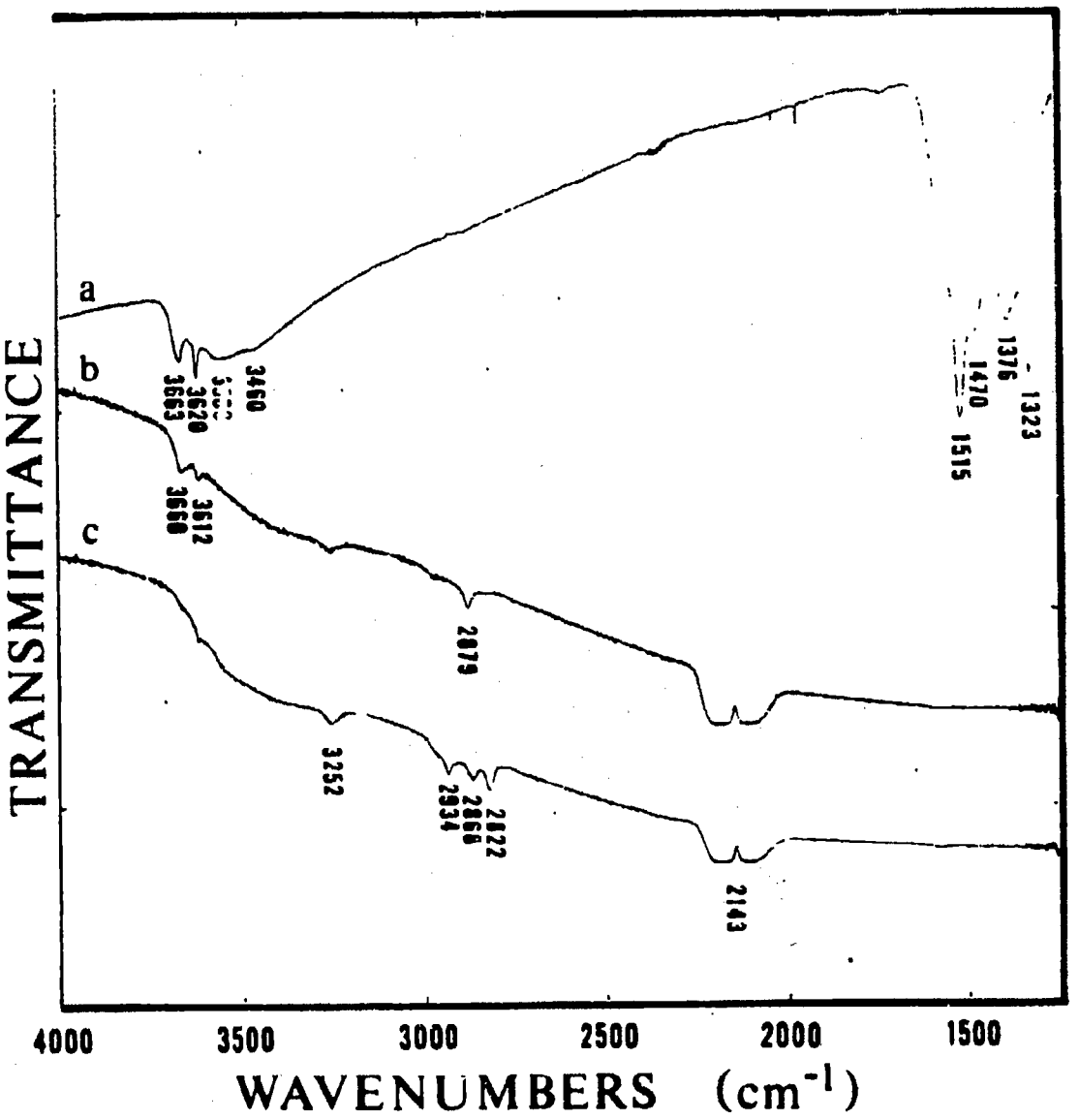
a
b
c
3663
3520
3460
3660
3612
2079
3252
2934
2866
2822
2143
1595
1470
1376
1323
TRANSMITTANCE
4000
3500
3000
2500
2000
1500
WAVENUMBERS (cm-1)

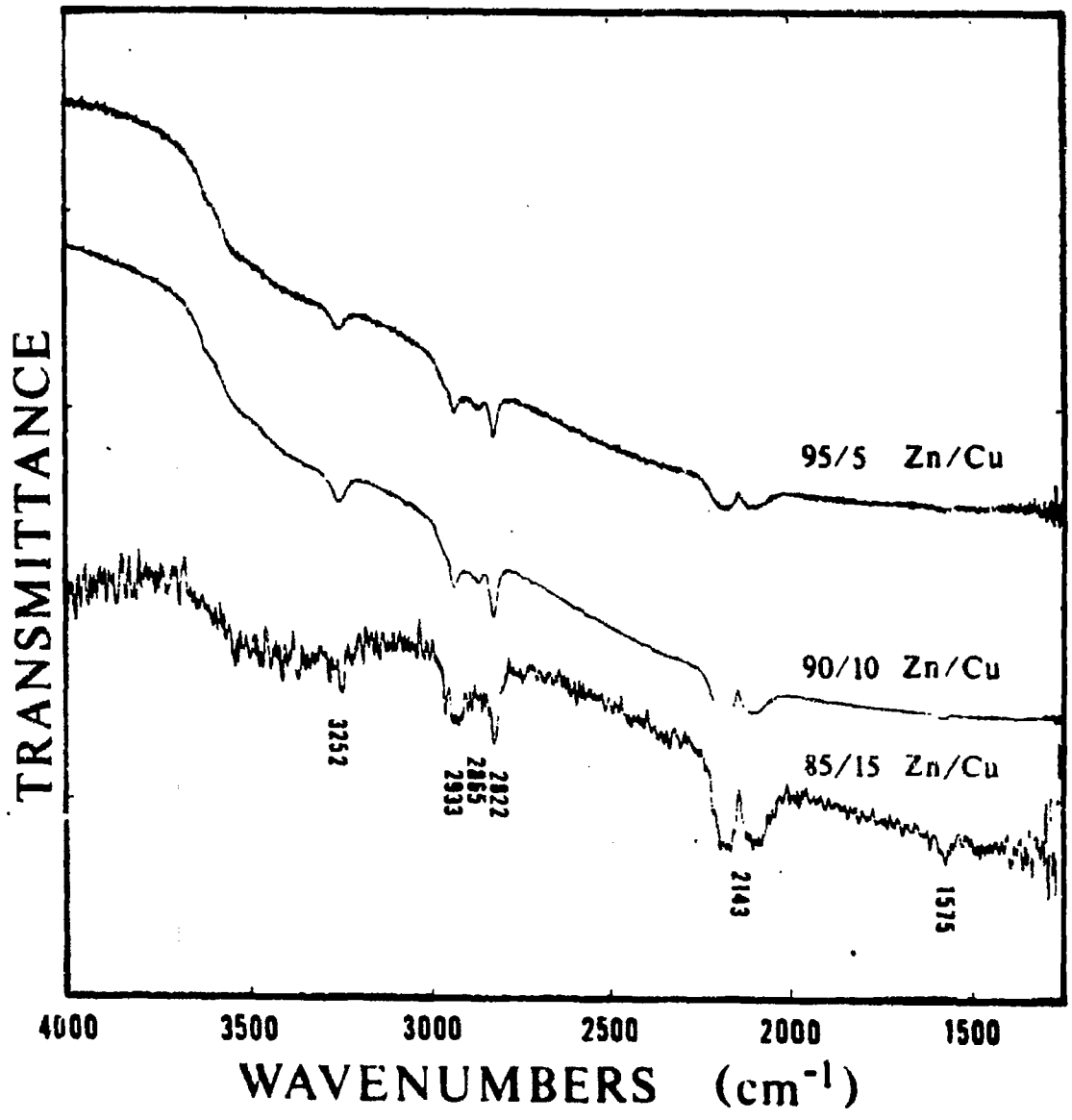

Figure 72. Adsorption of $CO-H_2$ mixture on binary oxides at 50 atm

the bands for gaseous carbon monoxide (band at 2143 cm^{-1}).

Because methanol synthesis normally includes some carbon dioxide in the feed mixture, the adsorption of a 27/7/66 $CO/CO_2/H_2$ mixture on 95/5 Zn/Cu catalyst (pretreatment #3) at 200°C and 50 atmospheres was examined. Surface species at high pressure were identical with those using only hydrogen and carbon monoxide in the feed. Figure 73 shows that after the pressure was dropped to 1 atmosphere, some decomposition of methoxy groups (bands at 2934 and 2826 cm^{-1}) occurred. After the cell had been thoroughly flushed with nitrogen, greater detail of surface groups was revealed. Further decomposition of methoxy groups restored the isolated hydroxyl groups (bands at 3663 and 3614 cm^{-1}), revealed a Type I hydroxyl species (band at 3524 cm^{-1}), a carbonyl group (band at 2010 cm^{-1}), an adsorbed formaldehyde species (bands at 2938, 2830, 2737, and 1616 cm^{-1}), and bidentate carbonate groups (bands at 1516 and 1327 cm^{-1}). The presence of some carbon dioxide (band at 2350 cm^{-1}) in the spectrum without the vibrational-rotational lines indicated that the carbon dioxide was trapped in the catalyst pores.

Methanol synthesis also occurred when formic acid solution was used in a hydrogenating feed stream. Figure 74 shows the spectrum of the adsorption of formic acid solution (73% HCOOH, 27% H_2C) in a carrier gas of 50% H_2-50% N_2 on a 95/5 Zn/Cu catalyst at 200°C and 47 atmospheres. The surface species during formic acid hydrogenation were very similar to those during carbon monoxide hydrogenation except for the lack of gaseous CO or any surface carbonyl species. The surface had some methoxy groups (bands at 2934 and 2820 cm^{-1}), formate groups (bands at 2868 and

Figure 73. Adsorption of $CO-CO_2-H_2$ mixture on 95/5 Zn/Cu oxide at 50 atm

a) exposure for 4 hours and pressure drop

b) 15-minute flush with nitrogen

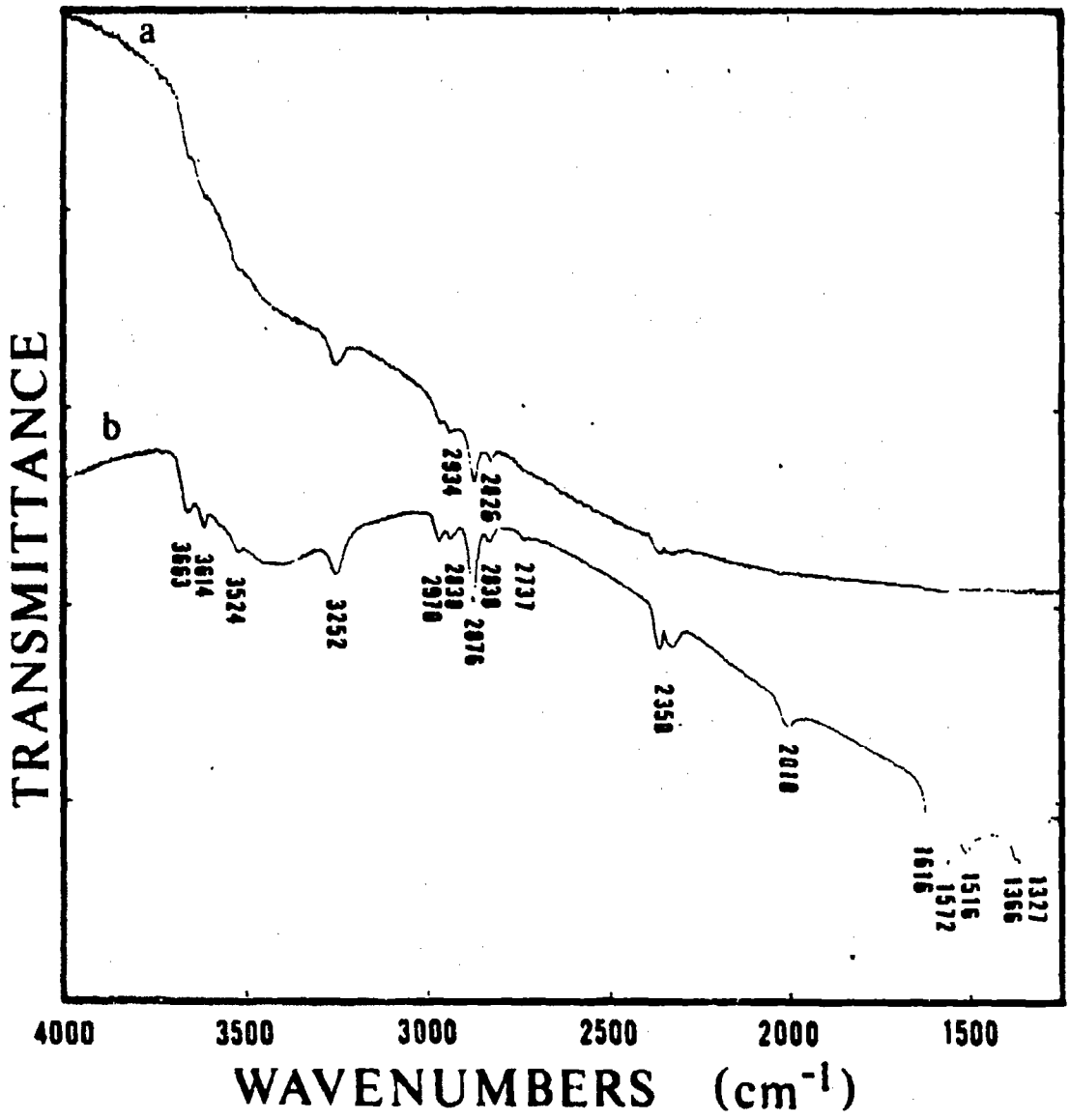
a
b
TRANSMITTANCE
4000
3500
3000
2500
2000
1500
WAVENUMBERS (cm-1)
3660
3614
3524
3252
2934
2826
2930
2870
2137
2350
2018
1616
1572
1516
1366
1327

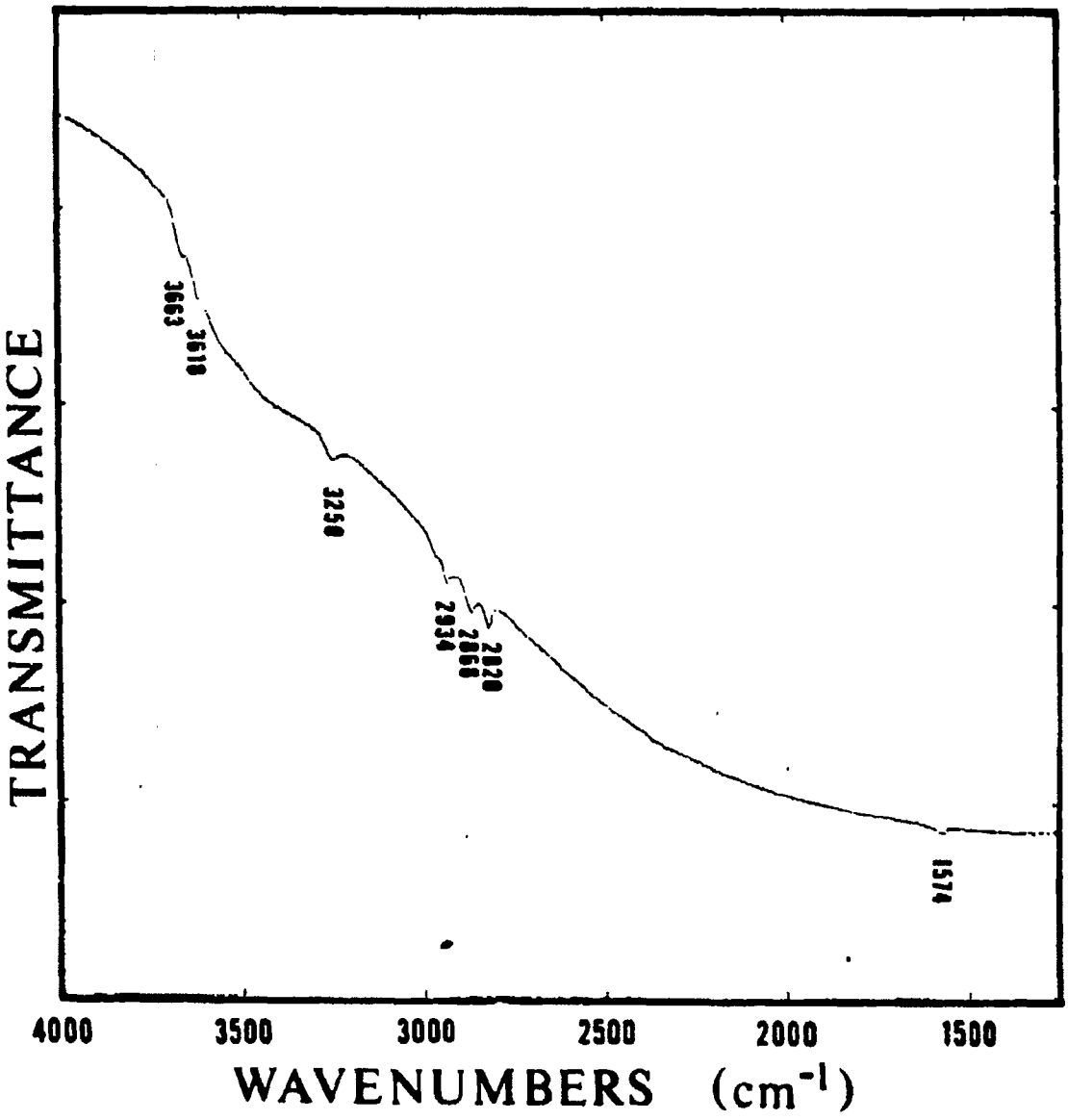

Figure 74. Adsorption of formic acid on 95/5 Zn/Cu oxide at 47 atm

1574 cm^{-1}), the hydroxyl of reduction (band at 3250 cm^{-1}), and isolated hydroxyl groups (bands at 3663 and 3618 cm^{-1}).

Species on ternary catalysts

The zinc-copper-chromium oxide catalysts were superior to binary catalysts in high-pressure infrared experiments because the transmittance remained high throughout the mid-infrared range. Better surface detail provided more information for identifying adsorbed species during methanol synthesis conditions.

The reaction of carbon monoxide and hydrogen on a 90/5/5 Zn/Cu/Cr catalyst at 200°C and 50 atmospheres is shown in Figure 75. The initial surface species on the reduced catalyst (pretreatment #3) after exposure to a 2/1 H_2/CO mixture were formate groups (bands at 2963, 2872, 1582, 1381, and 1360 cm^{-1}), adsorbed formaldehyde species (bands at 2934 and 2843 cm^{-1}), and methoxy groups (bands at 2934 and 2824 cm^{-1}). The adsorbed formaldehyde species disappeared and the amount of methoxy groups had maximized in an hour, followed by a gradual decrease in methoxy groups. A pressure drop to 1 atmosphere revealed an adsorbed carbonyl species at 2010 cm^{-1}.

Because the decrease over time of methoxy groups might have occurred owing to severe reduction of the catalyst, a similar experiment was conducted at the same conditions except that the 2/1 H_2/CO mixture was passed through the high-pressure saturator containing distilled water. Figure 76 shows the same general behavior of adsorbed species as the previous experiment without any water in the feed. The initial spectrum did not have any adsorbed formaldehyde and the final spectrum

Figure 75. Adsorption of CO-H_2 mixture on 90/5/5 Zn/Cu/Cr oxide at 50 atm

a) exposure for 15 minutes

b) exposure for 30 minutes

c) exposure for 8 hours

d) after pressure drop

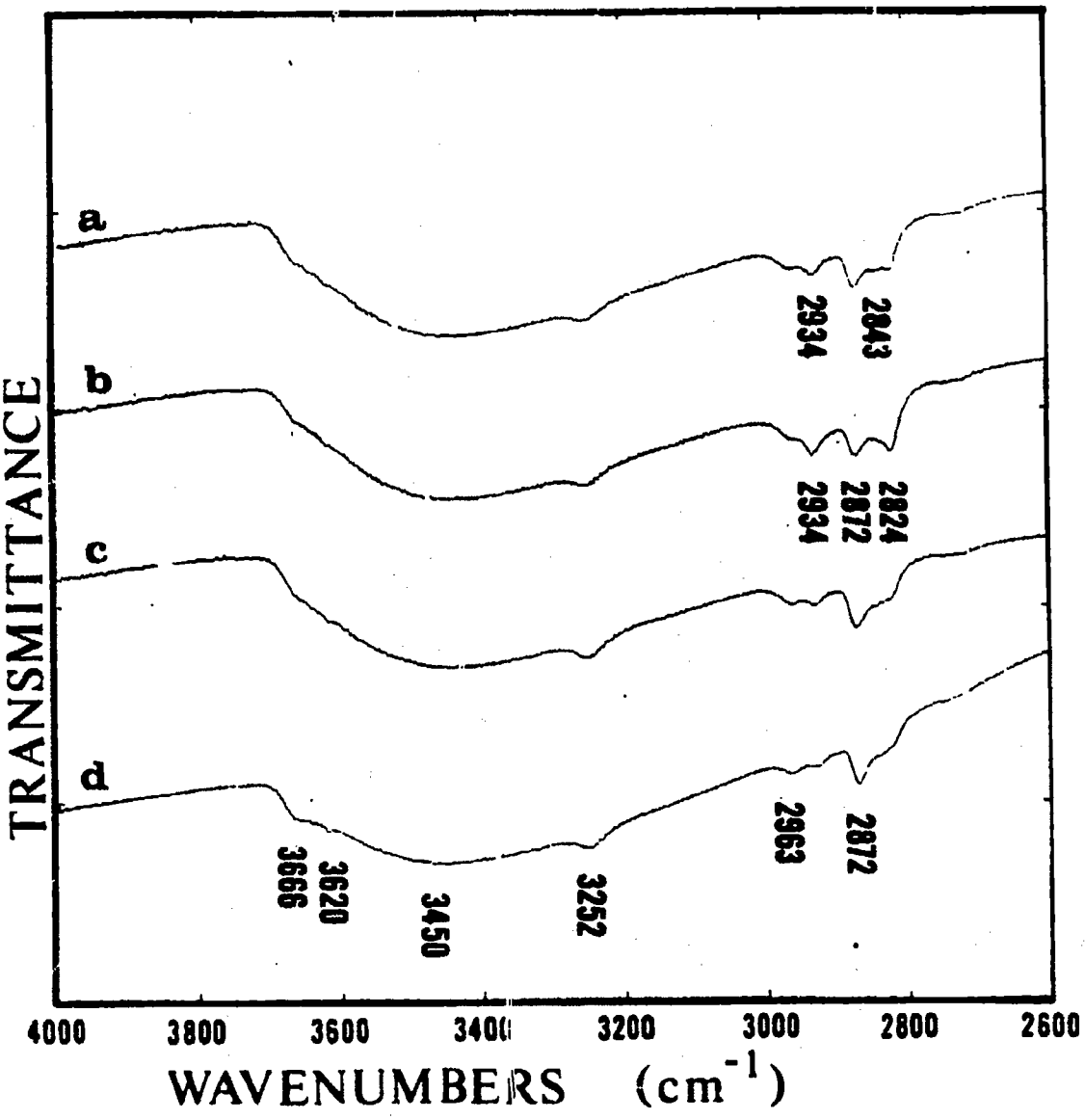
a
b
c
d
2934
2843
2824
2872
2934
3666
3620
3450
3252
2963
2872
TRANSMITTANCE
4000
3800
3600
3400
3200
3000
2800
2600
WAVENUMBERS (cm-1)

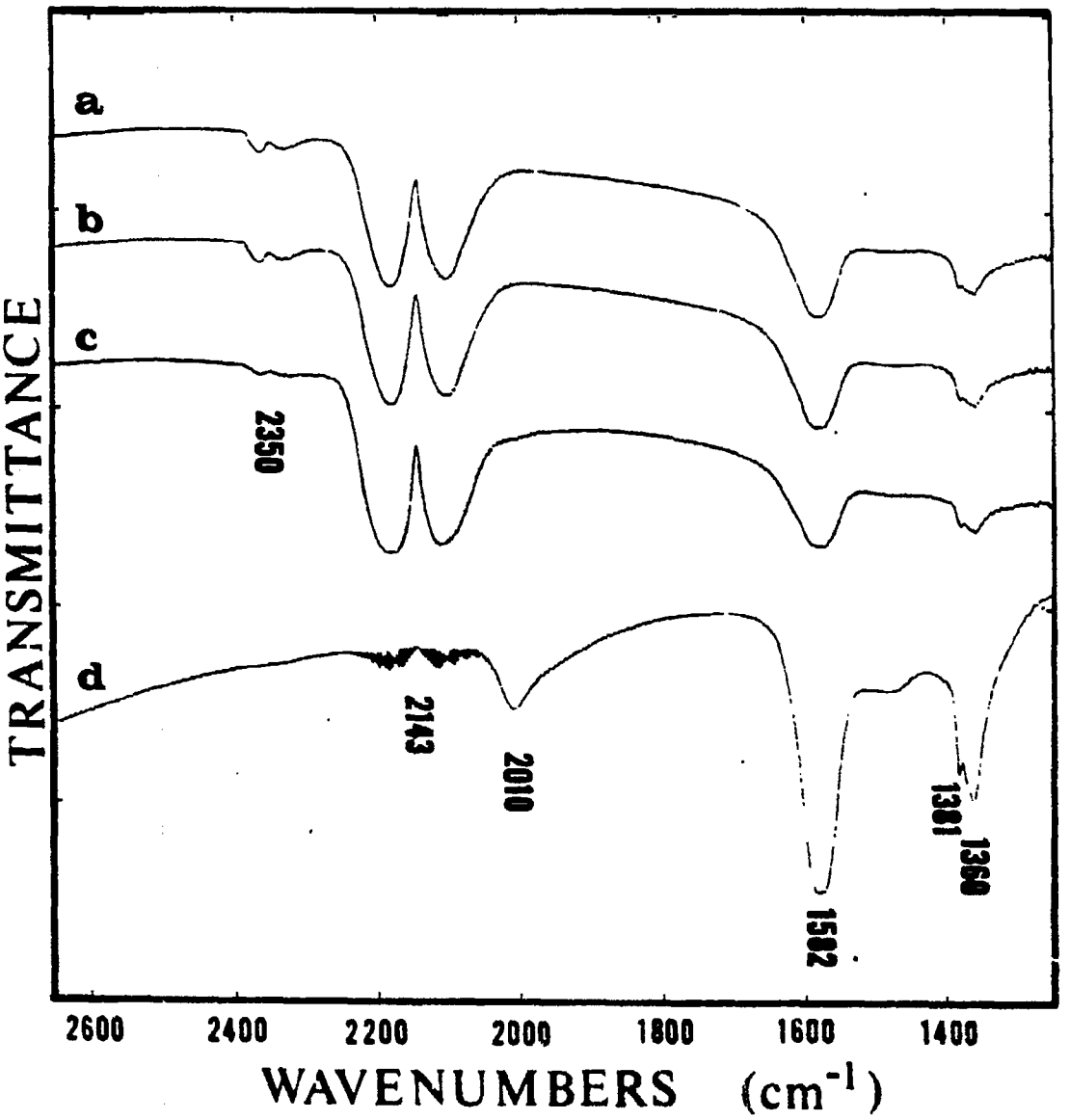

Figure 75. Continued

Figure 76. Adsorption of CO-H_2-H_2O on 90/5/5 Zn/Cu/Cr oxide at 50 atm

a) exposure for 15 minutes

b) exposure for 1 hour

c) exposure for 8 hours

d) after pressure drop

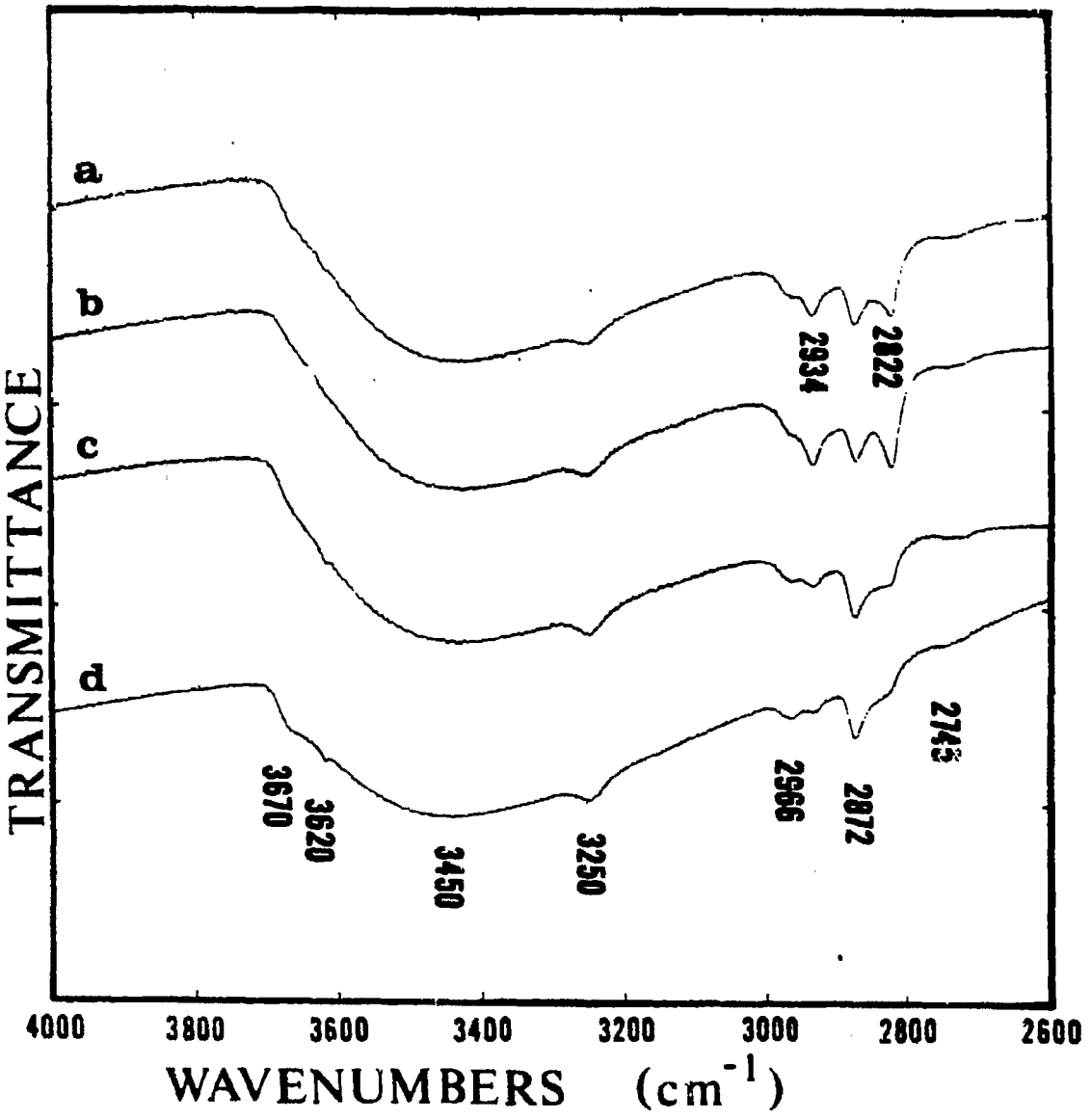
a
b
c
d
2934
2822
3670
3620
3450
3250
2966
2872
2743
TRANSMITTANCE
4000
3800
3600
3400
3200
3000
2800
2600
WAVENUMBERS (cm-1)

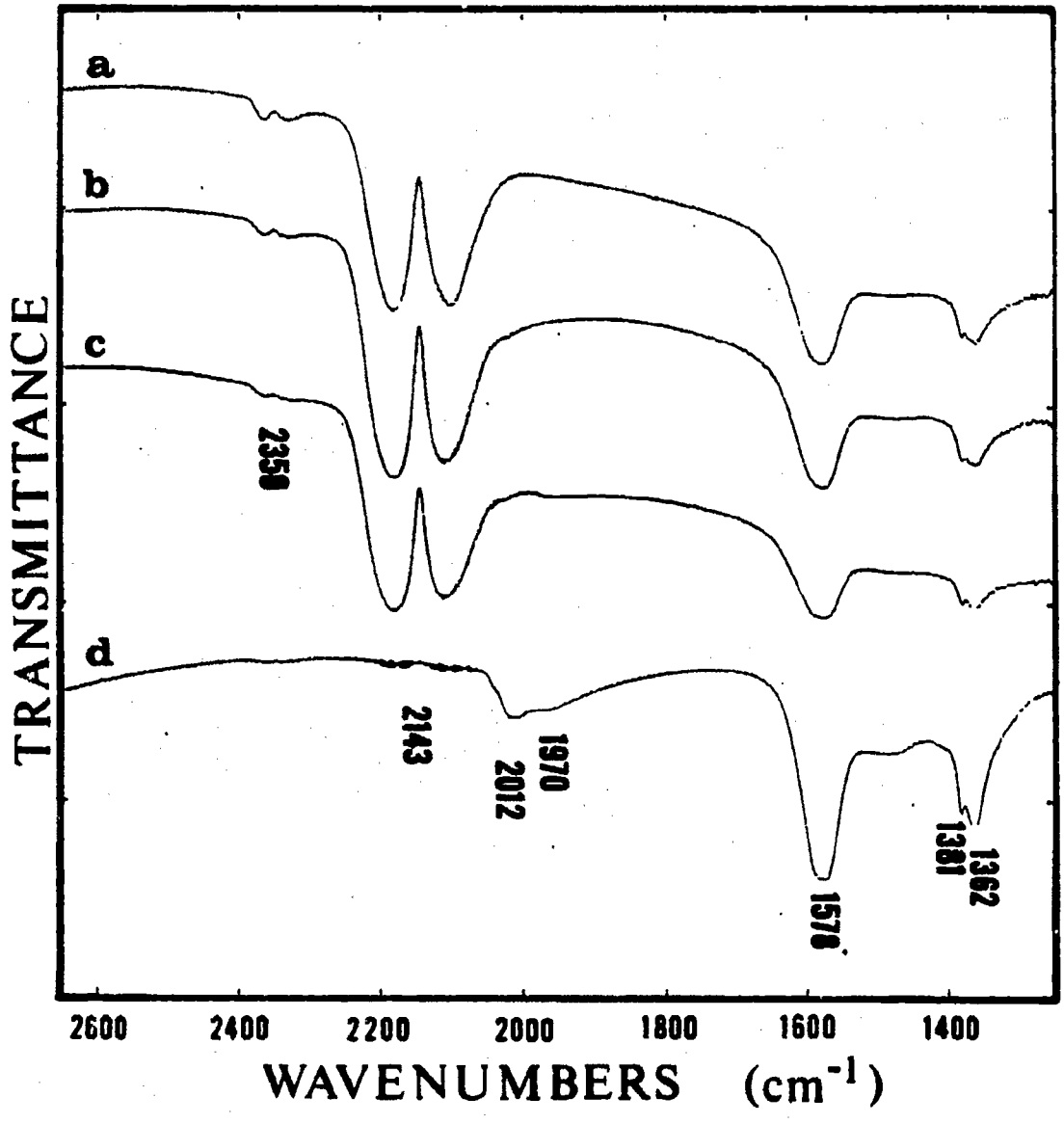

Figure 76. Continued

revealed carbonyl groups at 2012 and 1970 cm^{-1}.

The reaction of carbon monoxide and hydrogen (H_2/CO = 2/1) on a 80/10/10 Zn/Cu/Cr catalyst (pretreatment #3) at 200°C and 50 atmospheres is shown in Figure 77. The initial spectrum showed formate groups (bands at 2870, 1576, 1381, and 1360 cm^{-1}), methoxy groups (bands at 2932 and 2822 cm^{-1}), and a carbonyl species at 2089 cm^{-1}. The methoxy groups increased and reached a stable concentration as steady-state conditions were approached. The carbonyl species shifted from 2089 to 2021 cm^{-1}. A pressure drop to 1 atmosphere revealed in sharper detail the carbonyl species (band at 2010 cm^{-1}).

The reactor tests established that although a binary catalyst was active for formic acid hydrogenation to methanol, the 80/10/10 Zn/Cu/Cr catalyst was inactive for this reaction during the same operating conditions. The adsorption of formic acid solution (73% HCOOH, 27% H_2O) in a carrier gas of 50% H_2-50% N_2 on a 80/10/10 Zn/Cu/Cr catalyst (pretreatment #3) at 200°C and 50 atmospheres is shown in Figure 78. Initially, the surface species were a carbonyl species (band at 1983 cm^{-1}) with minor amounts of formate groups (bands at 2872, 1580, 1381, and 1360 cm^{-1}). Prolonged exposure began to produce some methoxy groups (bands at 2934 and 2818 cm^{-1}), but not much since the isolated hydroxyl groups (bands at 3668 and 3618 cm^{-1}) were not completely displaced. At high pressure, the decomposition of formic acid into formate and methoxy groups on zinc-copper-chromium oxides was unfavorable, hence, the poor methanol synthesis activity.

Figure 77. Adsorption of CO-H_2 mixture on 80/10/10 Zn/Cu/Cr oxide at 50 atm

a) exposure for 15 minutes

b) exposure for 1 hour

c) exposure for 4 hours

d) after pressure drop

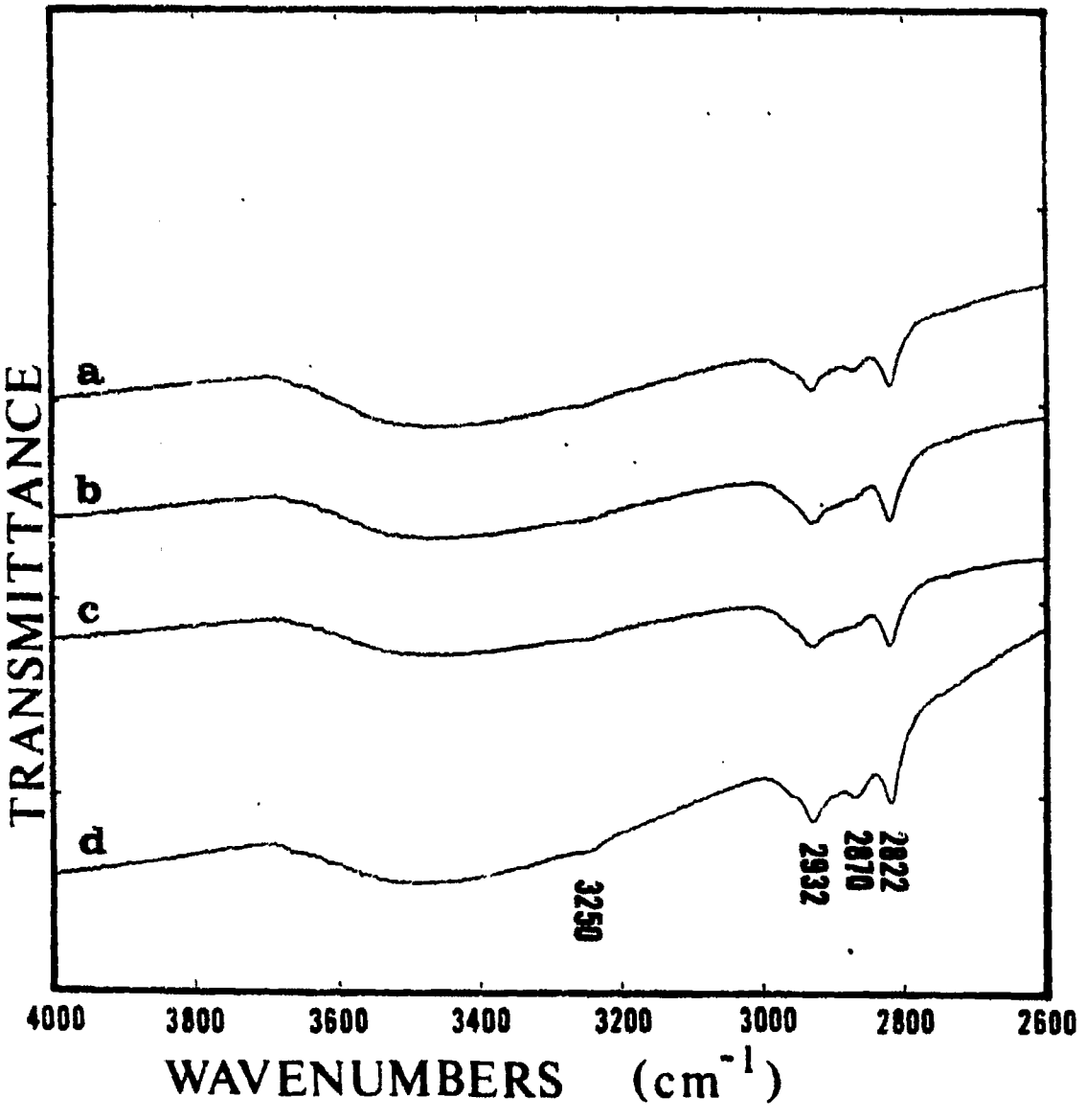
TRANSMITTANCE
a
b
c
d
3250
2932
2870
2822
4000
3800
3600
3400
3200
3000
2800
2600
WAVENUMBERS (cm-1)

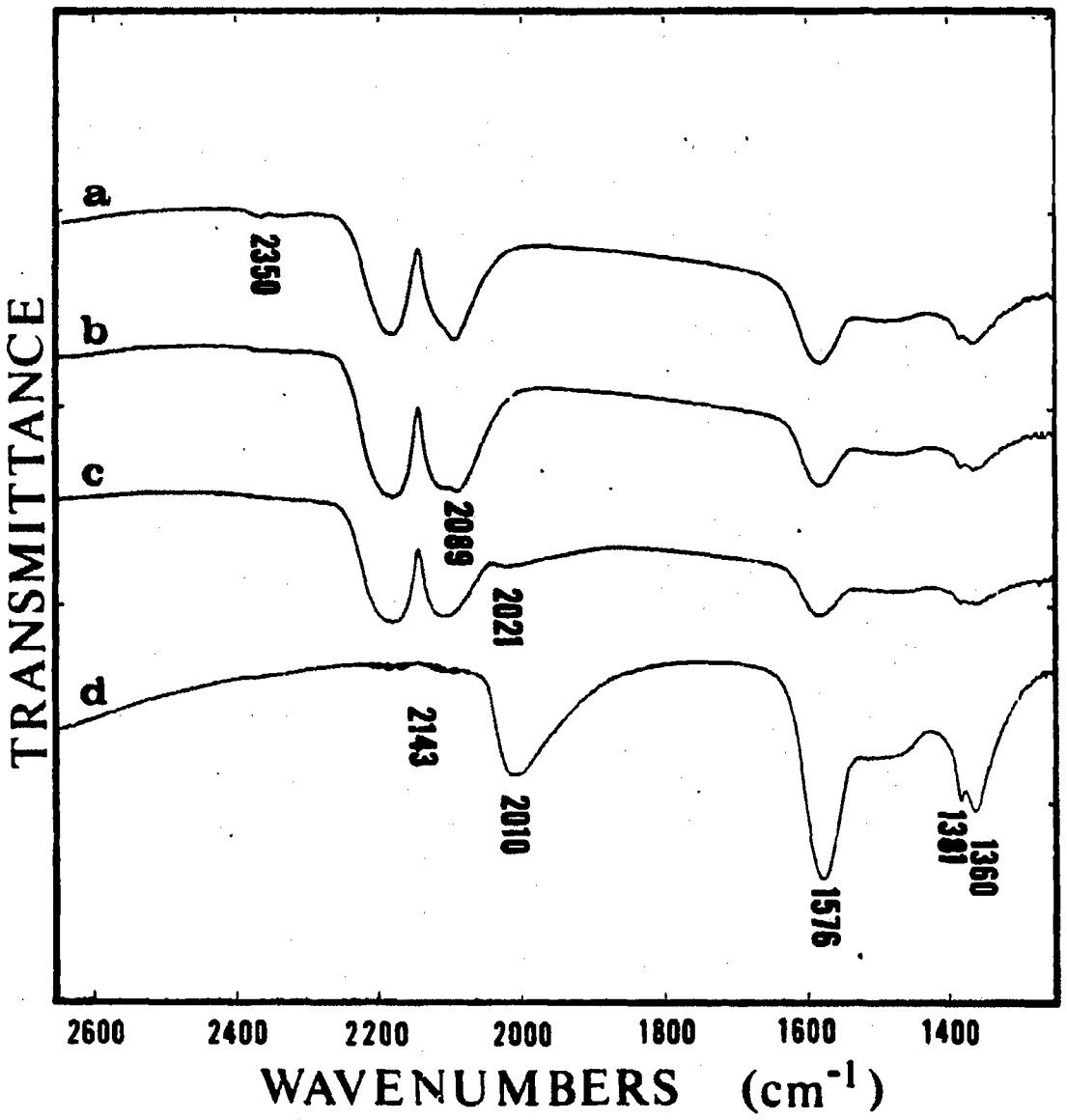

Figure 77. Continued

Figure 78. Adsorption of formic acid on 80/10/10 Zn/Cu/Cr oxide at 50 atm

a) reduced surface

b) exposure for 1 hour

c) exposure for 3 hours

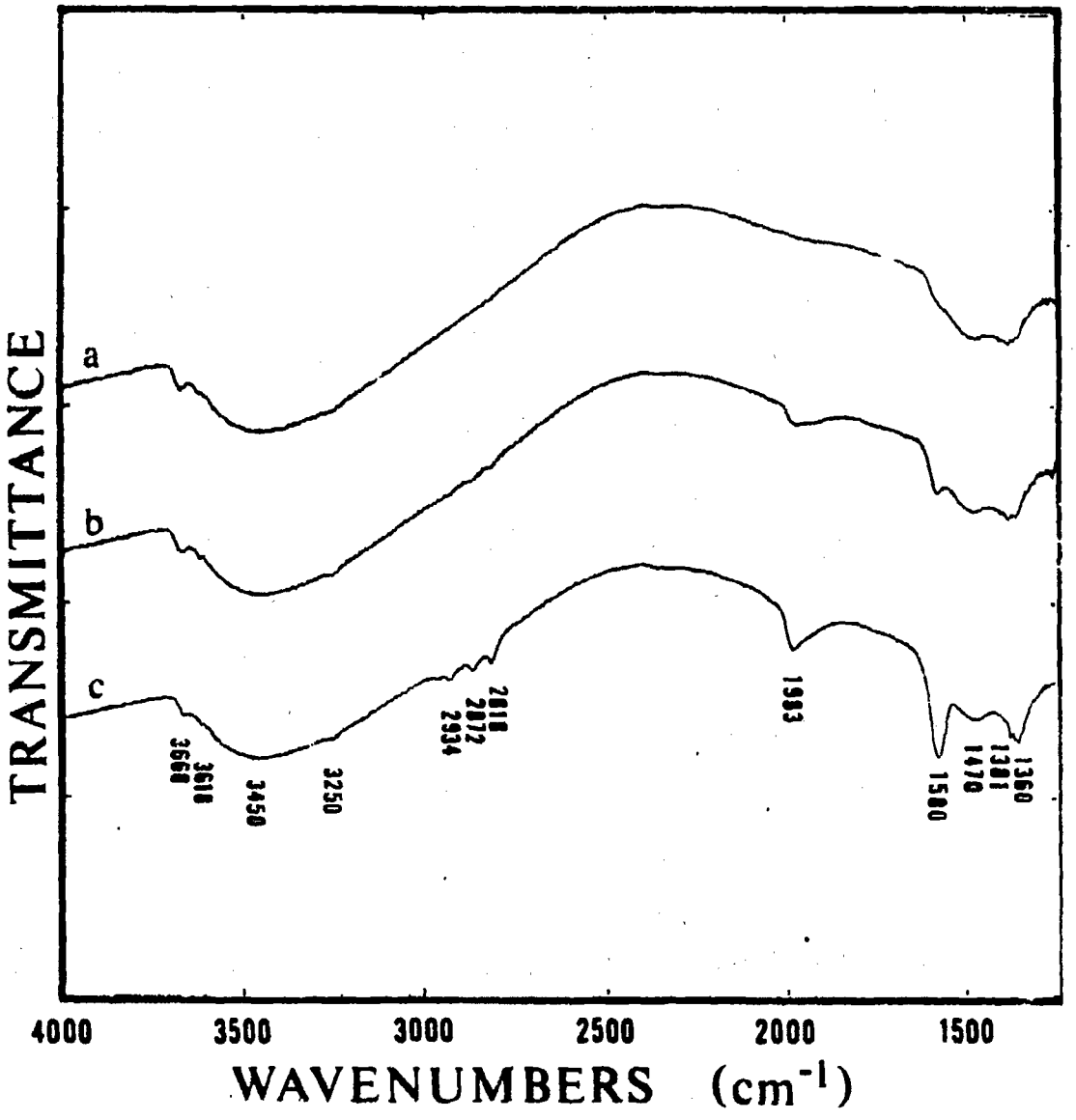
TRANSMITTANCE
a
b
c
3668
3618
3450
3250
2934
2872
2818
1983
1580
1470
1381
1360
4000
3500
3000
2500
2000
1500
WAVENUMBERS (cm-1)

DISCUSSION OF RESULTS

The reactor tests established that coprecipitated binary and ternary catalysts were active and highly selective for methanol synthesis at 50 atmospheres and 200-250°C, even though the copper contents in these compositions were much lower than those used in industrial catalysts. The methanol synthesis reaction was far from equilibrium in all the reaction experiments. At equilibrium, the conversion of carbon monoxide to methanol using a stoichiometric mixture of CO and H_2 would be 82% and 60% at 200°C and 250°C, respectively. The experimental conversions, including values from feeds containing an oxidizing promoter, were generally under 15%. A small addition of water into a CO-H_2 feed stream produced an effluent with carbon dioxide rather than water, indicating that the water-gas shift reaction was near equilibrium.

At 200°C, zinc oxide and impregnated CuO/ZnO were inactive for methanol synthesis, whereas the coprecipitated binary and ternary oxides possessed some activity. A feed stream of CO and H_2 would usually be expected to deactivate these catalysts, but some carbon dioxide was formed during the initial stage of reaction (some CO_2 was detected initially in the reactor effluent and CO_2 was observed in the infrared spectra). This carbon dioxide could be formed either from further reduction of the catalyst by carbon monoxide or via the water-gas shift reaction as carbon monoxide reacts with water in catalyst pores (the water would be the product of the prior reduction using hydrogen). The activity was maintained over an 8-hour period because some carbon dioxide persisted in the catalyst pores. The gradual decrease in

activity coincided with a gradual decrease in the CO_2 band intensity in infrared spectra. The addition of carbon dioxide or water to the $CO-H_2$ feed stream generally decreased the yield of methanol at 200°C. The initial decrease of the oxidant concentration in the reactor effluent and the release of relatively large amounts of the oxidant when the pressure was reduced suggested that the oxidant was adsorbed by the catalyst. Reaction rates were inhibited by relatively high concentrations of the oxidant in the catalyst pores.

At 250°C, the effect of an oxidizing additive was positive on the reaction rate. The increased temperature improved the yields on all catalysts, but catalyst deactivation was also increased as evident by the promotional effect of oxidant additions to the $CO-H_2$ feed stream. Assuming that Cu(I) sites are necessary for methanol synthesis (Herman et al., 1979), the function of small amounts of CO_2 or H_2O was to prevent the reduction of Cu(I) sites to copper in the zero valent state. Even pure zinc oxide showed some activity for methanol synthesis at 250°C, although the yield was an order of magnitude less than the binary and ternary catalysts.

The infrared spectra taken at 50 atmospheres in CO/H_2 mixtures had much less transmission than previous spectra taken at atmospheric pressure, especially the binary catalyst results. However, despite some lack of detail in the high pressure spectra, it was apparent that the surface species were essentially the same at the various pressures. Thus, band assignments that were given to adsorbed species on these metal oxides at atmospheric pressure have been applied to surface species at 50 atmospheres. The primary effects of elevated pressure were to

stabilize the surface hydroxyls at 3520 cm^{-1} and to weaken the carbon-oxygen bond of the surface carbonyl (band shift to lower frequency).

Information about the sequence of reaction steps and adsorption sites was obtained from transient experiments. Despite the low activity of these catalysts at 200°C, the infrared spectra showed that steady-state surface conditions were quickly reached when a stoichiometric CO/H_2 feed mixture was used. The surface reactions could be slowed by decreasing the amount of hydrogen in the feed mixture. Even in the extreme case of having only carbon monoxide in the gas phase, gradual hydrogenation of surface groups occurred because the residual hydroxyls were a source of hydrogen. The adsorption of carbon monoxide at 50 atm on zinc oxide produced formate groups, whereas on a binary catalyst formate, formaldehyde, and methoxy groups were formed. The greater extent of surface hydrogenation on a binary catalyst as compared to zinc oxide indicated that the copper component of the binary catalyst enhanced hydrogenation as well as carbon monoxide adsorption. Formate groups were clearly formed before formaldehyde and methoxy groups. The order of formaldehyde and methoxy formation at high pressure was difficult to establish because the intensity of the formaldehyde bands was low, but results from the atmospheric studies suggested that the formaldehyde species was the precursor of the methoxy species.

At 200°C, the adsorption of hydrogen caused a reduction in transmittance without forming any new species of adsorbed hydrogen observable in the infrared spectra, except the hydroxyl at 3250 cm^{-1} on mixed metal oxides. This new hydroxyl species, however, was determined in Part II to be a bulk species which was unaffected by surface reactions.

Hydrogenation of surface species during CO adsorption in the absence of gaseous hydrogen demonstrated that hydrogen was mobile on the surface at 200°C.

The spectra of Zn/Cu/Cr ternary catalysts during methanol synthesis conditions provided the most detailed information on surface species. The adsorbed carbonyl gradually shifted from 2090 to 2020 cm^{-1}, indicating a weakening of the carbon-oxygen bond without changing the nature of the carbonyl (linear bonded). Formate, formaldehyde, and methoxy species were produced during the experiment; the best methanol catalyst (80/10/10 Zn/Cu/Cr oxide) had mainly methoxy groups on the surface at steady state and no observable formaldehyde groups. The hydroxyl region was too indistinct to detect any band at 3520 cm^{-1}.

The steady-state spectrum of surface species on a binary catalyst during methanol synthesis using a feed with formic acid was the same as the spectra for feed mixtures of CO/H_2 or $CO/CO_2/H_2$. Because the spectrum from the formic acid experiment showed no surface carbonyl or gaseous carbon monoxide, the evidence for a reaction sequence involving formate and methoxy intermediates was strengthened. The ternary catalysts were unsatisfactory for methanol synthesis using a feed with formic acid. The infrared spectrum showed very little formate and methoxy groups on this catalyst, apparently because formic acid decomposition at these conditions was difficult. This study provided additional proof of the importance of formate and methoxy groups in methanol synthesis because these species were lacking on the surface of ternary catalysts.

A mechanism for methanol synthesis based on the results from this study is shown in Figure 79. Carbon monoxide was adsorbed on Cu(I)

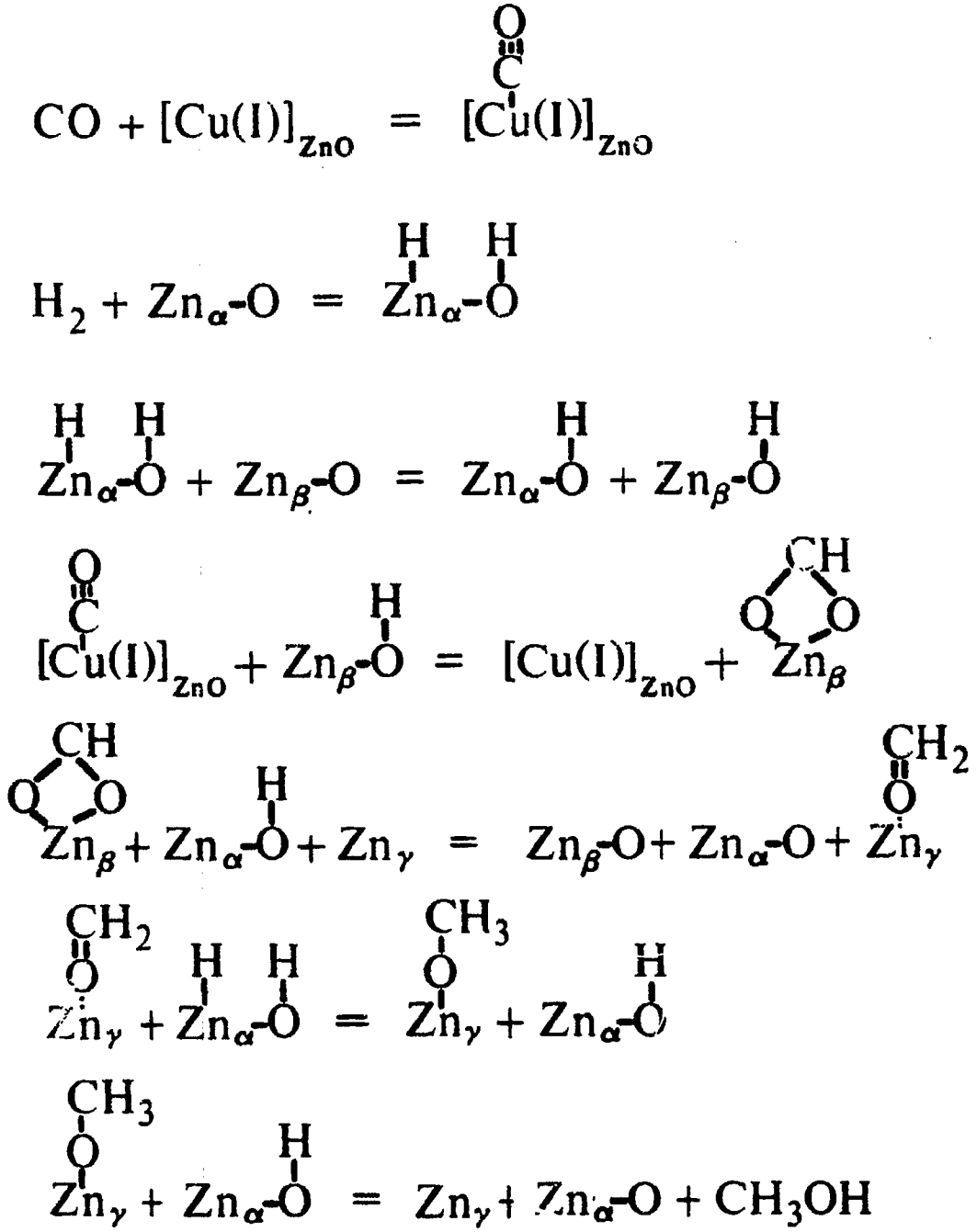

Figure 79. Methanol synthesis mechanism from infrared studies

sites in the zinc oxide lattice to form a linear carbonyl species (band at 2020 cm^{-1}). Hydrogen was adsorbed dissociatively on adjacent zinc-oxygen sites to form a hydroxyl and hydride species (Type I adsorption), but only the hydroxyl species (band at 3520 cm^{-1}) was stable enough to be seen in the infrared spectra. Hydrogen migrated to other sites to form other types of hydroxyl species (bands at 3550 and 3450 cm^{-1}) which were stable at these conditions. The surface carbonyl can insert itself into a hydroxyl group to form a bidentate formate species (bands at 2875, 1575, 1381, and 1365 cm^{-1}). Hydrogenation of the formate species produced an adsorbed formaldehyde species (bands at 2935, 2850, 2740, and 1600 cm^{-1}) which was adsorbed to a different surface site than the formate species. The formaldehyde species was quickly hydrogenated to form a methoxy species (bands at 2935 and 2820 cm^{-1}). The rate determining step was the hydrogenation of the methoxy species to methanol.

The various zinc sites proposed to be involved in this mechanism can be associated with specific hydroxyl groups. The hydroxyl band at 3520 cm^{-1} is the site of hydrogen adsorption. This band was very prominent during methanol or formic acid adsorption. The hydroxyl bands at 3550 and 3450 cm^{-1} are the sites where the formate species was adsorbed. The formate groups occupy only part of these hydroxyl sites since the formation of formate groups has little effect on the intensity of the hydrogen-bonded hydroxyl groups. The isolated hydroxyl bands at 3665 and 3620 cm^{-1} are the sites where the formaldehyde and methoxy species were adsorbed. These hydroxyl groups are completely displaced during methanol synthesis.

SUMMARY AND FUTURE RECOMMENDATIONS

This study has contributed significantly to an understanding of methanol synthesis on the type of mixed metal oxide known as the industrial low-pressure catalyst. This experimental work has placed emphasis on the characterization of binary catalysts with 95/5 and 90/10 Zn/Cu compositions, and ternary catalysts with 90/5/5 and 80/10/10 Zn/Cu/Cr compositions. Carbonyl, formate, and methoxy groups were identified by transmission infrared spectroscopy as stable surface species during methanol synthesis conditions (200°C and 50 atmospheres). The adsorption site of the carbonyl species was established to be a Cu(I) site because 1) only catalysts containing copper had this carbonyl species, 2) Auger spectra showed the presence of copper in the first valence state in reduced catalysts, and 3) the carbonyl stretching frequency in organometallic copper(I) complexes was very close to this carbonyl stretching frequency at atmospheric pressure. The carbonyl species was the only surface species to shift significantly when the pressure was increased from 1 to 50 atmospheres; the carbonyl stretching frequency shifted from 2085 to 2020 cm^{-1}. The formate species was adsorbed to a zinc site (Zn_β) which did not affect the isolated hydroxyls (bands at 3665 and 3620 cm^{-1}). The methoxy species, however, displaced the isolated hydroxyl groups, indicating that the methoxy species was adsorbed on a different zinc site (Zn_γ). A formaldehyde species, also adsorbed on a Zn_γ site, was unstable at 200°C. Some evidence suggested that a hydroxyl species adsorbed on a Zn_α site (Type I hydrogen adsorption) was stable at high pressure and 200°C, and was the source of the hydrogen

for methoxy hydrogenation to methanol. The rate-determining step in methanol synthesis was determined to be the hydrogenation of methoxy groups.

The formate species was identified as a reaction intermediate in methanol synthesis by using a feed stream containing formic acid and hydrogen. Adsorbed formate and methoxy groups were formed on a binary catalyst which produced methanol as the only product. The addition of carbon dioxide to a feed of carbon monoxide and hydrogen had little effect on the methanol yield at 200°C but substantially improved the yield at 250°C. Carbon dioxide apparently prevented the reduction of some Cu(I) active sites at the higher temperature. Carbon dioxide was absorbed in the catalyst pores at high pressure. At reaction conditions, any water in the feed or in the catalyst pores rapidly reacted with carbon monoxide to form carbon dioxide and hydrogen at thermodynamic equilibrium (water-gas shift reaction). The methanol synthesis reaction was always far from equilibrium with these catalysts.

At atmospheric pressure and 200°C, the surface species produced by a feed of carbon monoxide and hydrogen were carbonyl, formate, and methoxy groups. A feed of carbon dioxide and hydrogen only produced formate groups. It was determined that the adsorbed copper carbonyl species promoted the hydrogenation of formate groups to methoxy groups. Methanol adsorption produced methoxy groups and hydroxyls adsorbed on Zn_α sites while displacing the isolated hydroxyls adsorbed on Zn_γ sites. Adsorption with deuterated methanol established that the hydrogen in the Zn_α hydroxyl had come from the hydroxyl group of methanol. Formic acid adsorption produced formate groups and hydroxyls adsorbed on Zn_α sites without displacing the isolated hydroxyls. Formaldehyde adsorption at

200°C produced formate and methoxy groups, whereas at 100°C, an adsorbed formaldehyde species bonded to the surface through the oxygen end of the molecule to a Zn_γ site was formed. A summary of surface species, band assignments, and adsorption sites is given in Table 24. Information for deuterated species is presented in Table 25.

This work has raised many new questions about these catalysts and the behavior of adsorbed species which may be addressed with techniques that were not used in this study. It is currently thought that some copper exists as a solid solution within the zinc oxide crystallites (Herman et al., 1979). The Guinier results in Part I showed no change in the zinc oxide lattice parameters for catalysts with copper contents up to 10 atomic % in both oxidized and reduced states. These results can be explained as either 1) no copper is in the zinc oxide crystallites, or 2) the coordination of the copper in the reduced catalyst is different than the coordination in the oxidized catalyst. This problem could be resolved by conducting an EXAFS study of both oxidized and reduced binary catalysts to determine the local geometry around copper atoms,

Solid-state NMR spectroscopy may be able to provide additional information about the nature and behavior of adsorbed species. At 200°C, the adsorption of carbon monoxide on a coprecipitated binary catalyst produced both formate and methoxy groups. There is no question but that this hydrogenation involves an adsorbed form of hydrogen, but only surface hydroxyl groups are observed in the infrared spectra. Hydrogen adsorption at room temperature forms new bands at 3490 and 1710 cm^{-1} corresponding to ZnOH and ZnH species, but at 200°C, hydrogen adsorption does not affect any residual hydroxyls nor are any new bands formed.

Table 24. Infrared band assignments for surface species

Band (cm^{-1})	Assignment	Adsorbed site
Bidentate formate		Zn_β
ν_1 2875 ± 5	CH stretching	
ν_4 1575 ± 5	Asym. OCO stretching	
ν_5 1380 ± 2	CH bending	
ν_2 1365 ± 5	Sym. OCO stretching	
2966 ± 4	$\nu_4 + \nu_5$	
2740 ± 4	$\nu_2 + \nu_5$	
Methoxy		Zn_γ
2935 ± 2	Asym. CH_3 stretching	
2820 ± 2	Sym. CH_3 stretching	
Formaldehyde		Zn_γ
2935 ± 5	CH_2 scissoring overtone	
2850 ± 10	Asym. CH_2 stretching	
2740 ± 5	Sym. CH_2 stretching	
1600 ± 10	C=O stretching	
Carbonyls		
2200 ± 20	C≡O stretching	Zn
2085 ± 5	C≡O stretching (1 atm)	Cu
2020 ± 10	C≡O stretching (50 atm)	Cu
Hydroxyls		
3665 ± 5	OH stretching	Zn_γ
3640 ± 4	OH stretching	Zn_γ
3620 ± 2	OH stretching	Zn_γ
3550 ± 20	OH stretching	Zn_β
3525 ± 5	OH stretching	Zn^α
3450 ± 20	OH stretching	Zn_β
Unidentate carbonate		Zn_β
1470 ± 5	Asym. OCO stretching	
1380 ± 5	Sym. OCO stretching	

Table 24. Continued

Band (cm^{-1})	Assignment	Adsorbed site
Bidentate carbonate		Zn_β
1512 ± 5	Asym. OCO stretching	
1325 ± 5	Sym. OCO stretching	

Table 25. Infrared band assignments for deuterated species

Band (cm^{-1})	Assignment	Adsorbed site
Bidentate formate		Zn_β
2166 ± 5	CD stretching	
1575 ± 5	Asym. OCO stretching	
1335 ± 5	Sym. OCO stretching	
Methoxy		Zn_γ
2220 ± 2	Asym. CD_3 stretching	
2056 ± 2	Sym. CD_3 stretching	
Hydroxyls		
2706 ± 5	OD stretching	Zn_γ
2667 ± 2	OD stretching	Zn^γ
2630 ± 20	OD stretching	Zn^γ_β
2608 ± 5	OD stretching	Zn^α
2560 ± 20	OD stretching	Zn^α_β

The questions to be resolved are 1) the forms of adsorbed hydrogen which may be infrared inactive, and 2) the surface mobility of the species that are identified. Reduced binary catalysts also have a band at 3250 cm^{-1} which has been assigned to a bulk copper hydroxide. Because deuterium readily shifts all surface hydroxyl groups but not the band

at 3250 cm^{-1}, this species can be isolated and characterized by solid-state NMR.

The technique of mass spectrometry can be utilized in many types of experiments. The most powerful application of this method involves the use of isotopic reactants to elucidate the reaction mechanism. If a formate species is a reaction intermediate, then the carbon and oxygen atoms in methanol could be different from the carbon and oxygen atoms in the carbon monoxide molecule. A mixture containing $^{12}C^{18}O$ and $^{13}C^{16}O$ would establish whether or not any mixing occurs in methanol formation. The role of carbon dioxide in methanol synthesis can be determined by using an isotopic compound. Mass spectrometry can be very useful in adsorption and desorption studies. The adsorption of methanol forms methoxy groups on sites containing isolated hydroxyl groups. By using deuterated methanol as the adsorbate, the detection of HOD would establish that the hydroxyl hydrogen from methanol combines with a surface hydroxyl to form water. Infrared studies could easily be coupled with temperature programmed desorption to correlate changes in surface species with the gaseous products evolved.

REFERENCES

Abbati, I.; Braicovich, L.; De Michelis, B.; Fasana, A. Zn(0001) water interaction: An ultraviolet photoelectron spectroscopy investigation. Solid State Commun. 26: 515-517; 1978.

Amberg, C. H.; Seanor, D. A. An infrared study of CO adsorbed on surfaces of zinc oxide. Influence of pre-oxidation and doping. Sachtler, W. M. H.; Schuit, G. C. A.; Zwietering, P., eds. Proceedings of the 3rd International Congress on Catalysis. New York: Interscience; 1965; 450-460.

Atherton, K.; Newbold, G.; Hockey, J. A. Infra-red spectroscopic studies of zinc oxide surfaces. Disc. Faraday Soc. (52): 33-43; 1971.

Au, C. T.; Roberts, M. W.; Zhu, A. R. Surface hydroxylation at a Zn(0001)-O surface. Surface Sci. 115: L117-L123; 1982.

Badische Anilin und Soda Fabrik (BASF), assignee. D. R. patents 415,686; 441,433; 462,837. U.S. patents 1,558,559; 1,569,775. 1923.

Ballintine, Thomas A.; Schmulbach, C. David. High pressure reactor and cell for electronic and infrared spectral studies. J. Organometal. Chem. 164: 381-390; 1979.

Bardet, Robert; Thivolle-Cazat, Jean; Trambouze, Yves. Méthanolation des oxydes de carbone sur des catalyseurs Cu-Zn, à la pression atmosphérique. J. Chim. Phys. 78 (2): 135-138; 1981.

Bell, Alexis T. Applications of Fourier transform infrared spectroscopy to studies of adsorbed species. Bell, Alexis T.; Hair, Michael L. eds. Vibrational spectroscpies for adsorbed species. Washington, D.C.: American Chemical Society; 1980; 13-35.

Bell, Robert John. Introductory Fourier transform spectroscopy. New York: Academic Press; 1972.

Berry, Reginald I. Gasoline or olefins from an alcohol feed. Chem. Eng. 87 (Apr. 21): 86-88; 1980.

Boccuzzi, F.; Borello, E.; Zecchina, A.; Bossi, A.; Camia, M. Infrared study of ZnO surface properties I. Hydrogen and deuterium chemisorption at room temperature. J. Catal. 51: 150-159; 1978a.

Boccuzzi, F.; Garrone, E.; Zecchina, A.; Bossi, A.; Camia, M. Infrared study of ZnO surface properties II. H_2-CO interaction at room temperature. J. Catal. 51: 160-168; 1978b.

Borowitz, J. L. On the mechanism of the synthesis $CO + 2H_2 \rightarrow CH_3OH$. J. Catal. 13: 106-108; 1969.

Bowker, M.; Madix, R. J. XPS, UPS and thermal desorption studies of alcohol adsorption on Cu(110) I. Methanol. Surface Sci. 95: 190-206; 1980.

Bowker, Michael; Houghton, Hilary; Waugh, Kenneth C. Mechanism and kinetics of methanol synthesis on zinc oxide. Chem. Soc., Faraday Trans. I 77: 3023-3036; 1981.

Bozon-Verduraz, F. Difficulties concerning the infrared identification of surface species on metal oxides. J. Catal. 18: 12-18; 1970.

Brown, Kevin L.; Clark, George R.; Headford, Christine E. L.; Marsden, Karen; Roper, Warren R. Organometallic models for possible Fischer-Tropsch intermediates. Synthesis, structure, and reactions of a formaldehyde complex of osmium. J. Am. Chem. Soc. 101: 503-505; 1979.

Brynestad, J. Iron and nickel carbonyl formation in steel pipes and its prevention – Literature survey. Oak Ridge National Laboratory TM-5499; 1976; 16 p.

Budneva, A. A.; Davydov, A. A.; Mikhal'chenko, V. G. IR spectroscopic study of hydrocarbon adsorption on oxide catalysts III. Adsorption of propylene on chromium oxide. Kinet. Catal. 16: 409-412; 1975. Translated from Kinet. Katal. 16: 468-490; 1975.

Bulko, John B.; Herman, Richard G.; Klier, Kamil; Simmons, Gary W. Optical properties and electronic interactions of microcrystalline Cu/ZnO catalysts. J. Phys. Chem. 83: 3118-3122; 1979.

Busca, Guido; Lorenzelli, Vincenzo. Infrared study of methanol, formaldehyde, and formic acid adsorbed on hematite. J. Catal. 66: 155-161; 1980.

Chang, C. C.; Dixon, L. T.; Kokes, R. J. The nature of molecular hydrogen adsorbed on zinc oxide. J. Phys. Chem. 77: 2634-2640; 1973.

Chemical engineers' handbook. 5th ed. Perry, Robert H.; Chilton, Cecil H. eds. New York: McGraw-Hill Book Co.; 1973; 3.137-3.144.

Cheng, W. H.; Kung, H. H. Interaction of CO, CO_2, and O_2 with nonpolar, stepped and polar Zn surfaces of ZnO. Surface Sci. 122: 21-39; 1982.

Cheng, W. H.; Akhter, S.; Kung, H. H. Structure sensitivity in methanol decomposition on ZnO single-crystal surfaces. J. Catal. 82: 341-350; 1983.

Chow, Yuan L.; Buono-Core, Gonzalo E. Triplet-state benzophenone-sensitized photoreduction of bis(acetylacetonato)copper(II): The generation and stability of copper(I) complexes. Can. J. Chem. 61: 795-800; 1983.

Churchill, Melvyn Rowen; DeBoer, Barry G.; Rotella, Frank J.; Abu Salah, Omar M.; Bruce, Michael I. Determination of the crystal structure and molecular geometry of (hydrotris(1-pyrazolyl)borato)-copper(I) carbonyl. A unique structural investigation of a copper-carbonyl linkage. Inorg. Chem. 14: 2051-2056; 1975.

Cimino, A.; Molinari, E.; Cramarossa, F.; Ghersini, G. Hydrogen chemisorption and electrical conductivity of zinc oxide semiconductors. J. Catal. 1: 275-292; 1962.

Collman, J. P.; Winter, S. R. Isolation and characterization of a kinetically stable transition metal formyl complex. J. Am. Chem. Soc. 95: 4089-4090; 1973.

Davydov, A. A.; Shchekochikhin, V. M.; Zaitsev, P. M.; Shchekochikhin, Yu. M.; Keier, N. P. Investigation of the reactivity of forms of adsorbed oxygen on chromic oxide. Kinet. Catal. 12: 611-615; 1971. Translated from Kinet. Katal. 12: 694-699; 1971.

Deluzarche, A.; Kieffer, R.; Muth, A. Réactions CO, H_2 — Synthèse du méthanol sur chromite de zinc. Étude d'espèces chimisorbées à la surface du catalyseur. Schémas réactionnels possibles. Tetrahedron Lett. 38: 3357-3360; 1977.

Denise, B.; Sneeden, R. P. A.; Hamon, C. Hydrocondensation of carbon dioxide: IV. J. Mol. Catal. 17: 359-366; 1982.

Denny, P. J.; Whan, D. A. The heterogeneously catalysed hydrogenation of carbon monoxide. Catalysis 2: 46-86; 1978.

Dent, A. L.; Kokes, R. J. Hydrogenation of ethylene by zinc oxide I. Role of slow hydrogen chemisorption. J. Phys. Chem. 73: 3772-3780; 1969a.

Dent, A. L.; Kokes, R. J. Hydrogenation of ethylene by zinc oxide II. Mechanism and active sites. J. Phys. Chem. 73: 3781-3790; 1969b.

Dodge, Barnett F., inventor. Catalyst for methanol manufacture and method of producing same. U.S. patent 1,908,696. 1933 May 16.

Dolgov, B. N.; Karpinskii, M. H. Khim. Tverdogo Topliva 3: 559; 1932.

Dombek, D. Duane. Hydrogenation of carbon monoxide to methanol and ethylene glycol by homogeneous ruthenium catalysts. J. Am. Chem. Soc. 102: 6855-6857; 1980.

Eastman Kodak Company. Kodak Irtran infrared optical materials. Kodak publication U-72. Rochester, NY: Eastman Kodak Co., 1971; 51 p.

Eischens, R. P.; Pliskin, W. A.; Low, M. J. D. The infrared spectrum of hydrogen chemisorbed on zinc oxide. J. Catal. 1: 180-191; 1962.

Ewell, Raymond H. Calculation of chemical equilibrium at high pressures. Ind. Eng. Chem. 32: 147-153; 1940.

Fahey, Darryl R. Rational mechanism for homogeneous hydrogenation of carbon monoxide to alcohols, polyols, and esters. J. Am. Chem. Soc. 103: 136-141; 1981.

Fenske, M. R.; Frolich, P. K. Catalysts for the formation of alcohols from carbon monoxide and hydrogen. V. Decomposition and synthesis of methanol with a zinc-copper-chromium oxide catalyst. Ind. Eng. Chem. 21: 1052-1055; 1929.

Fink, Peter. Über die CO_2-chemisorption auf γ-aluminiumoxid. Z. Chem. 7: 324; 1967.

Friedrich, J. B.; Wainwright, M. S.; Young, D. J. Methanol synthesis over Raney copper-zinc catalysts I. Activities and surface properties of fully extracted catalysts. J. Catal. 80: 1-13; 1983a.

Friedrich, J. B.; Young, D. J.; Wainwright, M. S. Methanol synthesis over Raney copper-zinc catalysts II. Activities and surface properties of a partially leached alloy. J. Catal. 80: 14-24; 1983b.

Frolich, P. K.; Lewis, W. K. Synthesis of methanol from carbon monoxide and hydrogen. Ind. Eng. Chem. 20: 285-290; 1928.

Gagné, Robert R.; Allison, Judith L.; Gall, Robert S.; Koval, Carl A. Models for copper-containing proteins: Structure and properties of novel five-coordinate copper(I) complexes. J. Am. Chem. Soc. 99: 7170-7178; 1977.

Gallei, E.; Schadow, E. Ultrahigh-vacuum, high pressure and temperature infrared-ultraviolet-visible spectrophotometer cell. Rev. Sci. Instrum. 45: 1504-1506; 1974.

Gay, Robert R.; Nodine, Mark H.; Henrich, Victor E.; Zeiger, H. J.; Solomon, Edward I. Photoelectron study of the interaction of CO with ZnO. J. Am. Chem. Soc. 102: 6752-6761; 1980.

Geerts, Rolf L.; Huffman, John C.; Folting, Kirsten; Lemmen, Timothy H.; Caulton, Kenneth G. Concerning the structure and stability of a copper(I) alkoxy carbonyl. J. Am. Chem. Soc. 105: 3503-3506; 1983.

Gerasimova, G. F.; Keier, N. P.; Isaenko, L. I. Nature of the hydrogen adsorption centers on zinc oxide. Kinet. Catal. 14: 1087-1092; 1973. Translated from Kinet. Katal. 14: 1239-1245; 1973.

Giamello, E.; Fubini, B. Characterization of the interaction of CO and H_2 at the ZnO surface by adsorption microcalorimetry. React. Kinet. Catal. Lett. 16: 355-358; 1981.

Green, David W.; Reedy, Gerald T. Matrix-isolation studies. Ferraro, John R.; Basile, Louis J. eds. Fourier transform infrared spectroscopy. Vol. 1. New York: Academic Press; 1978; 18-37.

Greenler, Robert G. Infrared study of the adsorption of methanol and ethanol on aluminum oxide. J. Chem. Phys. 37: 2094-2100; 1962.

Gregg, S. J.; Ramsay, J. D. F. A study of the adsorption of carbon dioxide by alumina using infrared and isotherm measurements. J. Phys. Chem. 73: 1243-1247; 1969.

Griffiths, Peter R. Chemical infrared Fourier transform spectroscopy. New York: John Wiley & Sons, 1975.

Hair, M. L. Infrared spectroscopy in surface chemistry. New York: Marcel Dekker; 1967.

Hammaker, R. M.; Walters, J. P. The infrared spectra of C-13 enriched sodium formate. Spectrochim. Acta 20: 1311-1317; 1964.

Harvey, K. B.; Morrow, B. A.; Shurvell, H. F. The infrared absorption of some crystalline inorganic formates. Can. J. Chem. 41: 1181-1187; 1963.

Hata, Kazuo; Kawasaki, Shoji; Kubokawa, Yutaka; Miyata, Hisashi. Infrared studies of oxidation of olefins adsorbed on zinc oxide. Bond, G. C.; Wells, P. B.; Tompkins, F. C. eds. Proceedings of the 6th International Congress on Catalysis. Vol. 2. London: Chemical Society; 1977; 1102-1110.

Henrici-Olivé, G.; Olivé, S. Mechanistic reflections on the methanol synthesis with Cu/Zn catalysts. J. Mol. Catal. 17: 89-92; 1982.

Herd, A. C.; Onishi, Takaharu; Tamaru, Kenzi. Studies on the mechanism of methanol oxidation on zinc oxide by dynamic treatments of chemisorbed species under the reaction conditions. Bull. Chem. Soc. Japan 47: 575-578; 1974.

Herman, R. G.; Klier, K.; Simmons, G. W.; Finn, B. P.; Bulko, J. B.; Kobylinski, T. P. Catalytic synthesis of methanol from CO/H_2 I. Phase composition, electronic properties, and activities of the $Cu/ZnO/M_2O_3$ catalysts. J. Catal. 56: 407-429; 1979.

Herman, R. G.; Simmons, G. W.; Klier, K. Catalytic synthesis of methanol from CO/H_2 III. The role of alumina and ceria in the Cu/ZnO system. Seiyama, T.; Tanabe, K. eds. New horizons in catalysis: Proceedings of the 7th International Congress on Catalysis. New York: Elsevier Scientific; 1981; 475-484.

Hertl, William; Cuenca, Angela Maria. Infrared kinetic study of reactions of alcohols on the surface of alumina. J. Phys. Chem. 77: 1120-1126; 1973.

Hicks, R. F.; Kellner, C. S.; Savatsky, B. J.; Hecker, W. C.; Bell, A. T. Design and construction of a reactor for in situ infrared studies of catalytic reactions. J. Catal. 71: 216-217; 1981.

Himelfarb, P. B.; Wawner, F. E., Jr.; Bieser, A., Jr.; Vines, S. N. Oxidation states of copper during reduction of cupric oxide in methanol catalysts. J. Catal. 83: 469-471; 1983.

Hollins, P.; Pritchard, J. Interactions of CO molecules adsorbed on Cu(111). Surface Sci. 89: 486-495; 1979.

Horn, K.; Pritchard, J. Infrared spectrum of CO chemisorbed on Cu(100). Surface Sci. 55: 701-704; 1976.

Hotan, W.; Göpel, W.; Haul, R. Interaction of CO_2 and CO with nonpolar zinc oxide surfaces. Surface Sci. 83: 162-180; 1979.

Hougen, O. A.; Watson, K. M. Solid catalysts and reaction rates. Ind. Eng. Chem. 35: 529-541; 1943.

Hougen, O. A.; Watson, K. M.; Ragatz, R. A. Chemical process principles charts. 2nd ed. New York: John Wiley & Sons; 1960.

Ito, K.; Bernstein, H. J. The vibrational spectra of the formate, acetate, and oxalate ions. Can. J. Chem. 34: 170-178; 1956.

Ivanov, K. N. Mem. Inst. Chem. Ukr. Akad. Sci. U.R.S.S. 1: 49; 1934a.

Ivanov, K. N. Acta Physicochim. U.R.S.S. 1: 493; 1934b.

John, C. S. Catalysis by zinc oxide. Catalysis 3: 169-188; 1980.

Kagan, Yu. B.; Lin, G. I.; Rozovskii, A. Ya.; Loktev, S. M.; Slivinskii, E. V.; Bashkirov, A. N.; Naumov, I. P.; Khludenev, I. K.; Kudinov, S. A.; Golovkin, Yu. I. The mechanism of the synthesis of methanol from carbon dioxide and hydrogen I. Kinetic regularities. Kinet. Catal. 17: 380-384; 1976. Translated from Kinet. Katal. 17: 440-446; 1976.

Kagel, R. O. Infrared investigation of the adsorption and surface reactions of the C_1 through C_4 normal alcohols on γ-alumina. J. Phys. Chem. 71: 844-850; 1967.

Kauffe, K.; Pschera, K. Z. Anorg. Allgem. Chem. 262: 147; 1950.

Ketchik, S. V.; Minyukova, T. P.; Plyasova, L. M.; Yurieva, T. M.; Boreskov, G. K. Peculiarities of formation of ZnO and CuO-based solid solutions. React. Kinet. Catal. Lett. 19: 345-349; 1982.

Kieffer, R.; Ramaroson, E.; Deluzarche, A.; Trambouze, Y. A comparison of reactivity in the synthesis of methanol from $CO_2 + H_2$ and $CO + H_2$ (catalysts $Cu,Zn/Al_2O_3$, $P = 515 \times 10^4$ Pa). React. Kinet. Catal. Lett. 16: 207-212; 1981.

King, R. B.; King, A. D., Jr.; Iqbal, M. Z.; Frazier, C. C. Transition metal alkyl chemistry at elevated carbon monoxide pressures. An infrared spectroscopic study of systems related to catalytic intermediates in homogeneous hydroformylation reactions. J. Am. Chem. Soc. 100: 1687-1694; 1978.

King, S. T. An infrared spectroscopic flow reactor for in situ studies of heterogeneous catalytic reactions at high temperature and the reactions of CO_2 and benzyl benzoate on alumina. Appl. Spectrosc. 34: 632-636; 1980.

Kiselev, A. V.; Lygin, V. I. Infrared spectra of surface compounds. New York: John Wiley & Sons; 1975. Translated from the Russian by N. Kaner.

Klier, K. Methanol synthesis. Adv. Catal. 31: 243-313; 1982.

Klier, K.; Chatikavanij, V.; Herman, R. G.; Simmons, G. W. Catalytic synthesis of methanol from CO/H_2 IV. The effects of carbon dioxide. J. Catal. 74: 343-360; 1982.

Kohn, Philip M. Bright future for CO feed. Chem. Eng. 86 (Jan. 29): 49-52; 1979.

Kokes, R. J.; Dent, A. L.; Chang, C. C.; Dixon, L. T. Infrared studies of isotope effects for hydrogen adsorption on zinc oxide. J. Am. Chem. Soc. 94: 4429-4436; 1972.

Kotera, Y.; Oba, M.; Ogawa, K.; Shimomura, K.; Uchida, H. The preparation of the catalysts for methanol synthesis and their characteristics. Delmon, B.; Jacobs, P. A.; Poncelet, G. eds. Preparation of catalysts. Amsterdam: Elsevier Scientific; 1976; 589-599.

Kung, Harold H. Methanol synthesis. Catal. Rev. — Sci. Eng. 22 (2): 235-259; 1980.

Kuznetsov, V. A.; Gerei, S. V.; Gorokhovat-skii, Ya. B.; Rozhkova, É. V. Interaction of hydrocarbons with oxide catalyst surfaces I. Infrared spectroscopic study of the reaction of hydrocarbons with chromic oxide. Kinet. Catal. 18: 355-359; 1977. Translated from Kinet. Katal. 18: 418-423; 1977.

Kuznetsov, V. D.; Shub, F. S.; Temkin, M. I. Role of carbon dioxide in methanol synthesis on the copper catalyst SNM-1. Kinet. Catal. 23: 788-791; 1983. Translated from Kinet. Katal. 23: 932-935; 1982.

Kuznetsova, L. I.; Yurieva, T. M.; Minyukova, T. P.; Ketchik, S. V.; Plyasova, L. M.; Boreskov, G. K. Nature of the active component of copper-zinc-aluminum catalyst for methanol synthesis. React. Kinet. Catal. Lett. 19: 355-359; 1982.

Lander, Elliot P.; Hubbard, J. Nathan; Smith, Lawrence A., Jr. Revving-up refining profits with catalytic distillation. Chem. Eng. 90 (Apr. 18): 36-39; 1983.

Lange's handbook of chemistry. 11th ed. Dean, John A. ed. New York: McGraw-Hill Book Co.; 1973; 3.118-3.123.

Larson, Alfred T., inventor. Production of methanol and other carbon compounds and catalytic agents for use therein. U.S. patent 2,061,470. 1936 Nov. 17.

Little, L. H. Infrared spectra of adsorbed species. New York: Academic Press; 1966.

London, Jack W.; Bell, Alexis T. Infrared spectra of carbon monoxide, carbon dioxide, nitric oxide, nitrogen dioxide, nitrous oxide, and nitrogen adsorbed on copper oxide. J. Catal. 31: 32-40; 1973.

Ludlum, K. H.; Eischens, R. P. Carbonyl formation in stainless steel infrared cells. Surface Sci. 40: 397-398; 1973.

Lüth, H.; Rubloff, G. W.; Grobman, W. D. Ultraviolet-photoemission studies of formic acid decomposition on ZnO nonpolar surfaces. Solid State Commun. 18: 1427-1430; 1976.

Matsushita, Sanjuro; Nakata, Toshiko. Infrared absorption of zinc oxide and of adsorbed CO_2. II. J. Chem. Phys. 36: 665-669; 1962.

McClellan, M. R.; Trenary, M.; Shinn, N. D.; Sayers, M. J.; D'Amico, K. L.; Solomon, Edward I.; McFeely, F. R. An angle resolved photoemission determination of the coordination of CO to the ZnO (0001) surface. J. Chem. Phys. 74: 4726-4731; 1981.

McIntyre, N. S. Analysis of corrosion films using XPS: Advantages and limitations. Windawi, Hassan; Ho, Floyd F.-L. eds. Applied electron spectroscopy for chemical analysis. New York: John Wiley & Sons; 1982; 99-101.

Mehta, S.; Simmons, G. W.; Klier, K.; Herman, R. G. Catalytic synthesis of methanol from CO/H_2 II. Electron microscopy (TEM, STEM, microdiffraction, and energy dispersive analysis) of the Cu/ZnO and $Cu/ZnO/Cr_2O_3$ catalysts. J. Catal. 57: 339-360; 1979.

Metallgesellschaft, assignee. Methanol production from carbon monoxide/dioxide and hydrogen. French patent 2,049,193. 1971 March 26.

Miyata, Hisashi; Nakajima, Takashi; Kubokawa, Yutaka. Infrared studies of oxidation of 2-butanol and 2-methyl-2-propanol adsorbed on ZnO. J. Catal. 69: 292-298; 1981.

Molstad, M. C.; Dodge, B. F. Zinc oxide — Chromium oxide catalysts for methanol synthesis. Ind. Eng. Chem. 27: 134-140; 1935.

Morimoto, Tetsuo; Morishige, Kunimitsu. Interaction between carbon dioxide and the zinc oxide surface. Bull. Chem. Soc. Japan 47: 92-94; 1974.

Morimoto, Tetsuo; Morishige, Kunimitsu. Relation between amounts of chemisorbed water and carbon dioxide on zinc oxide. J. Phys. Chem. 79: 1573-1577; 1975.

Morimoto, Tetsuo; Nagao, Mahiko. Adsorption anomaly in the system zinc oxide-water. J. Phys. Chem. 78: 1116-1120; 1974.

Morimoto, Tetsuo; Yanai, Hiromi; Nagao, Mahiko. Infrared spectra of ammonia adsorbed on zinc oxide. J. Phys. Chem. 80: 471-475; 1976.

Morterra, C.; Coluccia, S.; Ghiotti, G.; Zecchina, A. An IR spectroscopic characterization of alpha alumina surface properties. Carbon dioxide adsorption. Z. Phys. Chem. Neue Folge 104: 275-290; 1977.

Nagao, Mahiko; Morimoto, Tetsuo. Adsorption of alcohols on zinc oxide surfaces. J. Phys. Chem. 84: 2054-2058; 1980.

Nagao, Mahiko; Morishige, Kunimitsu; Takeshita, Toshie; Morimoto. Tetsuo. Porous structure formed by the decomposition of the surface product on ZnO preserved in the atmosphere. Bull. Chem. Soc. Japan 47: 2107-2110; 1974.

Nagao, Mahiko; Yunoki, Koji; Muraishi, Haruto; Morimoto, Tetsuo. Differential heat of chemisorption. I. Chemisorption of water on zinc oxide and titanium oxide. J. Phys. Chem. 82: 1032-1035; 1978.

Nakamoto, Kazuo. Infrared and Raman spectra of inorganic and coordination compounds. 3rd ed. New York: John Wiley & Sons; 1978; 243-245.

Natta, G. Synthesis of methanol. Emmett, P. H. ed. Catalysis. Vol. 3. New York: Reinhold; 1955; 349-411.

Natta, G.; Pino, P.; Mazzanti, G.; Pasquon, I. Kinetic interpretation of the heterogeneous catalysis of high pressure reactions — Synthesis of methanol. Chim. Ind. (Milan) 35: 705-725; 1953.

Newman, Roger. Polarized infrared spectrum of sodium formate. J. Chem. Phys. 20: 1663-1664; 1952.

Newsome, David S. The water-gas shift reaction. Catal. Rev. — Sci. Eng. 21 (2): 275-318; 1980.

Nguyen, Tam T.; Sheppard, Norman. The adsorption of allylbenzene on zinc oxide: An infrared spectroscopic study. J. Catal. 67: 402-409; 1981.

Noto, Yuko; Fukuda, Kenzo; Onishi, Takaharu; Tamaru, Kenzi. The dehydrogenation of formic acid over zinc oxide. Bull. Chem. Soc. Japan 40: 2722; 1967.

Oba, M. Zinc oxide catalysts. V. Catalytic activity for methanol synthesis of catalysts prepared by precipitation method. Tokyo Kogyo Shikensho Kokoku 60: 121-123; 1965.

Okamoto, Yasuaki; Fukino, Kiyotaka; Imanaka, Toshinobu; Teranishi, Shiichiro. A study of the catalytically active copper species in the synthesis of methanol on Cu-ZnO by x-ray photoelectron spectroscopy. J. Chem. Soc., Chem. Commun.: 1405-1407; 1982.

Okamoto, Yasuaki; Fukino, Kiyotaka; Imanaka, Toshinobu; Teranishi, Shiichiro. Surface characterization of CuO-ZnO methanol-synthesis catalysts by x-ray photoelectron spectroscopy. 1. Precursor and calcined catalysts. J. Phys. Chem. 87: 3740-3747; 1983a.

Okamoto, Yasuaki; Fukino, Kiyotaka; Imanaka, Toshinobu; Teranishi, Shiichiro. Surface characterization of CuO-ZnO methanol-synthesis catalysts by x-ray photoelectron spectroscopy. 2. Reduced catalysts. J. Phys. Chem. 87: 3747-3754; 1983b.

Ostrovskii, V. E.; Dyatlov, A. A.; Ogneva, T. P. Adsorption of carbon monoxide on the low-temperature methanol synthesis catalyst. Kinet. Catal. 19: 410-413; 1978. Translated from Kinet. Katal. 19: 514-518; 1978.

Parkinson, Gerald; Skole, Robert; McQueen, Silke; Payne, Adam. California puts methanol plan into high gear. Chem. Eng. 89 (Nov. 1): 30-33; 1982.

Parkyns, N. D. Surface properties of metal oxides. Part I. Infrared studies of the adsorption and oxidation of carbon monoxide on alumina. J. Chem. Soc. (A): 1910-1913; 1967.

Parkyns, N. D. The surface properties of metal oxides. Part II. An infrared study of the adsorption of carbon dioxide on γ-alumina. J. Chem. Soc. (A): 410-417; 1969.

Pasquali, Marco; Marchetti, Fabio; Floriani, Carlo. Synthesis, properties, and x-ray structure of (diethylenetriamine)copper(I) carbonyl: A highly thermally stable copper(I) amine carbonyl. Inorg. Chem. 17: 1684-1688; 1978.

Pasquali, Marco; Marini, Giuliana; Floriani, Carlo; Gaetani-Manfredotti, Amelia. The role of halide ligands in copper(I) carbonyl chemistry: Synthesis of monohalogen-bridged dinuclear copper(I) carbonyls, and x-ray crystal structure of $(Cu_2(Me_2NCH_2CH_2NMe_2)_2(CO)_2Cl)(BPh_4)$. J. Chem. Soc., Chem. Commun.: 937-938; 1979.

Pasquali, Marco; Floriani, Carlo; Gaetani-Manfredotti, Amelia. Copper-amine-carbonyl chemistry. Solution and solid-state studies of the copper(I)-ethylenediamine-carbon monoxide system: Synthesis and x-ray structures of mononuclear and binuclear copper(I)-carbonyl complexes. Inorg. Chem. 19: 1191-1197; 1980a.

Pasquali, Marco; Marini, Giuliana; Floriani, Carlo; Gaetani-Manfredotti, Amelia; Guastini, Carlo. Model compounds for copper(I) sites in hemocyanins: Synthesis, structure, and properties of copper(I) — Histamine complexes. Inorg. Chem. 19: 2525-2531; 1980b.

Pasquali, M.; Fiaschi, P.; Floriani, C.; Zanazzi, P. F. Copper(I) binds carbon monoxide in a cubane-like structure: Chemistry and x-ray crystal structure of tetrakis((2-methylquinolin-8-olato)-carbonylcopper(I)). J. Chem. Soc., Chem. Commun.: 613-614; 1983.

Penninger, Johannes M. L. A spectroscopic flow reactor for in situ studies of heterogeneous catalysts at elevated pressure and temperature by means of IR transmission spectroscopy. J. Catal. 56: 287-289; 1979.

Peri, J. B. Infrared and gravimetric study of the surface hydration of γ-alumina. J. Phys. Chem. 69: 211-219; 1965.

Pinchas, S.; Laulicht, I. Infrared spectra of labelled compounds. New York: Academic Press; 1971.

Plotnikov, V. A.; Ivanov, K. N.; Pospekhov, D. A. J. Chem. Ind. (Moscow) 8: 119, 472; 1931.

Pritchard, J.; Sims, M. L. Infra-red reflection spectra of adsorbed CO on copper. Trans. Faraday Soc. 66: 427-433; 1970.

Pritchard, J.; Catterick, T.; Gupta, R. K. Infrared spectroscopy of chemisorbed carbon monoxide on copper. Surface Sci. 53: 1-20; 1975.

Rálek, M.; Gunsser, W.; Knappwost, A. ESR studies on ZnO-Cr_2O_3 catalysts. J. Catal. 11: 317-325; 1968.

Reid, Robert C.; Prausnitz, John M.; Sherwood, Thomas K. The properties of gases and liquids. 3rd ed. New York: McGraw-Hill Book Co.; 1977; Appendix A.

Rozovskii, A. Ya. New data on the mechanism of catalytic reactions with the participation of carbon oxides. Kinet. Catal. 21: 78-87; 1980. Translated from Kinet. Katal. 21: 97-107; 1980.

Rozovskii, A. Ya.; Kagan, Yu. B.; Lin, G. I.; Slivinskii, E. V.; Loktev, S. M.; Liberov, L. G.; Bashkirov, A. N. Mechanism for the synthesis of methanol from carbon monoxide and hydrogen. Kinet. Catal. 16: 706; 1975. Translated from Kinet. Katal. 16: 810; 1975.

Rozovskii, A. Ya.; Lin, G. I.; Loktev, S. M.; Kagan, Yu. B.; Bashkirov, A. N. Transformations of methanol on a copper-containing oxide catalyst. Kinet. Catal. 17: 933; 1976a. Translated from Kinet. Katal. 17: 1071; 1976.

Rozovskii, A. Ya.; Kagan, Yu. B.; Lin, G. I.; Slivinskii, E. V.; Loktev, S. M.; Liberov, L. G.; Bashkirov, A. N. Mechanism of methanol synthesis from carbon dioxide and hydrogen II. Selection of the reaction mechanism. Kinet. Catal. 17: 1132-1138; 1976b. Translated from Kinet. Katal. 17: 1314-1320; 1976.

Rozovskii, A. Ya.; Lin, G. I.; Liberov, L. G.; Slivinskii, E. V.; Loktev, S. M.; Kagan, Yu. B.; Bashkirov, A. N. Mechanism of methanol synthesis from carbon dioxide and hydrogen III. Determination of rates of individual stages using ^{14}CO. Kinet. Catal. 18: 578-585; 1977. Translated from Kinet. Katal. 18: 691-699; 1977.

Rubloff, G. W.; Lüth, H.; Grobman, W. D. Orbital energy shifts associated with chemical bonding of organic molecules on ZnO nonpolar surfaces. Chem. Phys. Lett. 39: 493-496; 1976.

Rudnitskii, L. A.; Maksimova, N. P.; Alekseev, A. M. Investigation of the adsorption isotherms of hydrogen on zinc-chromium and zinc-chromium-copper catalysts. Kinet. Catal. 14: 1331-1337; 1973. Translated from Kinet. Katal. 14: 1505-1513; 1973.

Ruggeri, O.; Trifirò, F.; Vaccari, A. Catalysts for low-temperature methanol synthesis I. A study of the reduction process. J. Solid State Chem. 42: 120-124; 1982.

Ryberg, Roger. Carbon monoxide adsorbed on Cu(100) studied by infrared spectroscopy. Surface Sci. 114: 627-641; 1982.

Saussey, Jacques; Lavalley, Jean-Claude; Lamotte, Jean; Rais, Taoufik. I.R. spectroscopic evidence of formyl species formed by CO and H_2 co-adsorption on ZnO and Cu-ZnO. J. Chem. Soc., Chem. Commun.: 278-279; 1982.

Sayers, M. J.; McClellan, M. R.; Gay, R. R.; Solomon, Edward I.; McFeely, F. R. Angle resolved photoemission investigation of the bonding geometry of CO to ZnO ($10\bar{1}0$). Chem. Phys. Lett. 75: 575-578; 1980.

Sayers, M. J.; McClellan, M. R.; Shinn, N. D.; Trenary, M.; McFeely, F. R. A novel bonding geometry of CO on Cu(311) as determined by angle-resolved photoemission spectroscopy. Chem. Phys. Lett. 80: 521-525; 1981.

Scholten, J. J. F.; van Montfoort, A. An I.R. and volumetric study of hydrogen chemisorption on zinc oxide. Hightower, Joe W. ed. Proceedings of the 5th International Congress on Catalysis. New York: Elsevier Scientific; 1973; 385-395.

Semenova, T. A.; Lyudkovskaya, B. G.; Markina, M. I.; Volynkina, A. Ya.; Cherkasov, G. P.; Sharkina, V. I.; Khitrova, N. F.; Shpiro, G. P. Phase transformations and properties of the low-temperature carbon monoxide conversion catalyst during the time of its reduction and operations. Kinet. Catal. 18: 834-838; 1977. Translated from Kinet. Katal. 18: 1014-1020; 1977.

Sexton, Brett A. Surface vibrations of adsorbed intermediates in the reaction of alcohols with Cu(100). Surface Sci. 88: 299-318; 1979.

Shannon, R. D.; Prewitt, C. T. Effective ionic radii in oxides and fluorides. Acta Cryst. B25: 925-946; 1969.

Shimomura, Kin'ya; Ogawa, Kiyoshi; Oba, Masaaki; Kotera, Yoshihide. Copper oxide-zinc oxide-alumina catalyst: The structure of a copper oxide-zinc oxide-alumina catalyst for methanol synthesis. J. Catal. 52: 191-205; 1978.

Shishkov, D. S.; Kasabova, N. A.; Gatev, E. M. Aging processes in low-temperature catalysts for carbon monoxide conversion and methanol synthesis. Kinet. Catal. 20: 429-432; 1979. Translated from Kinet. Katal. 20: 521-524; 1979.

Smith, Garry; Cole-Hamilton, David J. Cationic formyl complexes of ruthenium(II). J. Chem. Soc., Chem. Commun.: 490-491; 1982.

Stiles, Alvin B., inventor. Methanol synthesis catalyst. U.S. patent 4,111,847. 1978 Sep. 5.

Strelzoff, Samuel. Methanol: Its technology and economics. Danner, G. A. ed. Methanol technology and economics. Chem. Eng. Progr. Symposium Ser. No. 98 66: 54-68; 1970.

Taylor, J. H.; Amberg, C. H. Infrared spectra of gases chemisorbed on zinc oxide I. CO and CO_2. Can. J. Chem. 39: 535-539; 1961.

Thomas, W. J.; Portalski, Stanislaw. Thermodynamics in methanol synthesis. Ind. Eng. Chem. 50: 967-970; 1958.

Thorn, David L. Hydrido-formyl complexes of iridium. The first cationic formyl complex and its reduction to a stable cis-hydrido-methyl compound. J. Am. Chem. Soc. 102: 7109-7110; 1980.

Tinker, H. Burnham; Morris, Donald E. High-pressure, high-temperature spectrophotometer cell for in situ catalyst identification. Perkins, A. J.; Grove, E. L.; Kaelble, Emmett F.; Westermeyer, Joan E. eds. Developments in applied spectroscopy. Vol. 10. New York: Plenum Press; 1972; 123-135.

Tsuchiya, Susumu; Shiba, Tadao. Mutual influence of adsorption of hydrogen and carbon monoxide on a methanol synthesis catalyst. J. Catal. 4: 116-122; 1965.

Ueno, Akifumi; Onishi, Takaharu; Tamaru, Kenzi. Dynamic technique to elucidate the reaction intermediate in surface catalysis. Trans. Faraday Soc. 66: 756-763; 1970.

Ueno, Akifumi; Onishi, Takaharu; Tamaru, Kenzi. Reaction intermediates in methyl alcohol decomposition on ZnO. Trans. Faraday Soc. 67: 3585-3589; 1971.

van Herwijnen, T.; de Jong, W. A. Kinetics and mechanism of the CO shift on Cu/ZnO I. Kinetics of the forward and reverse CO shift reactions. J. Catal. 63: 83-93; 1980.

van Herwijnen, T.; Guczalski, R. T.; de Jong, W. A. Kinetics and mechanism of the CO shift on Cu/ZnO II. Kinetics of the decomposition of formic acid. J. Catal. 63: 94-101; 1980.

Veltistova, M. V.; Dolgov, B. N.; Karpov, A. Z. J. Chem. Ind. (9): 24; 1934.

Vlasenko, V. Catalytic activity of precipitated zinc-chromium catalyst of various chemical compositions in the methanol synthesis. Ukr. Khim. Zh. 32: 348-353; 1966.

Wachs, Israel E.; Madix, Robert J. The selective oxidation of CH_3OH to H_2CO on a copper(110) catalyst. J. Catal. 53: 208-227; 1978.

Wachs, Israel E.; Madix, Robert J. The oxidation of H_2CO on a copper(110) surface. Surface Sci. 84: 375-386; 1979.

Wadayama, Toshimasa; Monma, Kiyoshi; Suĕtaka, Wataru. Multiple adsorbates on copper surfaces in formic acid vapor observed by polarization modulation infrared spectroscopy. J. Phys. Chem. 87: 3181-3183; 1983.

Wagner, C. D.; Riggs, W. M.; Davis, L. E.; Moulder, J. F.; Muilenberg, G. E. eds. Handbook of x-ray photoelectron spectroscopy. Eden Prairie, MN: Perkin-Elmer; 1979; 171.

Wayland, Bradford B.; Woods, Bruce A. Observation of a neutral metallo-formyl complex formed by the reaction of rhodium octaethylporphyrin hydride with carbon monoxide. J. Chem. Soc., Chem. Commun.: 700-701; 1981.

Weismantel, Guy E. Methanol supplies: Too much or too little? Chem. Eng. 87 (July 14): 75-78; 1980.

Williams, Roberto J. J.; Cunningham, Roberto E. Noncatalytic gas-solid reaction. Chromium oxide catalyst in methanol synthesis. Ind. Eng. Chem., Prod. Res. Develop. 13: 49-60; 1974.

Wood, Bernard J.; Isakson, William E.; Wise, Henry. Kinetic studies of catalyst poisoning during methanol synthesis at high pressures. Ind. Eng. Chem., Prod. Res. Develop. 19: 197-204; 1980.

Zecchina, A.; Coluccia, S.; Guglielminotti, E.; Ghiotti, G. An infrared study of surface properties of α-chromia. I. Preparation and adsorption of water, heavy water, and carbon monoxide. J. Phys. Chem. 75: 2774-2783; 1971a.

Zecchina, A.; Coluccia, S.; Guglielminotti, E.; Ghiotti, G. An infrared study of surface properties of α-chromia. III. Adsorption of carbon dioxide. J. Phys. Chem. 75: 2790-2798; 1971b.

ACKNOWLEDGMENTS

I am grateful to Professor Glenn Schrader for the opportunity to work on this research at the University of Delaware and Iowa State University. I am also indebted to the many colleagues at both of these institutions who have been helpful and cooperative during my professional activities. In particular, I thank Mr. David Studer for the construction of the high pressure infrared cell, Dr. John McClellan for use of his photoacoustic cell, Mr. Jim Anderegg for obtaining the XPS-Auger measurements, and Dr. Bernard Harbrecht for assistance with the Guinier X-ray technique. The encouragement and advice of Professor Alvin Stiles for catalyst preparation have been invaluable.

The pursuit of this degree has been more than a technical task; it has been a way of life for the last five years. Therefore, it is appropriate also to acknowledge the support and fellowship provided by my family and friends which have sustained me toward my goal.

APPENDIX A.

CALCULATION OF XPS BINDING ENERGIES

The calculations involved in the analysis of XPS and AES data from an oxidized 67/33 Zn/Cu oxide are carried through in detail. Table 5 gives a value of 1191.2 eV for the C 1s photoelectron. The correction term for this sample is calculated from the Einstein relation using a value of 285.0 eV for the binding energy of the C 1s electron:

$$\phi = h\nu - E_K - E_B = 1486.6 - 1191.2 - 285.0 = 10.4 \text{ eV}$$

Using this value for the correction term, the binding energy of the Zn $2P_{3/2}$ photoelectron is calculated from the Einstein relation using the value of 454.4 eV for the kinetic energy obtained from Table 5:

$$E_B = h\nu - E_K - \phi = 1486.6 - 454.4 - 10.4 = 1021.8 \text{ eV}$$

In the same manner, the Cu $2P_{3/2}$ photoelectron is evaluated using the kinetic energy value of 542.8 eV:

$$E_B = h\nu - E_K - \phi = 1486.6 - 542.8 - 10.4 = 933.4 \text{ eV}$$

These binding energies can be compared to values reported in the literature.

From Figure 12, the experimental kinetic energy of the Cu $L_3M_{4,5}M_{4,5}$ Auger electron can be determined to be 908.2 eV. A correction term is added to this value to adjust the kinetic energy value with respect to the Fermi level:

$$E_K^* = E_K + \phi = 908.2 + 10.4 = 918.6 \text{ eV}$$

This Auger kinetic energy can be compared to values reported in the literature.

APPENDIX B.

CALCULATION OF BET SURFACE AREA AND MICROPORE DISTRIBUTION

The procedures for analyzing physical adsorption/desorption processes on catalysts using the Accusorb 2100E instrument have been described in detail for a sample of 95/5 ZnO/CuO catalyst which had been removed from the reactor after activity tests. The catalyst, having a weight (W_s) of 0.5220 g, was placed into a BET bulb and heated overnight at 190°C under vacuum to remove adsorbed gases. Then, the sample was cooled to liquid nitrogen temperature (T_s) for adsorption measurements. The dead space (V_s) in the bulb varies with the amount of sample used, so the first measurement utilizes helium (a nonadsorbing gas) to determine the value of V_s. The system is composed of three sections: a manifold (V_D) held at a constant temperature (T_D) of 307.2°K, the dead space in the bulb, and the interconnecting tubing (V_i) which has a temperature (T_i) taken as the average of the manifold and liquid nitrogen temperatu. The initial manifold pressure (H_1) was 550 mmHg and the final pressure (H_2) in the system was 148.7 mmHg. The dead space was calculated from a material balance based on the ideal gas law:

$$V_s = (T_s/H_2)[(V_D/T_D)(H_1 - H_2) - V_i H_2/T_i]$$

$$V_s = (77.40^{\circ}K/148.7\ mmHg)[(29.79\ ml/307.2^{\circ}K)(550.0 - 148.7\ mmHg) - (3.65\ ml)(148.7\ ml)/192.3^{\circ}K]$$

$$= 18.79\ ml$$

After pumping off the helium in the bulb, the adsorption of nitrogen was measured. Because the nitrogen gas in the bulb does not behave ideally, a correction term of $(1 + \alpha P_e)$ is applied to the dead space. The perfect gas law correction factor, α, for nitrogen is 6.6×10^{-5} $mmHg^{-1}$. The volume of nitrogen adsorbed on the catalyst (V_a), which is given at STP conditions (760 mmHg and 273.1°K), can be calculated from a material balance:

$$V_a = \frac{273.1^{\circ}K}{760\ mmHg}\left[\frac{V_D}{T_D}(P_1 - P_2) - \left(\frac{V_s}{T_s} + \frac{V_i}{T_i}\right)(P_2 - P_e) - \frac{V_s}{T_s}\alpha(P_2^2 - P_e^2)\right]$$

where the initial manifold pressure (P_1), the final system pressure (P_2), and the final system pressure from the previous measurement (P_e) are experimental values. Usually, four or five sets of pressure readings are obtained in the range from 0.05 to 0.3 P_2/P_s, where P_s is the saturation pressure of nitrogen at 77.40°K (765 mmHg). Table 26 gives experimental values for P_1 and P_2, and the calculated values for the normalized volume of adsorbed nitrogen and the relative pressure. The BET equation utilizes this information to determine the monolayer volume (V_m):

$$(W_s/V_a)(P_2/P_s - P_2) = C/V_m + [(C - 1)/CV_m](P_2/P_s)$$

A plot of $(W_s/V_a)(P_2/P_s - P_2)$ vs. P_2/P_s will yield a straight line with a slope of $W_s(C - 1)/CV_m$ and an intercept of W_s/CV_m. The value of V_m is simply (slope plus intercept)$^{-1}$. A least-squares linear regression of the data points yielded a slope of 0.1681 and an intercept of 0.0012; the initial pair of data points were not used because the relative pressure was 0.0206 which was outside the linear region. The BET

Table 26. BET pressure readings and volume adsorbed

P_1 (mm Hg)	P_2 (mm Hg)	$\Sigma V_a/W_s$ (ml/g)	(P_2/P_s)
130.54	15.76	4.816	0.0206
151.36	48.92	5.654	0.0639
174.08	80.52	6.159	0.1053
197.82	110.20	6.597	0.1441
222.30	138.34	7.053	0.1808

surface area is the unit area per nitrogen molecule (S) times the number of molecules in a monolayer, which can be determined from the monolayer volume and the ideal gas law (the volume adsorbed was expressed at STP conditions). The BET surface area (S_w) was calculated to be:

$$S_w = SV_m(P/RT)_{STP}$$

$$= (16.2\ \text{Å}^2)(0.1681 + 0.0012)^{-1}(82.06 \times 273.1)^{-1}$$

$$(6.023 \times 10^{23}/10^{20}\ \text{Å}^2/\text{m}^2)$$

$$= 26\ \text{m}^2$$

Additional adsorption increments were made until the relative pressure (P_2/P_s) approached unity. Adsorbed nitrogen gradually filled the micropores during the adsorption process, with smaller pores filling before larger pores. Then, the pressure in the system was decreased by increments and a material balance made to determine the amount of nitrogen desorbed ($-V_a$) after each step. Both the adsorption and desorption isotherms were nearly the same, indicating that the desorption isotherm should be used for calculating the pore size distribution. A cylindrical pore model was utilized which assumes that the catalyst has

a distribution of pores of radii r_c with condensate of thickness t. The free radius, r, was determined from the Kelvin equation:

$$r = - 2\sigma M \cos\theta/(RT\rho \ln (P_2/P_s))$$

where σ is the surface tension of nitrogen, ρ is the density of liquid nitrogen, M is the molecular weight of nitrogen, and θ is the contact angle of the condensate (taken as zero). The condensate thickness was calculated from a Halsey-type expression:

$$t = 3.54[- 5/\ln (P_2/P_s)]^{0.33}$$

The pore radius was determined simply as:

$$r_c = r + t$$

Table 27 gives relative pressures, normalized volume of adsorbed nitrogen, pore radii, the change in pore radii between increments, the change in adsorbed nitrogen between increments, and the surface area of unfilled micropores ($\Sigma \Delta S_p$). The pore size distribution was plotted as $\Delta V/\Delta r$ vs. r_c. The surface area was calculated for each increment from geometrical considerations to be:

$$(\Sigma \Delta S_p)_i = \Sigma 2\Delta V_{p,i}/r_{c,i}$$

where

$$\Delta V_{p,i} = [\Delta V_i - \Delta t_i(\Sigma \Delta S_p)_{i-1}][r_c/(r_c - t)]_i^2$$

The total surface area of the micropores was determined to be 45 m^2/g, which is much higher than the BET surface area of 26 m^2/g. This

discrepancy indicates that the cylindrical pore model is not a true representation of the pore structure.

Table 27. Desorption pressure readings and volume desorbed

P_2/P_s	$\Sigma(V_a/W_s)$ (ml/g)	r_c (Å)	Δr (Å)	ΔV (ml)	$\Sigma \Delta S_p$ (m^2/g)
0.954	132.99	–	–	–	–
0.939	127.70	170	–	–	1.2
0.926	109.47	140	30	18.2	6.2
0.914	84.49	120	20	25.0	14
0.898	54.68	100	20	29.8	26
0.854	27.49	74	26	27.2	41
0.776	19.43	47	27	8.1	45

APPENDIX C.

THERMODYNAMICS OF METHANOL SYNTHESIS

A. $CO + 2H_2 = CH_3OH$ at 200°C and 50 atm

The standard-state free energy of formation for the reaction is

$$\Delta G^\circ = \Delta G^\circ_{CH_3OH} - \Delta G^\circ_{CO} - 2\Delta G^\circ_{H_2}$$
$$= -38.6 + 32.8 - 0.0 = -5.8 \text{ kcal/g mol}$$

The standard-state equilibrium constant is

$$K^\circ = \exp[-\Delta G^\circ/RT_o]$$
$$= \exp[5800/(1.99)(298)] = 1.8 \times 10^4$$

The standard-state heat of formation is

$$\Delta H^\circ = \Delta H^\circ_{CH_3OH} - \Delta H^\circ_{CO} - 2\Delta H^\circ_{H_2}$$
$$= -41.8 + 26.4 - 0.0 = -21.7 \text{ kcal/g mol}$$

The constants for the heat capacity expression are

$$\Delta a = \Sigma \nu_i a_i = a_{CH_3OH} - a_{CO} - 2a_{H_2}$$
$$= 5.052 - 7.373 - 2(6.483) = -15.287$$

$$\Delta b = \Sigma \nu_i b_i = b_{CH_3OH} - b_{CO} - 2b_{H_2}$$
$$= (1.694 + 0.307 - 2(0.2215)) \times 10^{-2} = 1.558 \times 10^{-2}$$

$$\Delta c = \Sigma \nu_i c_i = c_{CH_3OH} - c_{CO} - 2c_{H_2}$$
$$= (0.6179 - 0.6662 + 2(0.3298)) \times 10^{-5} = 0.6113 \times 10^{-5}$$

$$\Delta d = \Sigma \nu_i d_i = d_{CH_3OH} - d_{CO} - 2d_{H_2}$$
$$= (-6.811 + 3.037 - 2(1.826)) \times 10^{-9} = -7.426 \times 10^{-9}$$

The equilibrium constant at 473°K, using Equation 26, is

$$\ln K = 9.78 - (15.287/1.99) \ln (473/298) + (0.01558/2(1.99))$$
$$(473 - 298) + (0.6113 \times 10^{-5}/6(1.99))(473^2 - 298^2)$$
$$- (7.426 \times 10^{-9}/12(1.99))(473^3 - 298^3) + (1/1.99)$$

$$(21{,}700 - 15.287(298) + (.01558/2)(298)^2$$

$$+ (0.6113 \times 10^{-5}/3)(298)^3 - (7.426 \times 10^{-9}/4)(298)^4)$$

$$(1/473 - 1/298)$$

$$\ln K = -4.39$$

$$K = 0.0124$$

Using the fugacity coefficients from Table 22 and Equation 28,

$$y_1 = y_2 y_3^2 (0.0124)(0.98)(1.03)^2(50)^2/0.70$$

For an initial stoichiometric mixture of CO and H_2, the mole fraction of CO at equilibrium is $(1 - X)/(3 - 2X)$, the mole fraction of H_2 is $2(1 - X)/(3 - 2X)$, and the mole fraction of CH_3OH is $X/(3 - 2X)$.

Substituting and solving for X,

$$X^3 - 3.01X^2 + 3.02X - 1 = 0$$

$$X \approx 0.82$$

$$y_1 = X/(3 - 2X) = .82/(3 - 1.64) = 0.60$$

B. $CO_2 + 3H_2 = CH_3OH + H_2O$ at 200°C and 50 atm

The standard-state free energy of formation for the reaction is

$$\Delta G^o = \Delta G^o_{CH_3OH} + \Delta G^o_{H_2O} - \Delta G^o_{CO_2} - 3\Delta G^o_{H_2}$$

$$= -38.62 - 54.64 + 94.26 - 0.0 = 1.00 \text{ kcal/g mol}$$

The standard-state equilibrium constant is

$$K^o = \exp[-1000/(1.99)(298)] = 0.185$$

The standard-state heat of formation is

$$\Delta H^o = \Delta H^o_{CH_3OH} + \Delta H^o_{H_2O} - \Delta H^o_{CO_2} - 3\Delta H^o_{H_2}$$

$$= -48.1 - 57.8 + 94.1 - 0.0 = -11.8 \text{ kcal/g mol}$$

The constants for the heat capacity expression are

$$\Delta a = a_{CH_3OH} + a_{H_2O} - a_{CO_2} - 3a_{H_2}$$

$$= 5.052 + 7.701 - 4.728 - 3(6.483) = -11.424$$

$$\Delta b = b_{CH_3OH} + b_{H_2O} - b_{CO_2} - 3b_{H_2}$$
$$= (1.694 + .046 - 1.754 - 3(0.2215)) \times 10^{-2} = -0.679 \times 10^{-2}$$

$$\Delta c = c_{CH_3OH} + c_{H_2O} - c_{CO_2} - 3c_{H_2}$$
$$= (0.6179 + 0.2521 + 1.338 + 3(0.3298)) \times 10^{-5} = 3.197 \times 10^{-5}$$

$$\Delta d = d_{CH_3OH} + d_{H_2O} - d_{CO_2} - 3d_{H_2}$$
$$= (-6.811 - 0.859 - 4.097 - 3(1.826)) \times 10^{-9} = -17.25 \times 10^{-9}$$

The equilibrium constant at 473°K, using Equation 26, is

$$\ln K = -1.686 - (11.424/1.99) \ln (473/298) - (0.00679/2(1.99))$$
$$(473 - 298) + (3.197 \times 10^{-5}/6(1.99))(473^2 - 298^2)$$
$$- (17.25 \times 10^{-9}/12(1.99))(473^3 - 298^3) + (1/1.99)$$
$$(11{,}800 - 11.424(298) - (0.00679/2)(298)^2 + (3.197 \times 10^{-5}/3)$$
$$(298)^3 - (17.25 \times 10^{-9}/4)(298)^4)(1/473 - 1/298)$$

$$\ln K = -9.54$$

$$K = 7.21 \times 10^{-5}$$

Using the fugacity coefficients from Table 22 and Equation 27,

$$y_{CH_3OH} = y_{CO_2} y_{H_2}^3 (7.21 \times 10^{-5})(0.96)(1.03)^3(50)^2/y_{H_2O}(0.70)(0.38)$$

For an initial stoichiometric mixture of CO_2 and H_2, the mole fraction of CO_2 at equilibrium is $(1 - X)/2(2 - X)$, the mole fraction of H_2 is $3(1 - X)/2(2 - X)$, the mole fraction of CH_3OH is $X/2(2 - X)$, and the mole fraction of H_2O is $X/2(2 - X)$. Substituting and solving for X,

$$X^4 - 21X^3 + 35X^2 - 27X + 6.7 = 0$$

$$X \approx .44$$

$$y_{CH_3OH} = X/2(2 - X) = .44/2(2 - .44) = 0.14$$

C. $HCOOH + 2H_2 = CH_3OH + H_2O$ at 200°C and 50 atm

The standard-state free energy of formation for the reaction is

$$\Delta G^{o} = \Delta G^{o}_{CH_3OH} + \Delta G^{o}_{H_2O} - \Delta G^{o}_{HCOOH} - 2\Delta G^{o}_{H_2}$$
$$= -38.62 - 54.64 + 80.24 - 0.0 = -13.02 \text{ kcal/g mol}$$

The standard-state equilibrium constant is

$$K^{o} = \exp[13020/(1.99)(298)] = 3.43 \times 10^{9}$$

The standard-state heat of formation is

$$\Delta H^{o} = \Delta H^{o}_{CH_3OH} + \Delta H^{o}_{H_2O} - \Delta H^{o}_{HCOOH} - 2\Delta H^{o}_{H_2}$$
$$= -48.1 - 57.8 + 86.7 - 0.0 = -19.2 \text{ kcal/g mol}$$

The constants for the heat capacity expression are

$$\Delta a = a_{CH_3OH} + a_{H_2O} - a_{HCOOH} - 2a_{H_2}$$
$$= 5.052 + 7.701 - 2.798 - 2(6.483) = -3.011$$

$$\Delta b = b_{CH_3OH} + b_{H_2O} - b_{HCOOH} - 2b_{H_2}$$
$$= (1.694 + 0.046 - 3.243 - 2(0.2215)) \times 10^{-2} = -0.01946$$

$$\Delta c = c_{CH_3OH} + c_{H_2O} - c_{HCOOH} - 2c_{H_2}$$
$$= (0.6179 + 0.2521 + 2.009 + 2(0.3298)) \times 10^{-5} = 3.539 \times 10^{-5}$$

$$\Delta d = d_{CH_3OH} + d_{H_2O} - d_{HCOOH} - 2d_{H_2}$$
$$= (-6.811 - 0.859 - 4.187 - 2(1.826)) \times 10^{-9} = -15.51 \times 10^{-9}$$

The equilibrium constant at 473°K, using Equation 26, is

$$\ln K = 21.96 - (3.011/1.99) \ln (473/298) - (0.01946/2(1.99))$$
$$(473 - 298) + (3.539 \times 10^{-5}/6(1.99))(473^2 - 298^2)$$
$$- (1.551 \times 10^{-8}/12(1.99))(473^3 - 298^3)$$
$$+ (1/1.99)(19200 - 3.011(298) - (0.01946/2)(298)^2$$
$$+ (3.539 \times 10^{-5}/3)(298)^3 - (1.551 \times 10^{-8}/4)(298)^4)(1/473 - 1/298)$$

$$\ln K = 9.69$$

$$K = 1.62 \times 10^{4}$$

Using the fugacity coefficients from Table 22 and Equation 27,

$$y_{CH_3OH} = y_{HCOOH} y_{H_2}^2 (1.62 \times 10^4)(50)(0.30)(1.03)^2 / y_{H_2O}(0.70)(0.38)$$

For an initial stoichiometric mixture of HCOOH and H_2, the mole fraction of HCOOH at equilibrium is $(1 - X)/(3 - X)$, the mole fraction of H_2 is $2(1 - X)/(3 - X)$, the mole fraction of H_2O is $X/(3 - X)$, and the mole fraction of CH_3OH is $X/(3 - X)$. Substituting and solving for X,

$$X \approx 0.999$$

$$y_{CH_3OH} = 0.999/(3 - 0.999) = 0.50$$

D. $HCHO + H_2 = CH_3OH$ at 200°C and 50 atm

The standard-state free energy of formation for the reaction is

$$\Delta G^o = \Delta G^o_{CH_3OH} - \Delta G^o_{HCHO} - \Delta G^o_{H_2}$$
$$= -38.62 + 26.88 - 0.0 = -11.74 \text{ kcal/g mol}$$

The standard-state equilibrium constant is

$$K^o = \exp[11740/(1.99)(298)] = 3.96 \times 10^8$$

The standard-state heat of formation is

$$\Delta H^o = \Delta H^o_{CH_3OH} - \Delta H^o_{HCHO} - \Delta H^o_{H_2}$$
$$= -48.1 + 28.3 - 0.0 = -19.8 \text{ kcal/g mol}$$

The constants for the heat capacity expression are

$$\Delta a = a_{CH_3OH} - a_{HCHO} - a_{H_2}$$
$$= 5.052 - 5.607 - 6.483 = -7.038$$

$$\Delta b = b_{CH_3OH} - b_{HCHO} - b_{H_2}$$
$$= (1.694 - 0.754 - 0.222) \times 10^{-2} = .00718$$

$$\Delta c = c_{CH_3OH} - c_{HCHO} - c_{H_2}$$
$$= (0.6179 - 0.7130 + 0.3298) \times 10^{-5} = 2.347 \times 10^{-6}$$

$$\Delta d = d_{CH_3OH} - d_{HCHO} - d_{H_2}$$
$$= (-6.811 + 5.494 - 1.826) \times 10^{-9} = -3.143 \times 10^{-9}$$

The equilibrium constant at 473°K, using Equation 26, is

$$\ln K = 19.80 - (7.038/1.99) \ln (473/298) + (0.00718/2(1.99))$$
$$(473 - 298) + (2.347 \times 10^{-6}/6(1.99))(473^2 - 298^2)$$
$$- (3.143 \times 10^{-9}/12(1.99))(473^3 - 298^3)$$
$$+ (1/1.99)(19800 - 7.038(298) + (0.00718/2)(298)^2$$
$$+ (2.347 \times 10^{-6}/3)(298)^3 - (3.143 \times 10^{-9}/4)(298)^4)$$
$$(1/473 - 1/298)$$

$$\ln K = 7.26$$

$$K = 1.42 \times 10^3$$

Using the fugacity coefficients from Table 22 and Equation 27,

$$y_{CH_3OH} = y_{HCHO}y_{H_2}(1.42 \times 10^3)(50)(0.85)(1.03)/(0.70)$$

For an initial stoichiometric mixture of HCHO and H_2, the mole fraction of HCHO at equilibrium is $(1 - X)/(2 - X)$, the mole fraction of H_2 is $(1 - X)/(2 - X)$, and the mole fraction of CH_3OH is $X/(2 - X)$.

Substituting and solving for X,

$$X \approx 1.00$$

$$y_{CH_3OH} = 1.00$$

APPENDIX D.

THERMODYNAMICS OF THE WATER-GAS SHIFT REACTION

$CO + H_2O = CO_2 + H_2$ at 200°C and 50 atm

The standard-state free energy of formation for the reaction is:

$$\Delta G^\circ = \Delta G^\circ_{CO_2} + \Delta G^\circ_{H_2} - \Delta G^\circ_{CO} - \Delta G^\circ_{H_2O}$$
$$= - 94.26 + 0.0 + 32.81 + 54.64$$
$$= - 6.81 \text{ kcal/g mol}$$

The standard-state equilibrium constant is

$$K^\circ = \exp[- \Delta G^\circ/RT]$$
$$= \exp[6810/(1.99)(298)] = 9.71 \times 10^4$$

The standard-state heat of formation is

$$\Delta H^\circ = \Delta H^\circ_{CO_2} + \Delta H^\circ_{H_2} - \Delta H^\circ_{CO} - \Delta H^\circ_{H_2O}$$
$$= - 94.1 + 0.0 + 26.4 + 57.8 = - 9.9 \text{ kcal/g mol}$$

The constants for the heat capacity expression are

$$\Delta a = a_{CO_2} + a_{H_2} - a_{CO} - a_{H_2O}$$
$$= 4.728 + 6.483 - 7.373 - 7.701 = - 3.863$$

$$\Delta b = b_{CO_2} + b_{H_2} - b_{CO} - b_{H_2O}$$
$$= (1.754 + 0.222 + 0.307 - 0.046) \times 10^{-2} = 2.237 \times 10^{-2}$$

$$\Delta c = c_{CO_2} + c_{H_2} - c_{CO} - c_{H_2O}$$
$$= (- 1.338 - 0.330 - 0.666 - 0.252) \times 10^{-5} = - 2.586 \times 10^{-5}$$

$$\Delta d = d_{CO_2} + d_{H_2} - d_{CO} - d_{H_2O}$$
$$= (4.097 + 1.826 + 3.037 + 0.859) \times 10^{-9} = 9.819 \times 10^{-9}$$

The equilibrium constant at 473°K, using Equation 26, is

$$\ln K = 11.48 - (3.863/1.99) \ln (473/298) + (0.02237/2(1.99))$$
$$(473 - 298) - (2.586 \times 10^{-5}/6(1.99))(473^2 - 298^2)$$

$$+ (9.819 \times 10^{-9}/12(1.99))(473^3 - 298^3) + (1/1.99)(9900$$

$$- 3.863(298) + (0.02237/2)(298)^2 - (2.586 \times 10^{-5}/3)(298)^3$$

$$+ (9.819 \times 10^{-9}/4)(298)^4)(1/473 - 1/298)$$

$$\ln K = 5.33$$

$$K = 206.$$

Using the fugacity coefficients from Table 22 and Equation 27,

$$y_{CO_2} = y_{CO}y_{H_2O}(206)(0.98)(0.38)/y_{H_2}(1.03)(0.96)$$

For an initial stoichiometric mixture of CO and H_2O, the mole fractions of CO and H_2O at equilibrium are $(1 - X)/2$ and the mole fractions of CO_2 and H_2 are $X/2$. Substituting and solving for X,

$$X^2 = 2.03X + 1.01 = 0$$

$$X \approx 0.95$$

$$y_{CO_2} = X/2 = 0.95/2 = 0.48$$

APPENDIX E.

MASS FLOW CONTROLLER CALIBRATION CURVES

Although the manufacturer provided a calibration curve for each mass flow controller, flowrates were measured with a wet test meter at several pressures after the flow controllers had been installed in the flow system. Each flow setting was based on the digital indicator reading and not the potentiometer set point. Every point on a curve was an average of two flowrate measurements. Some of the low flowrates (< 200 cc/min STP) were checked with a bubble meter to ensure the accuracy of the results.

Calibration curves for nitrogen, hydrogen, and carbon monoxide at pressures of 1, 10, 30, and 50 atm are given in Figures 80, 81, and 82, respectively. The Brooks calibration curve, which was measured at 100 atm, has been included for comparison. The hydrogen line was also used with the premixed cylinder of hydrogen (90%) and carbon dioxide (10%); the calibration curve for this gas mixture at 1 and 50 atm is given in Figure 83. The curves for each gas show that the slope of each curve was pressure-dependent. This effect would not result from leakage because a leak would simply cause a shift in the entire curve without affecting the slope.

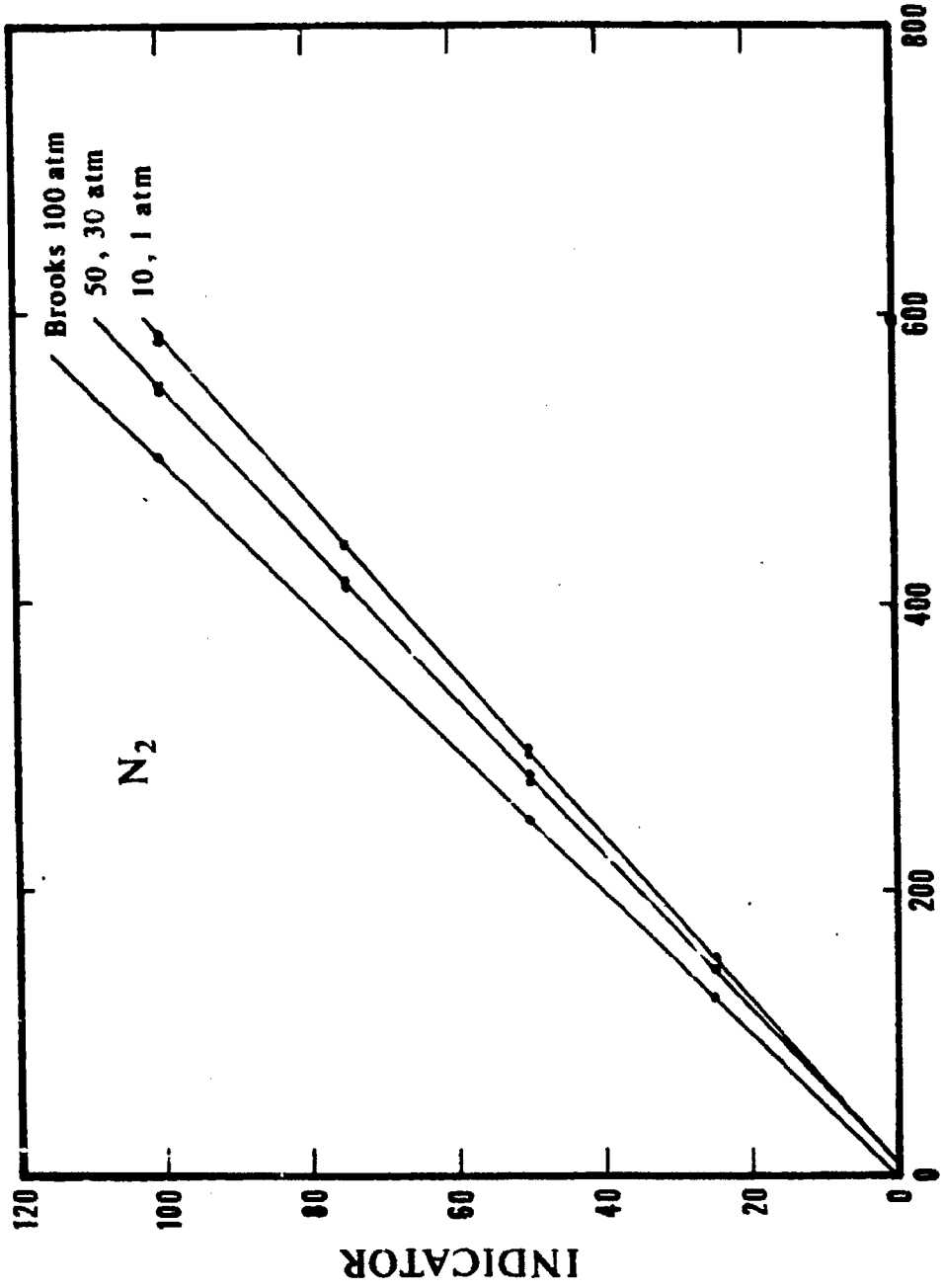

Figure 80. Calibration curves for nitrogen flowrates

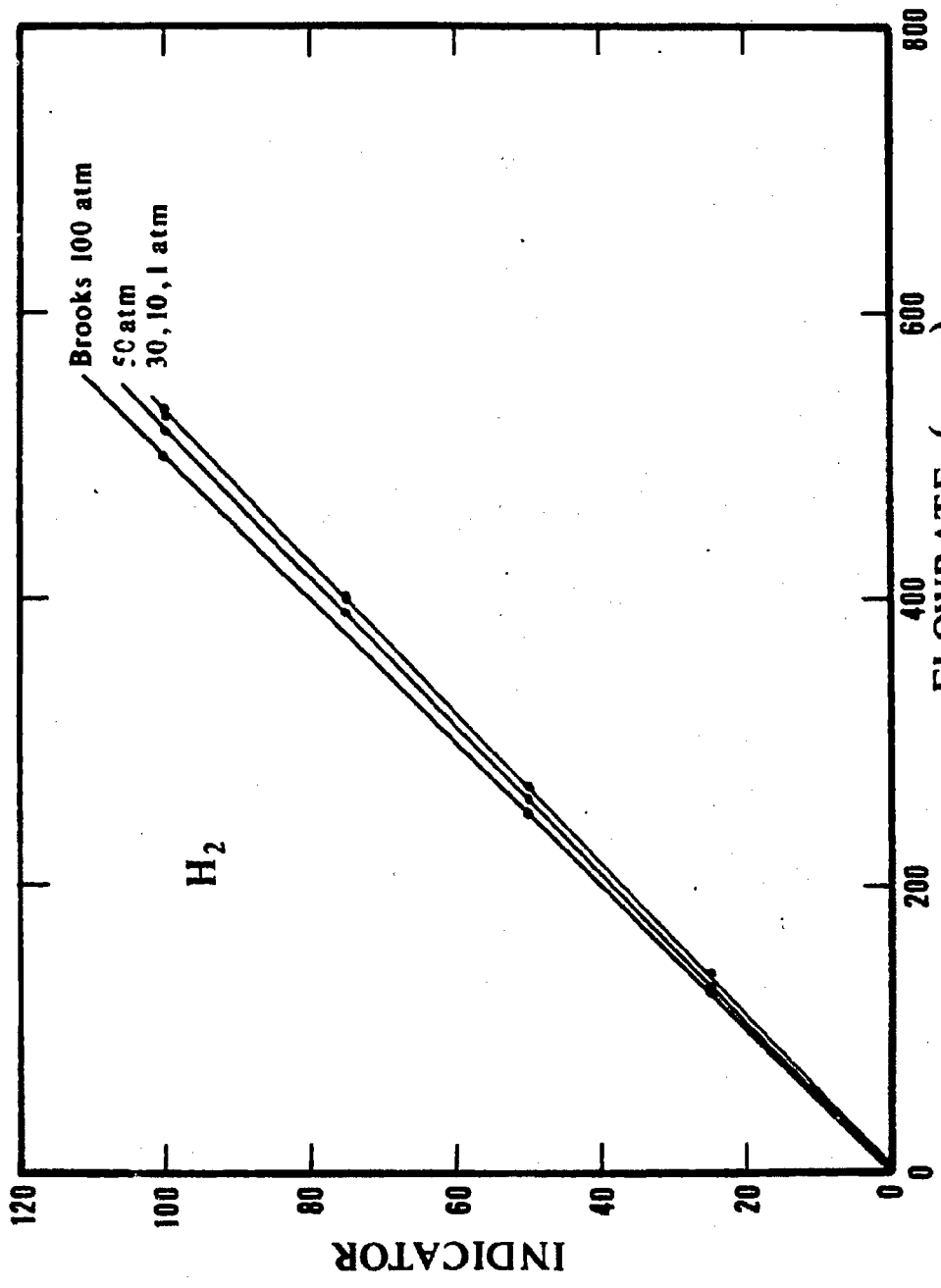

Figure 81. Calibration curves for hydrogen flowrates

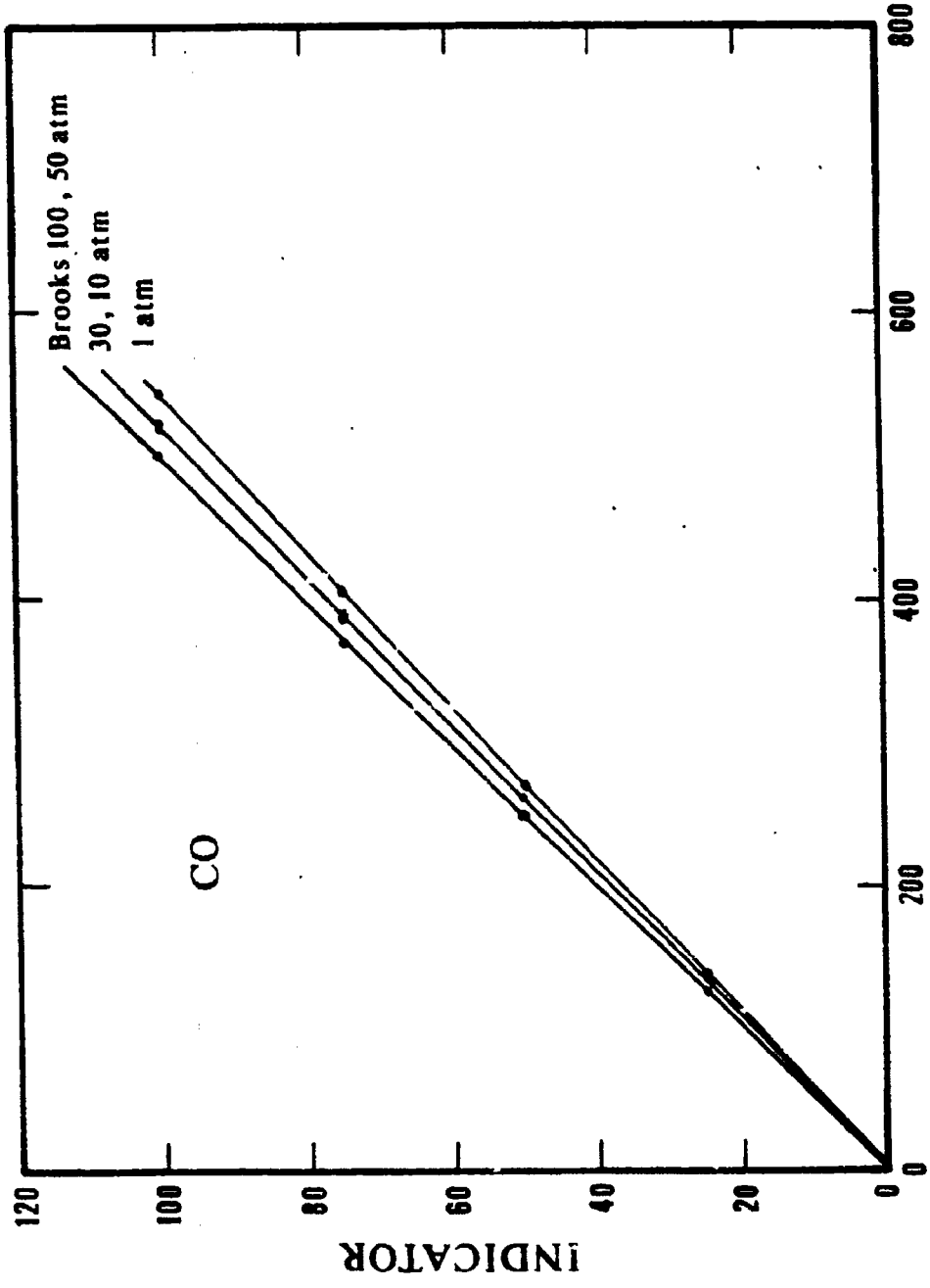

Figure 82. Calibration curves for carbon monoxide flowrates

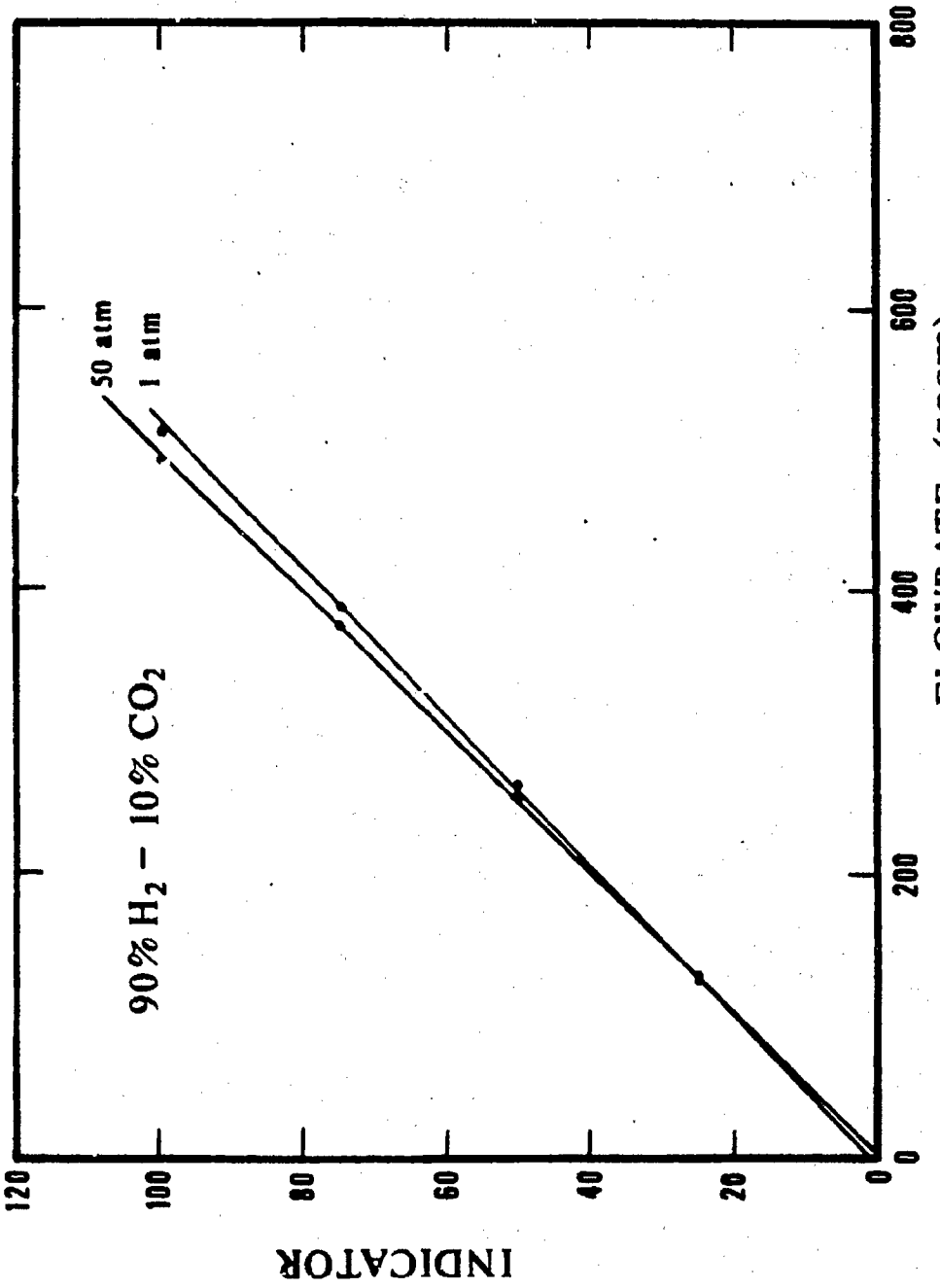

Figure 83. Calibration curves for 90% hydrogen-10% carbon dioxide flowrates

APPENDIX F.

RELATIVE RESPONSE FACTORS

A mixture of 95% CO, 4% CH_3OH, and 1% H_2O was prepared by injecting 17.6 µl of CH_3OH and 1.9 µl of H_2O into 250 cc of CO. After allowing enough time for the components to evaporate and mix, 0.5 cc samples were injected into the gas chromatograph. The response factor of CH_3OH was determined to be 1.11 and the response factor of H_2O to be 0.91. A mixture of 97.2% CO and 2.8% CH_3OH was prepared by injecting 12.0 µl of CH_3OH into 250 cc of CO. The response factor of CH_3OH was determined to be 1.19. A mixture of 99.0% CO and 1.0% CO_2 was prepared by injecting 2.5 cc of CO_2 into 250 cc of CO. The response factor of CO_2 was determined to be 0.98. A mixture of 52.9% CO and 47.1% N_2 was prepared by blending 35.5 cc/min CO with 31.6 cc/min N_2 and using the sampling loop to take samples. The response factor of N_2 was determined to be 1.10. Peak areas and relative response factor determinations have been given in Table 28.

Table 28. Relative response factors

1. 95% CO, 4% CH_3OH, 1% H_2O

   Area CO: 95.4, 95.2, 95.2, 95.4, 95.3; avg. = 95.3
   Area CH_3OH: 3.61, 3.66, 3.65, 3.54, 3.58; avg. = 3.61
   Area H_2O 1.01, 1.15, 1.13, 1.08, 1.14; avg. = 1.10

   RF_{CH_3OH} = (4.0/95)(95.3/3.61) = 1.11
   RF_{H_2O} = (1.0/95)(95.3/1.10) = 0.91

2. 97.2% CO, 2.8% CH_3OH

   Area CO: 97.6, 97.5, 97.6, 97.5, 97.6; avg. = 97.6
   Area CH_3OH: 2.40, 2.32, 2.38, 2.30, 2.43; avg. = 2.37

   RF_{CH_3OH} = (2.8/97.2)(97.6/2.37) = 1.19

3. 99.0% CO, 1.0% CO_2

   Area CO: 98.99, 98.98, 98.98, 98.98, 98.98; avg. = 98.98
   Area CO_2: 1.01, 1.02, 1.02, 1.02, 1.02; avg. = 1.02

   RF_{CO_2} = (1.0/99.0)(98.98/1.02) = 0.98

4. 52.9% CO, 47.1% N_2

   Area CO: 54.99, 55.18, 55.20, 54.90, 55.28; avg. = 55.11
   Area N_2: 44.94, 44.73, 44.72, 45.00, 44.66; avg. = 44.81

   RF_{N_2} = (47.1/52.9)(55.11/44.81) = 1.10

U.S. DEPARTMENT OF COMMERCE
Technology Administration
National Technical Information Service
Springfield, VA 22161 (703) 605-6000